

AD-A888 898

SCITECH CORP SANTA ANA CA  
LOW TEMPERATURE REGENERATOR STUDY. (U)  
AUG 79 P J WALSH

F/O 13/1

UNCLASSIFIED

F33615-78-C-3425  
NL

AFDOL-TR-79-2009

1 of 2  
AD-A888 898

The table consists of a grid of 10 columns and 10 rows. The top-left cell is white and contains the text '1 of 2' and 'AD-A888 898'. The rest of the grid is blacked out, obscuring any data that might have been present.

AFFDL-TR-79-3099

**LEVEL II**

**LOW TEMPERATURE REGENERATOR STUDY**

SCITECH CORPORATION  
SANTA ANA, CALIFORNIA 92704

AUGUST 1979

TECHNICAL REPORT AFFDL-TR-79-3099  
FINAL REPORT FOR PERIOD AUGUST 1978 TO AUGUST 1979

AD A 080892

DDC FILE COPY

APPROVED FOR PUBLIC RELEASE;  
DISTRIBUTION UNLIMITED.

DDC  
RECEIVED  
FEB 14 1980  
RECEIVED  
D

AIR FORCE FLIGHT DYNAMICS LABORATORY  
AIR FORCE WRIGHT AERONAUTICAL LABORATORIES  
AIR FORCE SYSTEMS COMMAND  
WRIGHT PATTERSON AIR FORCE BASE, OHIO 45433

80 2 14 030

NOTICE

When Government drawings, specifications, or other data are used for any purpose other than in connection with a definitely related Government procurement operation, the United States Government thereby incurs no responsibility nor any obligation whatsoever; and the fact that the government may have formulated, furnished, or in any way supplied the said drawings, specifications, or other data, is not to be regarded by implication or otherwise as in any manner licensing the holder or any other person or corporation, or conveying any rights or permission to manufacture, use, or sell any patented invention that may in any way be related thereto.

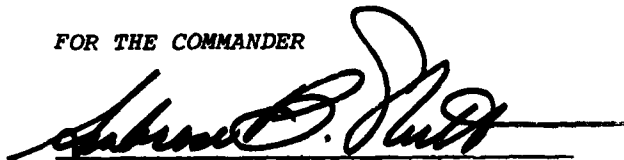
This report has been reviewed by the Information Office (OI) and is releasable to the National Technical Information Service (NTIS). At NTIS, it will be available to the general public, including foreign nations.

This technical report has been reviewed and is approved for publication.



RONALD WHITE  
Project Engineer

FOR THE COMMANDER



AMBROSE B. NUTT  
Director  
Vehicle Equipment Division

"If your address has changed, if you wish to be removed from our mailing list, or if the addressee is no longer employed by your organization please notify AFFDL/FEE, W-PAFB, OH 45433 to help us maintain a current mailing list".

Copies of this report should not be returned unless return is required by security considerations, contractual obligations, or notice on a specific document.

UNCLASSIFIED

SECURITY CLASSIFICATION OF THIS PAGE (When Data Entered)

(19) REPORT DOCUMENTATION PAGE		READ INSTRUCTIONS BEFORE COMPLETING FORM	
(18) 1. REPORT NUMBER AFFDL TR-79-3099	2. GOVT ACCESSION NO.	3. RECIPIENT'S CATALOG NUMBER	
(6) 4. TITLE (and Subtitle) LOW TEMPERATURE REGENERATOR STUDY.	(9) 5. TYPE OF REPORT & PERIOD COVERED Interim rpt. August 1978 to Aug 1979	6. PERFORMING ORG. REPORT NUMBER	
(10) 7. AUTHOR(s) P. J. Walsh	(15) 8. CONTRACT OR GRANT NUMBER(s) F33615-78-C-3425	9. PERFORMING ORGANIZATION NAME AND ADDRESS Scitech Corporation/ Santa Ana, CA 92704	
11. CONTROLLING OFFICE NAME AND ADDRESS United States Air Force AFSC Aeronautical Systems Division Wright-Patterson AFB, OH 45433	(11) 12. REPORT DATE August 1979	10. PROGRAM ELEMENT, PROJECT, TASK AREA & WORK UNIT NUMBERS Project 2402 (1904)	
14. MONITORING AGENCY NAME & ADDRESS (if different from Controlling Office) Air Force Flight Dynamics Laboratory/ Wright-Patterson AFB, Ohio 45433 FEE	13. NUMBER OF PAGES 138	15. SECURITY CLASS. (of this report) Unclassified	
16. DISTRIBUTION STATEMENT (of this Report) Approved for public release; distribution unlimited. (10) 151			
17. DISTRIBUTION STATEMENT (of the abstract entered in Block 20, if different from Report)			
18. SUPPLEMENTARY NOTES			
19. KEY WORDS (Continue on reverse side if necessary and identify by block number) Regenerators Cryogenics Refrigeration Low Temperature			
20. ABSTRACT (Continue on reverse side if necessary and identify by block number) This report covers the results of a study program to determine the extent to which low temperature regenerators can be improved by utilizing size or surface effects. Subjects include surface effect contribution to specific heat; conditions necessary for significant effect; effect upon refrigeration parameters; materials selection; configurations; and plans for producing and testing improved regenerators for the 50° to 300°K regions.			

DD FORM 1 JAN 73 1473 EDITION OF 1 NOV 65 IS OBSOLETE

UNCLASSIFIED

SECURITY CLASSIFICATION OF THIS PAGE (When Data Entered)

SLC 32000

JK

PREFACE

This Interim Technical Report on the Low Temperature Regenerator Study was prepared by Scitech Corporation, Santa Ana, California. Work on this program began 1 August 1978 under Contract F33615-78-C-3425, Project 2402, Task 240204 "Aerospace Vehicle Environmental Control", sponsored by the Air Force Flight Dynamics Laboratory, Air Force Systems Command, Wright-Patterson Air Force Base, Ohio. Initial funding was provided by AFFDL Laboratory Director's Fund. Mr. Ronald White was the Project Engineer for AFFDL/FEE.

The following key personnel at Scitech Corporation participated and made significant contribution to the program:

H. Yoshimoto	Program Manager
P. J. Walsh	Chief Scientist and Principal Investigator
L. A. Wade	Technical Staff
E. E. Payne	Technical Staff

<b>Accession For</b>	
NTIS GRA&I	<input checked="" type="checkbox"/>
DDC TAB	<input type="checkbox"/>
Unannounced	<input type="checkbox"/>
Justification	
By _____	
Distribution/	
Availability Codes	
Dist	Avail and/or special
A	

## TABLE OF CONTENTS

SECTION		PAGE
I	INTRODUCTION .....	1
II	SPECIFIC HEAT THEORY .....	4
	2.1 Background .....	4
	2.2 Bulk Lattice Specific Heat .....	5
	2.3 Surface Contributions to Specific Heat ..	12
	2.4 Electron System Contribution To Surface Specific Heat .....	20
	2.5 Survey of Reported Measurements .....	23
	2.6 The Question of Cluster Structures .....	27
	2.7 The Composite Specific Heat Model .....	31
	2.7.1 Comparison with Reported Measurements ...	32
	2.8 Candidate Materials for Surface Specific Heat Enhancements .....	40
	2.8.1 Interpretation of Specific Heat Enhancement Data .....	52
III	IDEALIZED REFRIGERATOR PERFORMANCE .....	64
	3.1 Introduction .....	64
	3.2 Stirling Cycle Analysis .....	71
	3.2.1 Simple Regenerator Model .....	73
	3.2.2 Multiple Stage Refrigeration .....	79
	3.2.3 Cold Stage Analysis .....	83
	3.3 Refrigerator Performance Calculation ....	91
	3.3.1 Interpretation of Calculated Results ....	98
IV	ULTRAFINE PARTICLE TECHNOLOGY .....	104
	4.1 Introduction .....	104
	4.2 Production of Particles .....	105

4.2.1	Measurement and Grading of Ultrafine Powders .....	107
4.2.2	Predicted Availability of Test Materials	.108
4.3	Methods of Regenerator Production .....	110
4.4	Safety Considerations .....	114
V	CONCLUSIONS .....	116
5.1	Small Particle Specific Heat .....	116
5.2	Small Particle Availability .....	116
5.3	Cryogenic Refrigerator Performance .....	117
5.4	Regenerator Element Producibility .....	117
5.5	Safety .....	118
5.6	Summary .....	118
	APPENDIX .....	123

## LIST OF ILLUSTRATIONS

<u>FIGURE</u>		<u>PAGE</u>
1	$\eta(v)$ models contrasted	11
2	Area Approximation to Integer Points	13
3	Magnesium Oxide, Small Particle $C_v$	33
4	Sodium Chloride, Small Particle $C_v$	34
5	Specific Heat of Palladium Ultrafines	36
6	Specific Heat of Lead Ultrafines	37
7	Specific Heat of Indium Ultrafines	38
8	Molar Specific Heat of Bismuth Ultrafines	44
9	Molar Specific Heat of Mercury Ultrafines	45
10	Molar Specific Heat of Indium Ultrafines	46
11	Molar Specific Heat of Lanthanum Ultrafines	47
12	Molar Specific Heat of Lead Ultrafines	48
13	Molar Specific Heat of Selenium Ultrafines	49
14	Molar Specific Heat of Mallium Ultrafines	50
15	Molar Specific Heat of Chromium Chloride Ultrafines	51
16	Volumetric Specific Heat of Bismuth Ultrafines	53
17	Volumetric Specific Heat of Mercury Ultrafines	54
18	Volumetric Specific Heat of Indium Ultrafines	55
19	Volumetric Specific Heat of Lanthanum Ultrafines	56
20	Volumetric Specific Heat of Lead Ultrafines	57
21	Volumetric Specific Heat of Selenium Ultrafines	58
22	Volumetric Specific Heat of Mallium Ultrafines	59
23	Volumetric Specific Heat of Chromium Chloride Ultrafines	60
24	Comparison of Specific Heat Calculations for Lead	62
25	Weighted Curves for Lead Particle $C_v$	63

LIST OF ILLUSTRATIONS

<u>FIGURE</u>		<u>PAGE</u>
26	Stirling Cycle Diagram	65
27	Ericsson Cycle Diagram	67
28	Minimum Required Regenerator Efficiency vs. $T_c$ (Cold Stage)	76
29	P-V Diagram Representation for Multiple Stage Refrigerator	80
30	Idealized Gas Flow Paths for Multiple Stage Refrigerator	81
31	Idealized Refrigerator Model with Segmented Cold Gradient Regenerator	89
32	Test Planning Network: Specific Heat Test & Regenerator Material Evaluation	133
33	Test Planning Network: Regenerator Performance Model Evaluation	138

List of Symbols for Section II

- $A$  = Constant (Eq. 7); number of degrees of freedom for cluster structure
- $a'$  = Bessel function index
- $B$  = Specific heat additive constant for cluster structure
- $C_{CL}$  = Specific heat term for cluster
- $C_E$  = Einstein's specific heat function
- $C_i$  = Weighted wave velocity defined by Eq. 18
- $C_L$  = Longitudinal wave velocity
- $C_s$  = Wave propagation velocity in a specific medium
- $C_T$  = Transverse wave velocity
- $C_v$  = Specific heat at constant volume
- $C_v^e$  = Specific heat of electron system
- $C_v^s$  = Surface specific heat
- $E$  = Electron energy
- $E_F$  = Fermi energy level
- $E_0$  = Internal energy of electron system at  $0^\circ K$
- $f(E)$  = Fraction of occupied energy states
- $f(\mathbf{z})$  = Lattice dynamics optical branch wave function
- $h$  = Planck's constant
- $I(\mathbf{z})$  = Lattice dynamics acoustical branch wave function
- $K_1$  = Constant
- $k$  = Boltzman's constant
- $L$  = Length of side of a cube
- $l$  = Bessel function index
- $M$  = Atomic weight

- $m$  = Mass  
 $m_e$  = Electron mass  
 $N$  = Number of lattice sites, number of molecules  
in crystal  
 $N'$  = Number of free electrons, number of particles  
in a system  
 $N_0$  = Avogadro's number  
 $\eta(E)$  = Energy density function  
 $\eta(\nu)$  = Density of vibrational modes  
 $n^+$  = Average number of conduction electrons per  
lattice site  
 $n_1, n_2, n_3, n_4, n_e$  = Positive integers  
 $O(\frac{1}{2})$  = Indicates numerical value "on the order of"  
 $P$  = Internal pressure in a system  
 $Q$  = Quantity of heat  
 $q$  = Dummy variable of integration  
 $R$  = Gas constant  
 $R$  = Radius of sphere  
 $r$  = Particle radius  
 $S$  = Surface area  
 $S'$  = Specific surface area  
 $\lambda$  = Bessel function index  
 $T$  = Temperature  
 $T_E$  = Einstein temperature  
 $t$  = Time  
 $U$  = Internal energy of a system  
 $\bar{u}_i$  = Average oscillator energy

- $u(x,y,z,t)$  = Wave deflections as function of location and time  
 $V$  = Volume  
 $V_m$  = Molar volume  
 $X$  = Dimensionless temperature ratio  
 $(x,y,z)$  = Location in three dimensional space  
 $\xi$  = Dummy variable of integration  
 $\alpha$  = Montroll constant defined in Eq. (22)  
 $\beta$  = Debye constant defined in Eq. (20)  
 $\delta$  = Electron system specific heat constant  
 $\epsilon$  = Montroll linear term enhancement coefficient  
 $\zeta(i)$  = Riemann zeta function  
 $\theta_0$  = Debye temperature  
 $\theta_0$  = Debye temperature near 0°K  
 $\nu$  = Frequency  
 $\nu_0$  = Debye Frequency  
 $f$  = Lattice dynamics velocity function  
 $\rho$  = Bulk density  
 $\omega, \omega_i$  = Angular velocities  
 $\omega_{A_i}, \omega_{A_i}^b, \omega_{O_i}, \omega_{O_i}^b$  = Angular velocities defined for small particles per Eq. (26)

List of Symbols for Section III

- $A$  = Cross-sectional area of flow bed  
 $A_c$  = Minimum free-flow area  
 $A_T$  = Heat transfer surface area  
 $C_g$  = Gas flow stream capacity rate  
 $C_R, C_R(L)$  = Matrix (thermal) stream capacity, as a function of axial length  
 $C_p$  = Specific heat at constant pressure  
 $C_v$  = Specific heat at constant volume  
 $C_m, C_m(L)$  = Specific heat of regenerator matrix, as a function of axial length  
COP = Theoretical coefficient of performance  
 $f$  = Fanning friction factor  
 $G$  = Regenerator flow stream mass velocity  
 $H$  = Total enthalpy  
 $\Delta H_{exp}$  = Enthalpy change during gas expansion process  
 $h$  = Convection heat transfer coefficient  
 $h_i, h_o$  = Specific enthalpy for inlet, outlet gas streams respectively  
 $I$  = Constant  
 $J$  = Heat transfer modulus  
 $K$  = Constant  
 $k$  = Thermal conductivity  
 $L$  = Length of flow path  
 $M_R$  = Total regenerator mass in flow cycle  
 $m$  = Mass

- $\bar{m}$  = Average mass flow rate
- $\dot{m}_c$  = Mass flow rate corrected for compressibility
- $m_R$  = Mass of (a single) regenerator
- $\dot{m}_{REQ}$  = Flow rate (theoretical) required to produce target refrigeration
- $N$  = Revolutions per minute
- $N_{PR}$  = Prandtl number
- $N_{ST}$  = Stanton number
- $\omega$  = Cycles per second
- $P$  = Pressure
- $P_i$  = Pressure at state i of a P-V diagram
- $\rho$  = Porosity of powder pack
- $Q$  = Quantity of heat
- $Q_{-exp}$  = Heat absorbed during expansion
- $Q_{-exp}^{ideal}$  = Heat absorbed during expansion (ideal gas assumption)
- $Q_{EXT}$  = External heat load on refrigerator cold station
- $Q_{Net}$  = Net heat rejected during refrigeration cycle
- $Q_R$  = Regenerator heat loss
- $Q_{SL}$  = Total stage loss of refrigerator
- $R$  = Gas constant
- $r_h$  = Hydraulic radius of flow path
- $S_v$  = Volume specific surface
- $T$  = Temperature
- $T_c$  = Temperature of coldest isothermal expansion
- $T_h$  = Temperature of warmest isothermal compression
- $T_i$  = Temperature at state i
- $T_{c1}, T_{c2}, T_{m1}, T_{m2}, T_{m3}$  = Regenerator segment temperatures as illustrated in Fig. 31

- $U$  = Internal energy  
 $U_{AV}$  = Overall conductance for heat transfer  
 $V$  = Volume  
 $v_i$  = Specific volume at state  $i$  of a P-V diagram  
 $W$  = Work  
 $W_{exp}$  = Work done during gas expansion process  
 $W_{Net}$  = Net work done by a system  
 $\gamma$  = Dimensionless ratio of specific heats  
 $E$  = Actual regenerator efficiency  
 $E_i$  = Efficiency of  $i^{th}$  stage of regenerator  
 $E_L^{(i)}$  = Achieved efficiency of the  $i^{th}$  segment of regenerator  
 $E_{MIN}$  = Minimum allowable regenerator efficiency  
 $E_M^{(i)}$  = Achieved efficiency of the  $i^{th}$  segment of  $n^{th}$  regenerator stage  
 $E_0$  = Theoretical design efficiency of regenerator  
 $\lambda$  = Actual number of heat transfer units  
 $\lambda_0$  = Theoretical number of heat transfer units  
 $\lambda_{REQ}$  = Theoretical required number of heat transfer units  
 $\mu$  = Gas viscosity  
 $\rho$  = Average gas density  
 $\tau_0$  = Regenerator blow time  
 $\tau_c$  = Cycle time

## I. INTRODUCTION

Miniature cryogenic refrigerators are used in a variety of military and civilian applications, probably chiefly to cool infrared detector elements to the appropriate operating temperature. Long wavelength sensors operating in the 8 - 14  $\mu\text{m}$  region commonly require refrigeration down to temperatures in the 4 - 30 $^{\circ}\text{K}$  range, and mid-wavelength detectors operating in the 2 - 8  $\mu\text{m}$  region usually perform satisfactorily at a temperature in the 70 - 80 $^{\circ}\text{K}$  neighborhood.

Historically, the 70 - 80 $^{\circ}\text{K}$  requirement was met by employing open cycle liquid nitrogen systems to provide the detector refrigeration. At least as early as about 1960 mechanical refrigerators were successfully used in this application. Early refrigerators employed were based on the Joule-Thompson process in which high pressure gas was expanded through a nozzle to produce either a liquid or a cold vapor capable of removing heat from the detector. Closed cycle Joule-Thompson devices were plagued with reliability problems stemming both from the high compression loads in the miniaturized compressors and from the stringent contamination requirements for the gas in order to avoid blocking the nozzle.

To improve the reliability situation, classes of refrigerators which employed a periodic flow heat exchanger, called a regenerator, and a piston-type expansion process were developed. Some of the earliest work on these regenerator-based machines was reported in the 1940s, and by 1960 Stirling cycle versions were already at a reasonably mature stage of development. Over the next decade nearly a half dozen variations of the Stirling cycle were explored, some rejected as mere laboratory curiosities and others developed to a high level of sophistication. All of these devices, in the final analysis, were limited in their capabilities by the performance of the periodic flow regenerator.

In regenerator heat exchanger matrix fabrication the search for suitable materials always came back to lead as the leading candidate since it (lead) has a higher specific heat at low temperatures than most other materials. Even with lead, however, the rapid decrease in specific heat at temperatures below about 15°K severely penalized refrigerator performance at the low end of the temperature range. Careful optimization of the various machines resulted in systematically reducing the "dead end" temperature over a period of years to values below 10°K.

At this low end of temperature, however, the machines normally provided very little excess capacity to account for variation in performance due to seal degradation, slight gas contamination, variation in crankcase temperature, or any of the multitude of off-design conditions that can be encountered in actual user environments. Consequently, variations in machine performance would directly translate into variations in the temperature platform provided for the infrared detector element.

Variations in the detector temperature are highly undesirable, since they can often directly show up as variations in the output signal. Output signal variations can cause confusion either by being interpreted as valid information to be decoded or by masking low level information content.

To minimize this temperature variation problem, the impetus for better regenerator design and the search for high specific heat materials continued. Various specific heat anomalies yielding high heat capacity values (but over very narrow temperature bands) have been identified. Many of these have been tried in regenerator experiments, usually with only limited success. One specific heat effect which has not yet been tried experimentally is achieved when a bulk material is subdivided into an ultra-fine powder form.

This specific heat enhancement, which is associated with the inherent high surface energy of powdered material,

has been reported several times in the literature. To this point in time, only a minimum amount of investigation into predicting the magnitude of the effect has taken place and no applications have been attempted. This surface enhanced specific heat effect is particularly attractive for refrigerator application since it is not limited to a narrow temperature band. So far as is known, it extends from the lowest temperatures of interest for these applications up to probably 30°K (or warmer), depending on the material.

The purpose of the research program reported herein has been to determine the suitability of this surface enhanced specific heat for use in low temperature regenerator applications. Objectives established to satisfy program requirements included:

- o Develop a predictive model for surface enhanced specific heat
- o Search literature and catalog experimental program results of measurements of this surface specific heat effect
- o Develop a model for predicting performance of a regenerator fabricated using finely divided powders
- o Apply this new regenerator model to predict performance capability of a refrigerator using the surface enhancement effect
- o Catalog current state of the art in small particle production
- o Develop concepts for producing practical regenerators which take advantage of the surface enhancement effect
- o Provide recommendations for further work and a system-oriented test plan for evaluating refrigerator improvements from this effect.

Each of these objectives is addressed in detail in the sections following.

## II SPECIFIC HEAT THEORY

### 2.1 Background

From thermodynamic considerations, the concept of heat capacity is best described as that amount of heat necessary to be added to a substance in order to raise its temperature by one measurement unit. Historical experiments to measure the specific heat\* of materials at moderate temperatures showed the surprising result that the constant volume specific heat of all monatomic solids ( $C_v$ ) approaches a definite value:

$$C_v = 3N_0R = 3R \approx 6 \text{ CAL/MOLE/K} \quad (1)$$

where  $N_0$  is Avogadro's number

$k$  is the Boltzmann constant

and  $R$  is the gas constant.

This relationship, known as the law of Dulong and Petit, has been found to hold over a broad temperature range. Its subsequent theoretical derivation, which was accomplished utilizing classical statistical mechanics principles, was considered to firmly establish it as a fundamental law of nature. The relationship was further strengthened when experimental results, in accord with the predictions of classical theory, demonstrated that diatomic solids had a value approximately double that of Eq. 1, triatomic solids triple, and so on.

It was a matter of considerable concern, then, that subsequent experiments indicated that the specific heat of solids in the cryogenic temperature region was a strong function of temperature, in sharp disagreement with the predictions of classical physics. A satisfactory explanation of this low temperature "anomaly" awaited the development of quantum mechanics concepts early in the twentieth century.

-----  
\* defined as heat capacity per unit mass

The turn of the twentieth century marked profound advances in our understanding of science. Planck's brilliant empirical approach quantizing the energy associated with black body radiation formed the basis for what was to become the quantum theory of physics. In 1906 Einstein applied these same quantum concepts to the model of specific heat with enough success to pave the way for later work which finally explained those early anomalous specific heat measurements. The most influential of the specific heat models, that developed by Debye, accurately predicted a low temperature  $T^3$  variation in specific heat.

Before developing the concept of improving the low temperature specific heat of a material by finely subdividing it into an ultrafine powder form -- the primary topic of this study program -- it is useful to review the Debye specific heat analysis for bulk material.

## 2.2 Bulk Lattice Specific Heat

The first law of thermodynamics is written as

$$\delta Q = dU + PdV \quad (2)$$

where  $\delta Q$  is heat absorbed by a system

$dU$  is the change in internal energy

$PdV$  is the work done by the system

and the notation  $\delta Q$  indicates the quantity is an inexact differential. Expressed as a function of volume ( $V$ ) and temperature ( $T$ ),

$$dU = \left(\frac{\partial U}{\partial T}\right)_V dT + \left(\frac{\partial U}{\partial V}\right)_T dV \quad (3)$$

Consequently,

$$\delta Q = \left(\frac{\partial U}{\partial T}\right)_V dT + \left[\left(\frac{\partial U}{\partial V}\right)_T + P\right] dV. \quad (4)$$

We then define specific heat at constant volume as:

$$C_V \equiv \left(\frac{\delta Q}{dT}\right)_V = \left(\frac{\partial U}{\partial T}\right)_V. \quad (5)$$

Eq. 5 will be the basis for computing specific heat once we derive an expression for the internal energy of a solid from quantum mechanics principles.

Quantum theories of specific heat all have in common the postulate that the total internal (vibrational) energy of a crystal of  $N$  lattice sites is equivalent to the energy of a system of  $3N$  harmonic oscillators. Consequently, in a three dimensional solid each atom can contribute three normal modes of oscillation to the overall vibrational frequency spectrum which we shall show determines the internal energy of the crystal.

It is not intuitively obvious that so-called vibrational modes of a crystal, which most readily bring to mind a wave traveling down a taut string, can be equated to the vibrations of a three dimensional harmonic oscillator, as the postulate requires. The text by Dekker<sup>1</sup> elegantly derives the mathematical correspondence between the two in a proof which won't be repeated here..

The specific heat model in general use today is the Debye equation which was derived only a few years after Einstein's classic work. This model provides highly accurate predictions of specific heat, even though it was derived using several simplifying assumptions, resulting in some theoretical shortcomings.

Although the Debye algorithm can be derived from quantum statistical mechanics principles, better insight to the physics of the specific heat mechanism is gained by the following less rigorous approach.

The three dimensional time dependent wave equation applicable to a harmonic oscillator is,

$$\frac{\partial^2 u}{\partial x^2} + \frac{\partial^2 u}{\partial y^2} + \frac{\partial^2 u}{\partial z^2} = \frac{1}{c_s^2} \frac{\partial^2 u}{\partial t^2} \quad (6)$$

where  $u(x, y, z, t)$  is the instantaneous wave deflection at a location  $(x, y, z)$  in space,  $t$  is time, and  $c_s$  is the propagation velocity in the medium.

A solution to this equation is the wave of frequency  $\nu$  described by:

$$u(x, y, z, t) = A \sin(m_x \pi x / L) \sin(m_y \pi y / L) \sin(m_z \pi z / L) \cos 2\pi \nu t, \quad (7)$$

provided that  $m_x, m_y$  and  $m_z$  are all positive integers  $\geq 1$ , and the solid is in the form of a cube of side  $L$ .

The frequencies allowed by Eq. 7 take the form:

$$\nu = \left[ \frac{c_s^2}{4L^2} (m_x^2 + m_y^2 + m_z^2) \right]^{1/2}. \quad (8)$$

This relationship exhibits the fact that only integral numbers of half-wave lengths are allowed to propagate through the crystal lattice.

In order to compute the internal energy from which to derive the specific heat, we are interested in determining the possible modes of vibration in the cube, multiplying each by the harmonic oscillator energy associated with it, and then summing all such mode energies to determine the total for the crystal.

Since the  $m_x$  of Eq. 8 are required to be all positive, we can associate them in integer space with

the first octant of a sphere of radius  $Q$ , where

$$Q^2 = n_x^2 + n_y^2 + n_z^2. \quad (9)$$

Now since each positive integer value gives rise to a discrete mode of vibration, the number of such modes in frequency space lying between  $Q$  and  $Q+dQ$ , designated  $\eta(Q)dQ$ , can be approximated by the volume of such an octant. Consequently,

$$\eta(Q)dQ \cong \left( \frac{4\pi V}{c^3} \right) Q^2 dQ \quad (10)$$

where  $V$ , the volume of the cube, is  $L^3$ .

The approximation sign in this equation is only to alert the reader that the number of integer points in such an octant is not rigorously determined by such an integration technique. This concept will be pursued in some depth later.

It must also be pointed out that elastic waves in a crystal propagate either as longitudinal or as transverse waves, and different velocities  $c_T, c_L$  may be associated with the two. Since there are two orthogonal transverse waves allowed, we modify Eq. 10 to the more general form (without carrying forward any longer the approximation symbol):

$$\eta(Q)dQ = 4\pi V \left( \frac{2}{c_T^3} + \frac{1}{c_L^3} \right) Q^2 dQ. \quad (11)$$

We see immediately, from our earlier assumptions, that

$$\int_0^{\nu_0} \eta(Q)dQ = 3N \quad (12)$$

where  $\nu_0$  is the so-called Debye frequency, which cuts off the number of modes added up by this integral at a

frequency  $\nu_0$  so the sum equates to the  $3N$  allowable modes in the crystal.

Since Planck showed that the average energy  $\bar{u}_i$  of a harmonic oscillator at temperature  $T$  is:

$$\bar{u}_i = \frac{h\nu}{e^{h\nu/(kT)} - 1} \quad (13)$$

where  $h$  is the Planck constant, then the total internal energy of the crystal is determined conceptually by multiplying each "shell" of modes described by Eq. 11 by the Planck relation applying to that shell, and adding them all up. Thus, internal energy of the crystal is expressed mathematically as,

$$U = \int_0^{\nu_0} \eta(\nu) \frac{h\nu}{e^{h\nu/(kT)} - 1} d\nu. \quad (14)$$

If we define the Debye temperature,  $\theta_0$ , as  $\frac{h\nu_0}{k}$ , then we find from Eq. 14 that at low temperatures the internal energy per mole is:

$$U = \frac{3}{5} \pi^4 N k T \left( \frac{T}{\theta_0} \right)^3 \quad \text{for } T \ll \theta_0 \quad (15)$$

and from Eq. (5)

$$C_v = \frac{12}{5} \pi^4 N k \left( \frac{T}{\theta_0} \right)^3. \quad (16)$$

Eq. 16 is the desired relationship for bulk lattice specific heat at low temperature, and shows the  $T$ -cubed dependence noted earlier.

In the Debye approach just outlined, we have implicitly assumed that the crystal could be represented as a continuum, and that all waves propagate as though they were embedded in a perfectly elastic medium. Although this can be shown to be a good approximation for low frequencies where the wavelength of such a disturbance is long compared

with the interatomic spacing of the crystal, for shorter wavelengths comparable to the lattice constant of the material such a model breaks down.

Consequently, the approach employed in arriving at Eq. 14 is generally valid, but the representation of  $\eta(\nu)$  as a continuous, simply derived function is misleading. If the lattice, instead of being treated as an elastic continuum is considered to be made up of an infinite array of mass points which interact with one another via harmonic restoring force, and it is further recognized that although nearest neighbor interactions predominate some coupling to further-removed lattice sites may exist, then a relationship for  $\eta(\nu)$  cannot in general be derived in closed form.

Even where appropriate simplifying assumptions are applied to the general discrete-lattice problem it is found that the velocity of propagation varies with the wavelength of the disturbance (in contrast to the constant value for  $C_T$  and  $C_L$  used in the Debye theory). Further it is found that the allowable range of frequencies which can propagate through the crystal is separated into a low frequency band (coinciding with the so-called acoustical waves of the Debye theory) and a high frequency band (associated with wavelengths comparable to the infrared energy spectrum). These are referred to respectively as the "acoustical" and "optical" branches of frequencies. Since an energy gap (or, more accurately, a band of "forbidden" frequencies) exists between the acoustical and the optical branches, it is apparent that a plot of  $\eta(\nu)$  against  $\nu$  for real substances will show a discontinuity in the gap region. Figure 1 contrasts the simple continuum assumption of Debye with the approximate model for a simple ionic crystal like sodium chloride<sup>2</sup>.

Although rigorous solutions to the form of  $\eta(\nu)$  cannot be obtained, in general, the lattice dynamics

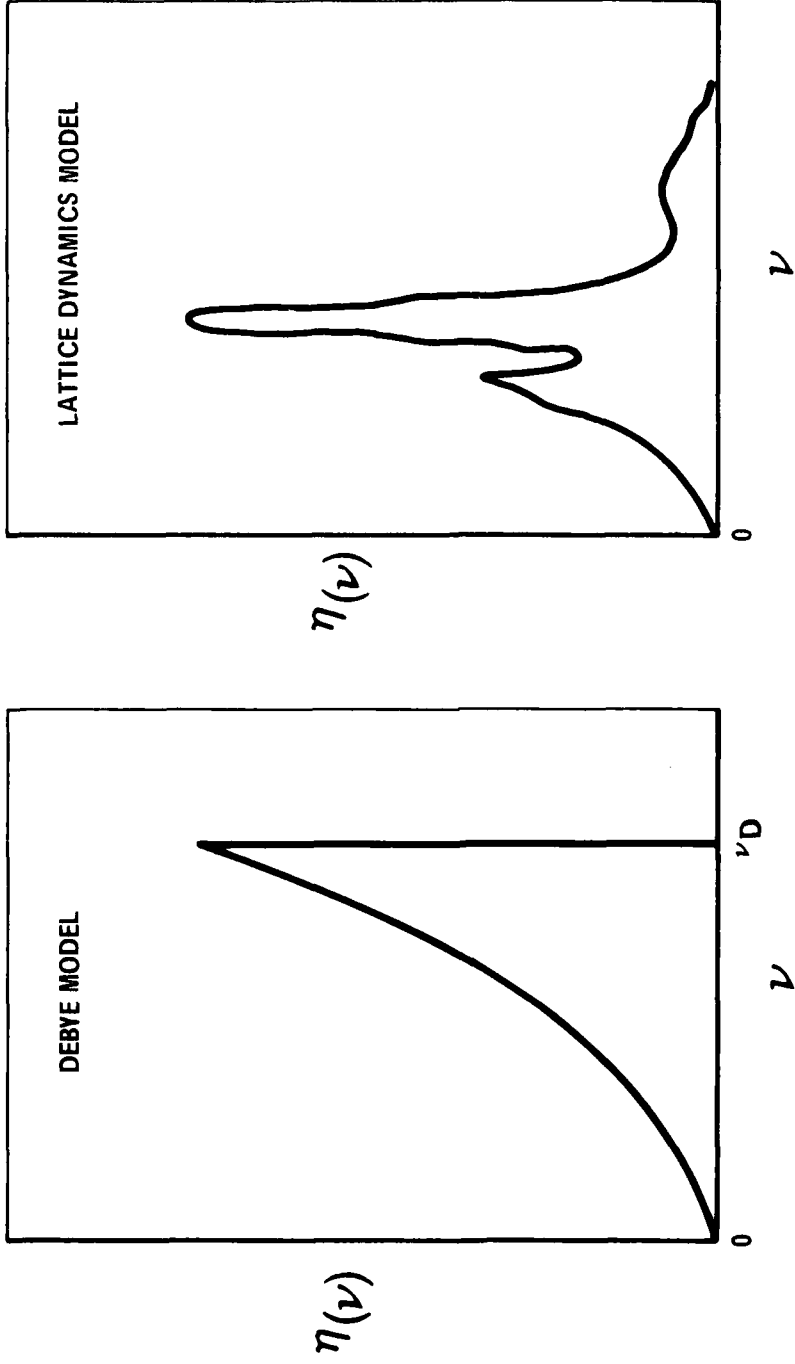


Figure 1.  $\eta(\nu)$  Models Contrasted

community has made considerable progress in the analytical approach to modeling its behavior for some of the simpler crystal structures.

### 2.3 Surface Contributions to Specific Heat

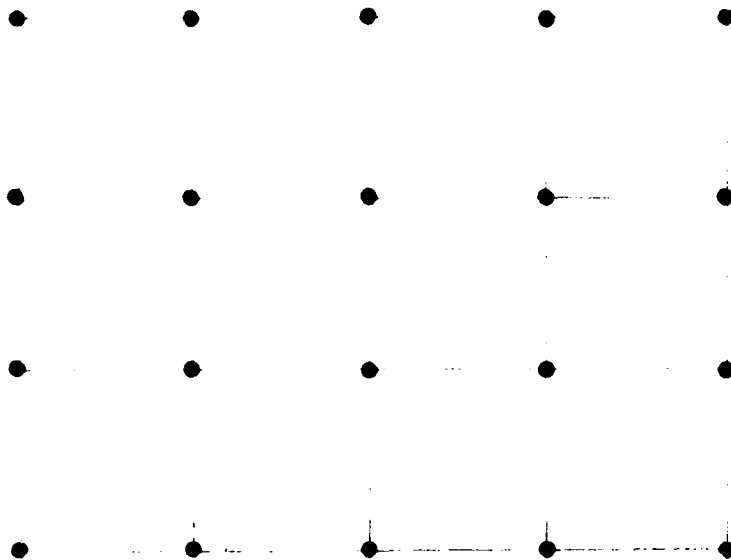
The Debye formulation, although an oversimplification of the physics of the situation, represents an outstanding success in applying the then-new concepts of quantum mechanics to a problem which couldn't be solved with classical techniques. That model, as just outlined, was derived from considerations of the three-dimensional characteristics of an elastic continuum as an approximation to a crystal lattice.

Since real substances exhibit a two-dimensional surface and not solely an infinite three-dimensional lattice, we may well inquire as to whether or not there can be a comparable energy contribution to the overall internal energy stemming from the crystal surface in addition to the contribution from the bulk lattice. Anticipating the discussion to follow, we will find that in exact analogy to Debye's derivation a surface contribution to internal energy (and thus via Eq. 5 to total specific heat) can be predicted. As we would intuitively expect from an analogy to Eq. 10, the contribution turns out to be proportional to the surface area of the sample and is only significant under conditions of very large surface-to-volume ratios and at low temperature.

It will be remembered that Eq. 10 was obtained by estimating the number of volume units in the first quadrant of a sphere in  $\nu$ -space. The estimation method used is accurate enough for large volumes, but, as noted, is not exactly equal to the actual count of non-negative integer points in the quadrant when the surface-to-volume ratio of the substance is large. Consequently, the actual number of allowable modes is greater than that indicated

by this equation. This can be conveniently illustrated with a two-dimensional example:

## AREA APPROXIMATION TO INTEGER POINTS



Number of integer points = 20  
Area of figure = 12 units  
Half perimeter of figure = 7 units.

### FIGURE 2

If the area of Figure 2 is used to approximate the number of non-negative integer coordinate points of the figure, the result is in error. Approximately one-half the points on the perimeter must be added to this two-dimensional area value as a correction.

In the three-dimensional case, the volume estimation is similarly in error, and half the surface area must be

added as a correction. E. W. Montroll<sup>3</sup> was one of the first workers to recognize this discrepancy in Debye's specific heat model. Drawing on earlier work from the field of acoustics<sup>4</sup>, he derived a frequency distribution function which accounted for lattice contributions plus the correction for allowable vibrational modes associated with the large surface area of powders and related geometries. Montroll's resulting form of Eq. 10 is,

$$\eta(\nu) = 4\pi V \frac{\nu^2}{c_3} + \frac{1}{2} \pi S \frac{\nu}{c_2} + \text{negligible edge correction terms,} \quad (16)$$

where  $S$  is the total surface area of the substance. Using the same Debye approach illustrated in Eq. 14 we find

$$\frac{c_v}{Nk} = \frac{12\pi^4}{5} \left(\frac{T}{\Theta_0}\right)^3 + \frac{9}{4} \zeta(3) (12\pi)^{4/3} \frac{1}{\left(\frac{c_3^{2/3}}{c_2}\right) \left(\frac{S}{V^{2/3}}\right) \left(\frac{T}{\Theta_0}\right)^2} N^{-1/3}, \quad (17)$$

$$\text{where } c_{\lambda} = \bar{c}_L^{-\lambda} + 2\bar{c}_T^{-\lambda}, \quad (18)$$

$\zeta(3)$  is the Riemann zeta function evaluated for a value of 3.

For a mole of the substance this can be expressed as:

$$c_v = \beta T^3 + \alpha T^2 \quad (19)$$

where the  $T^3$  coefficient has the bulk Debye value of:

$$\beta = \frac{464.5}{\Theta_0^3} \text{ CAL/MOLE/K.} \quad (20)$$

Ratioing the  $T^3$  term to the  $T^2$  term we find:

$$\frac{\beta T^3}{\alpha T^2} = \frac{\frac{12\pi^4}{5} \left(\frac{T}{\Theta_0}\right)^3 N^{1/3}}{\frac{9}{4} \zeta(3) (12\pi)^{4/3} \left(\frac{c_3^{2/3}}{c_2}\right) \left(\frac{S}{V^{2/3}}\right) \left(\frac{T}{\Theta_0}\right)^2}, \quad (21)$$

$$\text{or } \frac{\beta T}{\alpha} = K_1 \left( \frac{T}{\theta_0} \right) \left( \frac{V}{S} \right) \left( \frac{M}{V} \right)^{1/3} \left( \frac{C_2}{C_3^{2/3}} \right) \quad (21a)$$

where  $K_1 \approx 26$ .

Thus, the first Montroll coefficient is found to be:

$$\alpha = .039 \beta \theta_0 \left( \frac{S}{V} \right) \left( \frac{M}{\rho N_0} \right)^{1/3} \left( \frac{C_3^{2/3}}{C_2} \right) \quad (22)$$

where  $M$  is the atomic weight

and  $\rho$  is the bulk density of the material.

If we accept Montroll's statement that it can be shown that  $3^{-1/3} \leq \frac{C_3^{2/3}}{C_2} \leq 1$ , then

$$\alpha \approx .033 \beta \theta_0 \left( \frac{S}{V} \right) \left( \frac{M}{\rho N_0} \right)^{1/3} \quad (22a)$$

If specific surface area ( $S'$ ) is defined as:

$$S' = \frac{S}{m} = \frac{S}{\rho V} = \frac{1}{\rho} \left( \frac{S}{V} \right) \quad (23)$$

where  $m$  is the mass of the sample,

then an alternate equation for this Montroll coefficient is:

$$\alpha \approx .033 \beta \theta_0 S' \rho^{2/3} \left( \frac{M}{N_0} \right)^{1/3} \quad (24)$$

For discussion purposes this can be rearranged as:

$$\alpha \propto \frac{S' \rho^{2/3} M^{1/3}}{\theta_0^2} \quad (25)$$

It is not surprising to find that Eq. 25 indicates that potentially the largest coefficient value for the surface contribution to specific heat will be found for

heavy, dense materials having the lowest possible Debye temperature. The Debye temperature is obviously the most important selection parameter, according to Eq. 25 , and we see that bulk density is relatively more important than atomic number in choosing a material expected to show large surface specific heat effects in the finely subdivided state.

It is appropriate to briefly summarize the preceding mathematical derivations. If we consider a continuous three-dimensional lattice structure, a standard Debye-type derivation from quantum mechanics principles shows that the specific heat of solids varies with the cube of temperature in the cryogenic region. If, however, we consider a special configuration of the solid wherein a large surface-to-volume ratio exists -- e.g., for finely subdivided powders or thin films -- the Montroll approach predicts an additional contribution to specific heat which varies as the square of temperature; consequently, this surface contribution to specific heat does not decrease at low temperatures as rapidly as the Debye lattice term. The magnitude of this surface contribution can be predicted from physical characteristics of the substance, as indicated by Eq. 25 .

Montroll's approach is subject to the same theoretical criticism as was levied on the simple Debye model discussed earlier; e.g., an elastic continuum must be assumed instead of a discrete lattice of coupled mass points, and simple periodic boundary conditions are assumed in order to allow solution of the wave equation. In addition, it has been noted that this Montroll approach does not take into account the fact that longitudinal mode waves and transverse mode waves may undergo a mode interchange upon reflection at crystal boundaries, and that under certain conditions additional surface-localized and edge-localized modes are allowable.

The net result is that the Montroll approach also under-counts the number of allowable vibration modes (although not as flagrantly as the Debye model), and should tend to err in the direction of predicting too low a value for specific heat. This has been verified in the few reported measurements on finely divided powders which can be correlated to specific heat predictions of the model<sup>5</sup>.

There have been many other approaches to modeling surface specific heat in the twenty-odd years since the work of Montroll. At present none of the lattice dynamics models developed in the last decade appear to be superior to the simple model of Eq. 25 in predictive ability. It is recognized, however, that lattice dynamics approaches will eventually develop an accurate algorithm for computing surface specific heat contributions. The solution to the problem may, in fact, already be at hand, but unverified due to a lack of reported measurements on fine powders; however, any equations stemming from lattice dynamics work are likely to be complex and tedious to use.

Because of the fact that lattice dynamics approaches do not presently have a clear advantage in predictive ability over the simple Montroll model, we will not dwell on that approach in any depth. It would be remiss, however, to gloss over the subject without illustrating a recent effort to develop a simplified lattice dynamics equation for the surface specific heat. Naugle and Allen<sup>6</sup> have applied their approximate algorithm,

$$C_v = \frac{8k}{\pi^2 A} \sum_{i, \text{acoustic}} \left[ I\left(\frac{\hbar \omega_{ai}}{2\pi kT}\right) - I\left(\frac{\hbar \omega_{ai}^b}{2\pi kT}\right) \right] + \frac{k}{A} \sum_{i, \text{optical}} \left[ f\left(\frac{\hbar \omega_{ai}}{2\pi kT}\right) - f\left(\frac{\hbar \omega_{ai}^b}{2\pi kT}\right) \right]. \quad (26)$$

where  $f(z) = \frac{(z/2)^2}{\sinh^2(z/2)}$

$$I(z) = \int_0^1 \frac{\sin^{-1} g}{(1-g^2)^{1/2}} f(zg) dg$$

$$g = \frac{\omega}{\omega_{A_i}}$$

and  $\omega_j = 2\pi\nu_j$ ,

to noble gas solids and alkali halides with the result they have closely matched values computed from rigorous lattice dynamics equations. The  $\omega_{A_i}$ ,  $\omega_{A_i}^b$ ,  $\omega_{O_i}$ , and  $\omega_{O_i}^b$  in this equation correspond, respectively, to surface vibration frequencies of the acoustical and the optical branches after the formation of a surface, and before the surface is created (superscript b) -- i.e., in the bulk.

From a theoretical standpoint this mathematical approach is very satisfying. From an experimental standpoint, however, this equation and its more rigorous kindred are no better at predicting surface specific heat than the simple model outlined earlier.

The equation resulting from the Montroll approach is convenient to use, but as might be expected, it has some shortcomings. First, it is not really the most accurate predictor available. Based on the few published data sets to date, the most accurate algorithm is one derived by two different workers independently, circa 1960<sup>7</sup>. In this more accurate Depuis-Mazo-Onsager (DMO) model, the same Debye approach -- involving assumptions of an isotropic elastic continuum -- was employed. The primary difference from the Montroll work was that the DMO model attempts to impose more realistic boundary conditions on the wave

equation, and it recognizes that introduction of a surface into the continuum "scrambles" wave reflections in such a way that resulting vibrations can't be analyzed in terms of pure transverse and longitudinal modes. The form of this equation for surface specific heat  $C_V^s$  is,

$$C_V^s = 3\pi \frac{h^3}{4\pi^2} \int_0^{\infty} \int_0^{\infty} \frac{2C_T^4 - 3C_T^3 C_L^2 + 3C_L^4}{C_T^2 C_L^2 (C_L^2 - C_T^2)} S T^2 \quad (27)$$

where the symbols are as earlier defined.

In order to employ the DMO algorithm, it is necessary to know the low temperature elastic constants of the material of interest. Although  $C_T$  (average) can apparently be estimated from the experimental Debye temperature,  $\Theta_D$ , in the temperature range of interest  $C_L$  is not generally available. In addition, the low temperature  $\Theta_D$  varies widely as  $T \rightarrow 0$ , so even the determination of  $C_T$  from this relationship is less than satisfactory.

The most recent analytical treatment of surface enhanced specific heat seems to be that of Baltés and Hilf<sup>8</sup>. They developed the algorithm,

$$C_V^s = V_m \sum_l \sum_{\lambda} \frac{3(2l+1) k \xi^2 \xi^{\lambda}}{4\pi r^3 (\xi^{\lambda} - 1)^2} \quad (28)$$

where  $\xi = \frac{h C_T a'}{k r T}$ ,  $r$  denotes the particle radius,  $V_m$  is the mole volume of the sample, and  $a'$ ,  $\lambda$  and  $l$  are associated with spherical Bessel functions.

Although recent measurements show that this algorithm is potentially very accurate, like the DMO model it is very difficult to use because the effective sound velocity,

$C_T$ , varies strongly at low temperature and can best be determined by measuring the variation of the Debye temperature itself in the range of interest. Consequently,

the equation is probably not very useful for our purposes as a predictor, since knowledge of the Debye temperature variation is not usually available for a given material. Consequently, we again are led back to the simpler Montroll model.

In a recent survey<sup>9</sup> of the ability of the various models to accurately estimate the surface specific heat value for dielectric powders, it was noted that results from the Montroll approach underestimate the surface contribution to specific heat (i.e. give a value too low) by a factor of 4 - 6. The more complicated DMO model can improve upon the Montroll accuracy by only about 45 percent, and at this point in time there are no other models (including the most sophisticated lattice dynamics algorithms) which can do any better without requiring extensive knowledge of low temperature crystal parameters.

#### 2.4 Electron System Contribution To Surface Specific Heat

The preceding derivations used as a starting point the bulk lattice and "bulk surface" contributions to specific heat. It must be recognized that other mechanisms can also contribute to specific heat of a substance; e.g. order-disorder transitions in the crystal lattice, order-disorder transitions in the magnetic spin system of the substance, and energy level changes in the conduction band electron system, to name the most important. The latter effect is only significant in metals, due to the broad range of energy states available in the conduction band.

Since electrons, being particles of half-integral spin values, are represented by antisymmetrical wave functions, we must apply Fermi-Dirac statistics in order to compute average values for the conduction band energy (and consequently the electron contribution to specific heat). Rather than repeat the derivation for specific heat of an

electron "gas" as found in the literature, the main difference from the bulk lattice case can be illustrated as follows.

It can be shown from quantum mechanical principles<sup>10</sup> that in analogy to Eq. 10 the number of allowable energy states  $\eta(E)$  for electrons in the range between  $E$  and  $E+dE$  is

$$\eta(E)dE = \frac{4\pi V (2m_e)^{3/2}}{h^3} E^{1/2} dE \quad (29)$$

where  $m_e$  is the electron mass and it is recognized that each electron of opposite spin represents a distinct energy state.

The Fermi-Dirac distribution law states that the probability of finding an electron in any one of these energy states,  $E$ , is

$$f(E) = \frac{1}{e^{(E-E_F)/kT} + 1} \quad (30)$$

where  $E_F$  is the Fermi energy level of the crystal.

Consequently, the average energy per mole of the system can be shown to be:

$$\bar{E} = \int_0^{\infty} E f(E) \eta(E) dE \quad (31)$$

or

$$\bar{E} = \frac{1}{h^3} \int_0^{\infty} \frac{4\pi (2m_e)^{3/2} E^{3/2} V}{e^{(E-E_F)/kT} + 1} dE \quad (31a)$$

The solution to this integral is

$$\bar{E} = E_0 + \frac{1}{6} \pi^2 (kT)^2 \eta(E_F) \quad (31b)$$

which yields the specific heat equation of interest:

$$C_v^e = \frac{4\pi^3 m_e k^2}{3 h^2} \left( \frac{3N'V^2}{\pi} \right)^{1/3} T, \quad (32)$$

commonly written  $C_v^e = \beta T.$  (33)

Thus we conclude that the specific heat of the electron system at low temperature is proportional to the first power of the absolute temperature. It is known that because of the assumptions inherent in the model the numerical value of measured results sometimes deviates markedly from the computed value. However, the expected linear proportionality to  $T$  does indeed occur.

Now, if we apply the same rationale used earlier, the density of state function of Eq. 29 has again undercounted the number of allowable electron quantum states associated with a finely divided powder or similar substance showing a large surface-to-volume ratio. Montroll showed that for this case Eq. 29 must be rewritten as

$$\eta(E)dE = \left[ \frac{4\pi V}{h^3} (2m_e)^{3/2} E^{1/2} + \frac{\pi m_e S}{h^2} + \dots \right] dE. \quad (34)$$

Upon performing similar steps as just indicated to compute first the internal energy and then the specific heat, Montroll showed:

$$C_v^e = \frac{4N'k^2 T \pi^2 m_e}{h^2} \left[ 1 + \frac{1}{24} \frac{S}{V^{2/3}} \left( \frac{9\pi}{N'} \right)^{1/3} \right] \left( \frac{\pi V}{3N'} \right)^{2/3}. \quad (35)$$

It will be noted that upon rearrangement the first term is identical to the expression of Eq. 32. In analogy with that formula, we express the enhanced specific heat as:

$$C_v^e = \beta (1 + \epsilon) T \quad (36)$$

$$\text{where } \epsilon = \left( \frac{q\pi}{N_0} \right)^{1/3} \frac{S}{24V} \left( \frac{M}{\rho m^*} \right)^{1/3} \quad (37)$$

$$\text{or } \epsilon = \left( \frac{q\pi}{N_0} \right)^{1/3} \frac{S'}{24} \left( \frac{M}{m^*} \right)^{1/3} \rho^{2/3} \quad (37a)$$

and where  $m^*$  is the average number of conduction electrons per lattice site.

Numerical calculations show that this  $\epsilon$  term is small for most metals; consequently the enhanced electron contribution is a less important small particle effect than the surface vibrations described by the  $\alpha T^2$  term predicted by Montroll.

## 2.5 Survey of Reported Measurements

The interest in surface contributions to specific heat at low temperature was perhaps stimulated by early measurements on  $MgO$  microcrystals by Giaouque and Archibald<sup>11</sup>, reported in 1937. In the early 1950's a flurry of theoretical work in surface thermodynamics, highlighted (at least for our purposes) by the models of Montroll, spurred some additional experimental measurement work on finely divided powders.

Patterson, Morrison, and Thompson<sup>12</sup> reported in 1955 that they were unable to detect the  $\alpha T^2$  term in low temperature measurements on  $TiO_2$ , but did detect this  $T$ -squared effect on measurements of finely divided  $NaCl$ . It is generally conceded now that the effect in  $TiO_2$  was undoubtedly present, but masked by experimental errors.

In the case of  $NaCl$ , these researchers found perhaps the first indication that the magnitude of the  $T$ -squared term measured experimentally in dielectric powders is significantly larger than the value predicted by Montroll's relationship of Eq. 24. Their actual reported measurement values are suspect, however, because of several experimental difficulties they were not able to satisfactorily

resolve. Some significant errors were made, for example, in the measurement of powder surface area. The difficulty in determining the area of powder samples will be discussed in a later section of this report, but it is appropriate to introduce the methodology at this point since it bears on the problems encountered by these authors.

In 1938, Branauer, Emmett and Teller<sup>13</sup> developed a comprehensive gas adsorption theory which provided a means of determining the surface area of finely divided solids from isothermal gas adsorption measurements. The technique involves a determination of the mass quantity necessary to coat the solid with a monolayer of the gas. Even with the advent of X-ray diffraction methods and scanning electron microscope technology, this BET adsorption isotherm method still today remains the standard for determining the surface area of fine particles. In the measurements of Patterson, et al, however, an anomalous behavior of the adsorbent-adsorbate system resulted in a non-linear BET plot even in the range of gas adsorbate pressures previously believed suitable for measurements of this type, and gave rise to the error. The difficulty was subsequently resolved by MacIver and Emmett (of the original BET team)<sup>14</sup> and apparently has not hampered later workers.

Following Patterson's work, Lien and Phillips<sup>15</sup> reported the first data on small particle heat capacity which can be considered generally reliable. Their data on  $MgO$  in the  $1.5^{\circ}K$  to  $4^{\circ}K$  range clearly showed the  $\alpha T^2$  effect predicted by Montroll. The  $MgO$  sample was in the form of ultra fine particles, with a cube edge of  $100 \text{ \AA}$ . The  $\alpha$  coefficient determined by them was larger than the Montroll prediction by nearly an order of magnitude.

In 1966 Barkman, Anderson, and Brackett<sup>16</sup> performed a carefully designed set of experiments to show conclusively both that the  $T$ -squared term actually exists in the finely divided samples and that its magnitude is proportional to

surface area. Their classic work with  $\text{NaCl}$ , over a broad range of sample surface areas and for a temperature range from  $4.5^\circ\text{K}$  to  $18.1^\circ\text{K}$ , demonstrated the existence of the surface enhanced specific heat and further showed that the DMO equation is its most accurate predictor, with the Montroll equation giving values of the surface contribution too low by a factor of 4 - 6.

In the past few years there has been a flurry of interest in measurements of the surface specific heat of metal particles. In a very excellent experimental program in Germany, Comsa, Heitkamp and Råde<sup>17</sup> measured the specific heat of palladium ultrafines of 30 and 66 Å diameters. Their work has dramatic implications on several aspects of this regenerator improvement study, and will be cited in several following sections.

Their work on metal powders, similar to the Barkman work on dielectrics, shows conclusively that a strong surface enhancement in specific heat is associated with particle size. Comparable to the earlier indications, the Montroll equation is again found to predict values too low by a factor in the 4 - 6 range. Their results did not detect that the electron specific heat for the ultrafines was enhanced over the value associated with bulk palladium. This is not inconsistent with the analytical result noted earlier: that such an enhancement, if it exists, would be numerically small in comparison with the  $\alpha T^2$  terms attributed to surface mode vibration.

Several years before the palladium measurements were reported, Novotny and Meincke<sup>18</sup> also verified the surface enhancement term in 37 Å and 60 Å particles of lead, and 22 Å particles of both lead and indium. Especially in the case of lead, the surface enhancement contribution was considerably smaller than we would expect from a Montroll-type analysis. Consequently, it was of priority interest to determine whether the measurements indicate a valid deviation from the algorithm of Eq. 22, thereby

raising doubts as to the generality of the Montroll concept, or whether peculiarities of the experimental technique used will allow us to accept these results without invalidating the Montroll theory. These questions are addressed in Section 2.7.

As can be inferred from the brief length of the foregoing summary, there have been very few reported measurement programs on the specific heat of small particles. This is not due to a lack of scientific interest in surface thermodynamics of powders at low temperatures, since the literature contains many recent theoretical treatments of the problem. We can conclude that the lack of data is due at least in part to the difficulty in performing the required measurements. These difficulties can be grouped into several categories, each of which will be treated in more detail later in this report:

- 1) The production of sub-micron powders is difficult at best, and is not currently done on a commercial basis; consequently, a researcher traditionally had to produce his own powders for use in a measurement program of this nature.
- 2) All powders in this size range, and particularly metals, are typically very reactive, both in the sense that they tend to agglomerate into larger particles (thus losing the desired surface characteristics) and that they can be pyrophoric, tending toward spontaneous combustion and even explosion.
- 3) The inherent difficulty of the measurements to be made including in particular surface area determination, sample temperature determination, and determination of effective heat input during the calorimetry process can jeopardize even a well designed specific heat experiment program.

## 2.6 The Question of Cluster Structures

There are many different physical processes which tend to produce a numerical deviation from the Debye  $T^3$  specific heat law at low temperatures. Most of these, such as the low temperature order-disorder transitions and the various low temperature magnetic alignment effects occur only in a relatively small class of materials and only over a very narrow temperature range, on the order of a few  $^{\circ}\text{K}^{19}$ . In contrast, the surface enhanced excess specific heat which is the primary topic of this study is generally applicable to all substances which can be subdivided fine enough that the  $\alpha$  coefficient of Eq. 22 is measurable. Additionally, the surface effect is a "broad band" enhancement, varying as  $T^2$ , and is not limited to a narrow temperature range.

Although we can assume that a broad band effect is ultimately more useful for application as a heat exchanger (regenerator) matrix material in a cryogenic refrigerator, it is reasonable to suggest that selected narrow band materials might be useful in the cold end segment of the "segmented regenerator model" introduced later in this report. Consequently, some effort was invested during this study to screen other specific heat anomalies for their potential application to the cold segment. In the process of that survey, an interesting coincidence was discovered which may allow us to take advantage of the Montroll-type enhancement without the difficulty of having to work with finely powdered materials.

In 1961 Schroder<sup>20</sup> published an analytical model to describe a deviation from the expected linear and cubic specific heat terms for certain metal alloys containing

small ferro magnetic clusters which caused the entire lattice to exhibit evidence of superparamagnetism. Under the assumption that these clusters oscillate around a particular preferred orientation, the author showed that for large clusters a specific heat term  $C_{CL}$  of the Einstein form,

$$C_{CL} = A \left( \frac{k}{2} \right) C_E \left( \frac{T}{T_E} \right) \quad (38)$$

should be found experimentally. In this equation,

$A$  equals the number of degrees of freedom for the cluster,

$C_E$  is the Einstein specific heat function and

$T_E$  is the Einstein temperature (defined in a manner analogous to the Debye temperature).

He further argued that for these ferromagnetic clusters the effective Einstein temperature would be well below  $1^\circ\text{K}$ , so that the Einstein function would reach a constant value at temperatures above 2 or  $3^\circ\text{K}$ . By this analysis Schroder explained an anomaly first discovered in a series of Ni-Cu alloys wherein experimental specific heat measurements at low temperatures were apparently fit by an equation of the type,

$$C_v = \beta T^3 + \delta T + B \quad (39)$$

It seemed an interesting coincidence that some ten years earlier Jura and Pitzer<sup>21</sup> had predicted on solely theoretical grounds that finely divided powder particles would vibrate as if each was a separate molecule, thus giving rise to an extra specific heat term in addition to the Montroll correction. This contribution was expected to approach a constant value at low temperatures, similar to Schroder's superparamagnetic contribution.

In several ensuing experimental programs with fine powders, notably the work of Lien and Phillips discussed earlier, this Jura and Pitzer constant value term was never detected. We can only speculate that the inter-particle restoring forces postulated by them were too small in the loose powders to give rise to the required oscillations. However, in the case of a metal matrix containing fine cluster structures, such as those considered by Schroder, such restoring forces can be readily imagined.

Primarily because of the similarity in the final equation coming from Schroder's classic analysis and the early theoretical treatment of fine powders by Jura and Pitzer, the following hypothesis was suggested:

Hypothesis: The low temperature specific heat of certain metal alloys containing small ferromagnetic cluster structures can be treated similar to a matrix of finely divided powder and thus represented by a Montroll-type equation with the addition of a constant term representing the contribution of cluster oscillations.

Consequently, it is hypothesized that a Montroll equation of the type,

$$C_v = \beta T^3 + \alpha T^2 + (1 + \epsilon) \gamma T + B \quad (40)$$

can represent these metal cluster structures.

A recent series of low temperature measurements on several metal alloy materials which evidence such a structure was recently reported by Collings and Jelinek, et al<sup>22</sup>. Following Schroder's approach, they fitted the data to an algorithm similar to Eq. 39. The value they found for the  $\beta T^3$  term is several orders of magnitude smaller than the remaining two terms. Consequently, we can question the statistical validity of its determination

since the  $\beta T$  and  $B$  terms are the predominant contributors to specific heat at the lower temperatures.

Recognizing that the term  $\beta T^3$  is comparatively small in this temperature region, we attempted to fit the Collings and Jelinek data set to a Montroll-type equation with an additive Jura and Pitzer constant term, with the results (for 310S stainless steel):

$$C_v = \cancel{\beta T^3} + 0.029T^2 + 0.2936T + 0.7848 \quad (41)$$

compared with the authors' statistical fit for the same material,

$$C_v = 0.000268T^3 + \cancel{\alpha T^2} + 0.46T + 0.334 \quad (42)$$

Our statistical fit of Eq. 41 resulted in a high correlation coefficient. Realistically, however, the determination of the  $T^2$  term is open to the same criticism as the Collings and Jelinek determination of the  $T^3$  coefficient since it is an order of magnitude smaller than the other terms.

Since no other "raw" data has been located in the literature, it is not possible to further test this hypothesis and resolve the question as to whether the surface enhancement effect of interest in this study is automatically associated with metal alloy cluster structure materials. The production and handling of materials which evidence the Montroll-type enhanced specific heat may obviously be considerably simplified if cluster-forming alloys which meet the requirements for large surface specific heat defined by Eq. 22 are available.

In order to predict whether or not such characteristics may exist, it is necessary to determine the effective Debye temperature for alloys which form this type of cluster

structure. Debye temperature tabulations for a few of such alloys have been located. However, since a broad range of transition element metals can form alloys of the superparamagnetic cluster structure type, an analytical method must be utilized to predict the Debye value for the most likely candidates. The development of this methodology was not pursued during this phase of the study program.

## 2.7 The Composite Specific Heat Model

Since all Debye-type specific heat models, including Montroll's, undercount the allowable vibration modes of substances exhibiting a large surface-to-volume ratio, the computed value for specific heat is expected to be smaller than actual measurement results. Reinforcing this conclusion, the error in the  $T^2$  (surface contribution) term of the Montroll equation has been found to range in both dielectric and metal powders from a factor of four to nearly an order of magnitude too small, based on the few measurement programs reported to date.

The most reliable prediction of composite specific heat, then, can probably be obtained by an empirical modification to Eq. 40. The suggested form is:

$$C_v = \beta T^3 + 4\alpha T^2 + (1+4\epsilon)\delta T + B \quad (43)$$

The coefficients in this equation can be computed as follows:

$$\beta = \frac{464.5}{\Theta_D^3} \quad \text{CAL/MOLE/K}^4 \quad (20, \text{ref})$$

$$\alpha = .033 \beta \Theta_D s' \rho^{2/3} \left(\frac{M}{N_0}\right)^{1/3} \quad \text{CAL/MOLE/K}^3 \quad (24, \text{ref})$$

$$\gamma = 3.26 \cdot 10^{-5} \left( \frac{M}{\rho} \right)^{2/3} n^{\# 1/3} \text{ CAL/MOLE/K}^2 \quad (44)$$

$$\epsilon = \left( \frac{9\pi}{N_0} \right)^{1/3} \frac{S'}{24} \left( \frac{M}{n^{\#}} \right)^{1/3} \rho^{2/3} \quad (37a, \text{ ref})$$

$$B = O(\gamma) \quad \text{CAL/MOLE/K}^2 \quad (45)$$

The notation in Eq. 45 indicates that the coefficient  $B$  (associated with superparamagnetic metal alloys only) has a numerical value on the order of the linear coefficient, gamma. This approximation is based on limited test data stemming from the Collings and Jelinek work, and may not prove to be generally valid. There apparently has been no successful theoretical development of an equation to predict  $B$  as yet, since no work along these lines was discovered in the literature. It was noted earlier that cluster structure materials of this kind were not considered in depth in this phase of the study; consequently, there was no attempt as part of this program to model an equation for this term.

2.7.1 Comparison with Reported Measurements - In order to get some indication of the likely accuracy of Eq. 43, its specific heat predictions for dielectric materials were compared to the Lien and Phillips data on  $MgO$  and the Barkman, et al data on  $NaCl$ . Results are shown in Figures 3 and 4 respectively. Similarly, the computed predictions are compared to the palladium data of

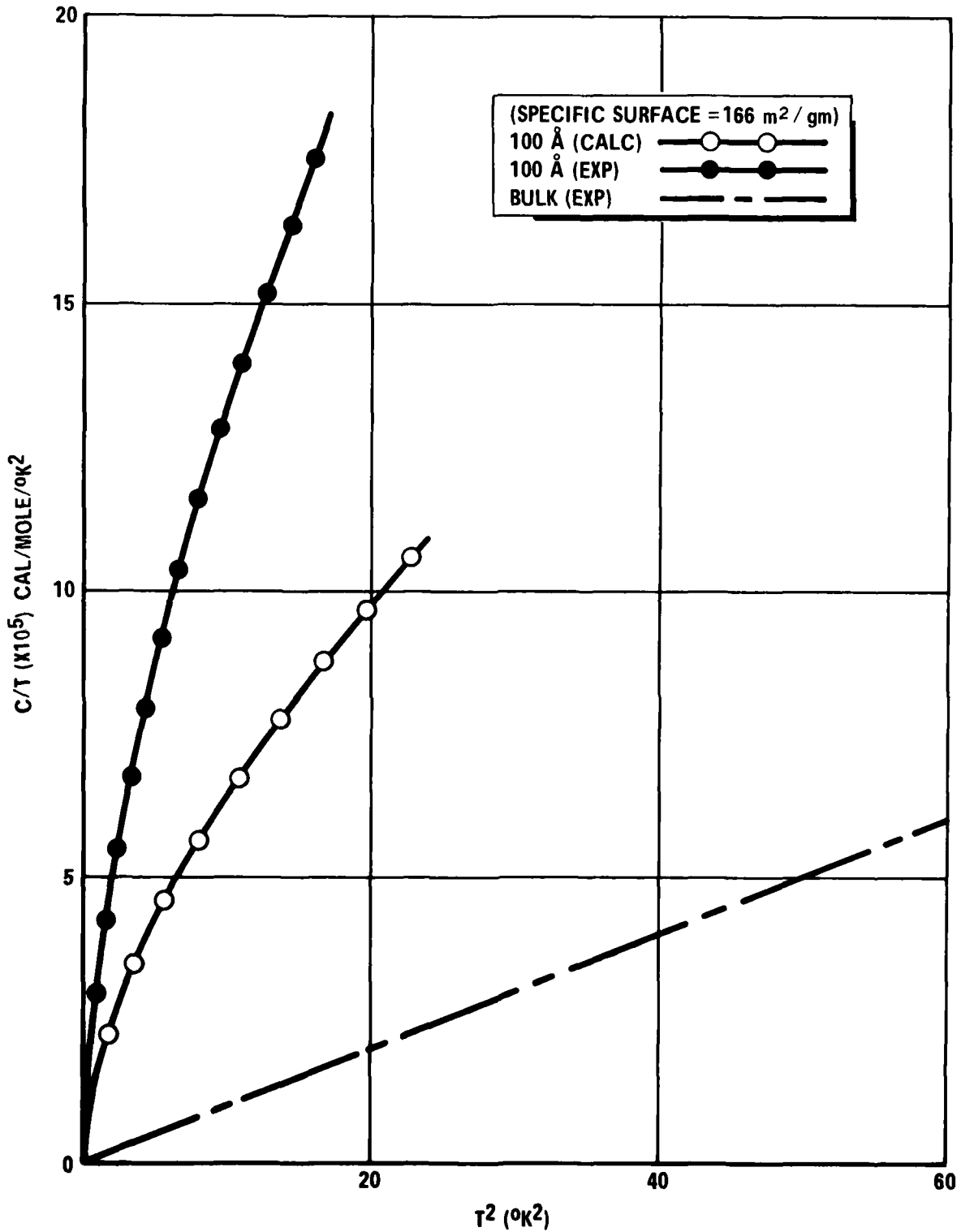


Figure 3. Magnesium Oxide Small Particle C<sub>v</sub>

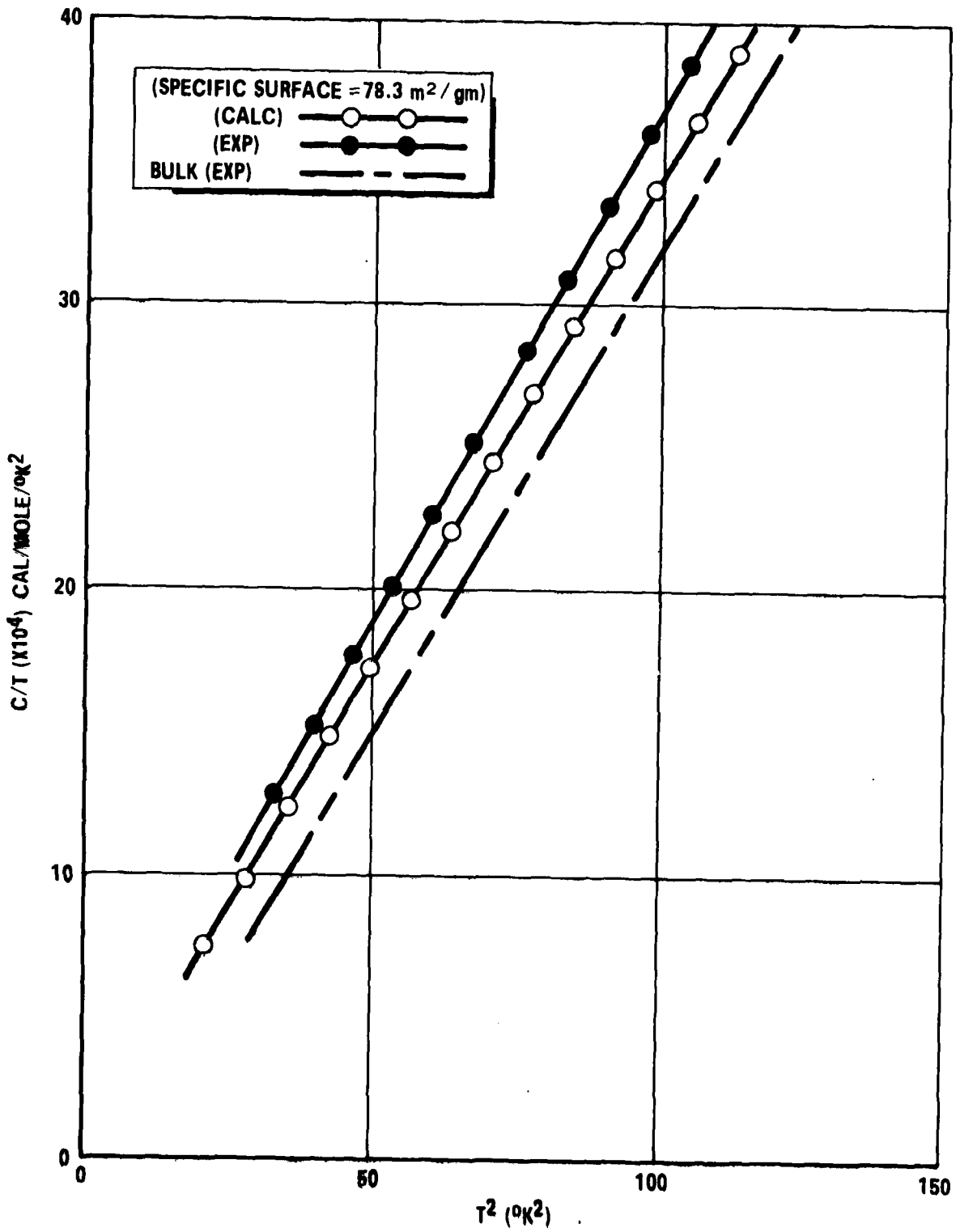


Figure 4. Sodium Chloride Small Particle Cv

Comsa, et al, in Figure 5 and the Novotny and Meincke data for lead and indium in Figures 6 and 7.

The Montroll theory and the empirical equation developed earlier in this section for surface enhanced specific heat can be correlated reasonably well with these few reported measurement sets except for the 1976 data of Novotny and Meincke on lead and indium particles. The correlation in this case is poor if we assume that the Eq. 43 specific surface value (which wasn't measured by Novotny) is the same as it would be for spherical particles. A failure of the theory for these materials would be particularly serious, since they both are low Debye temperature metals, and prime candidates for the regenerator improvement test program.

The Novotny measurement results were derived under unusual test conditions, which may have invalidated the conditions necessary for Eq. 43 to hold. To assess the probable influence of these test conditions on the reported measurements, it is necessary first to examine the more recent data set of Comsa, et al, performed on palladium ultrafines. This palladium data fits the predictions derived from the Montroll theory exceedingly well.

Comsa and his co-workers prepared the ultrafines by the inert gas evaporation technique, allowing the palladium vapor to condense in a helium environment to minimize particle size. Granqvist and Buhrman<sup>23</sup> recently showed that sub-200 Å ultrafines produced in this manner are spherical (as opposed to taking the characteristic crystalline shape), and have a narrow spread in their size distribution, characterized by a log normal distribution function (LNDF).

Since Eq. 43 strictly applies to a monodisperse, or single size, distribution of particles, it is apparent that any measurable quantity of ultrafines larger than the nominal size will invalidate the analytical prediction of specific heat. The larger particles will contribute less

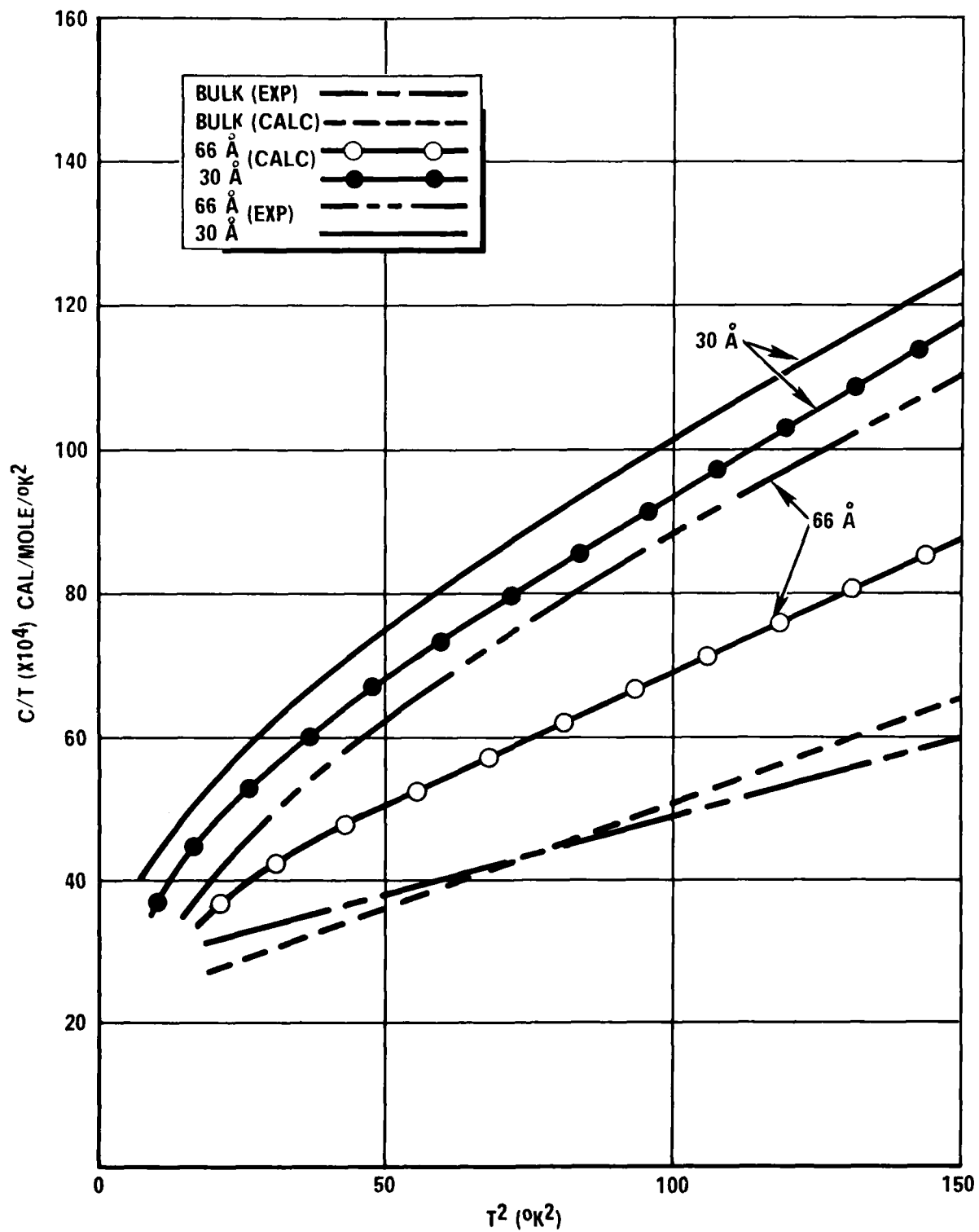
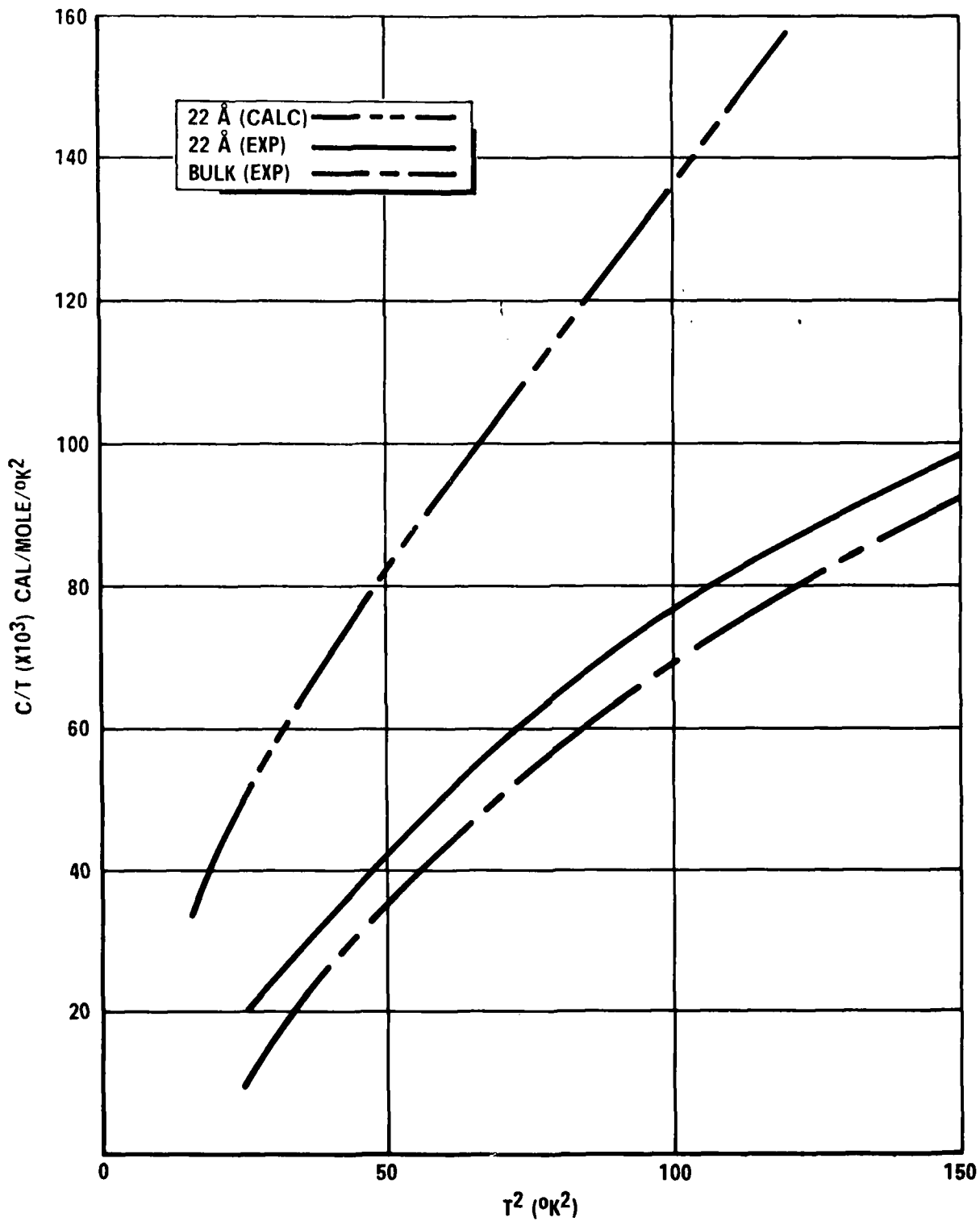


Figure 5. Specific Heat of Palladium ultrafines



**Figure 6. Specific Heat of Lead Ultrafines**

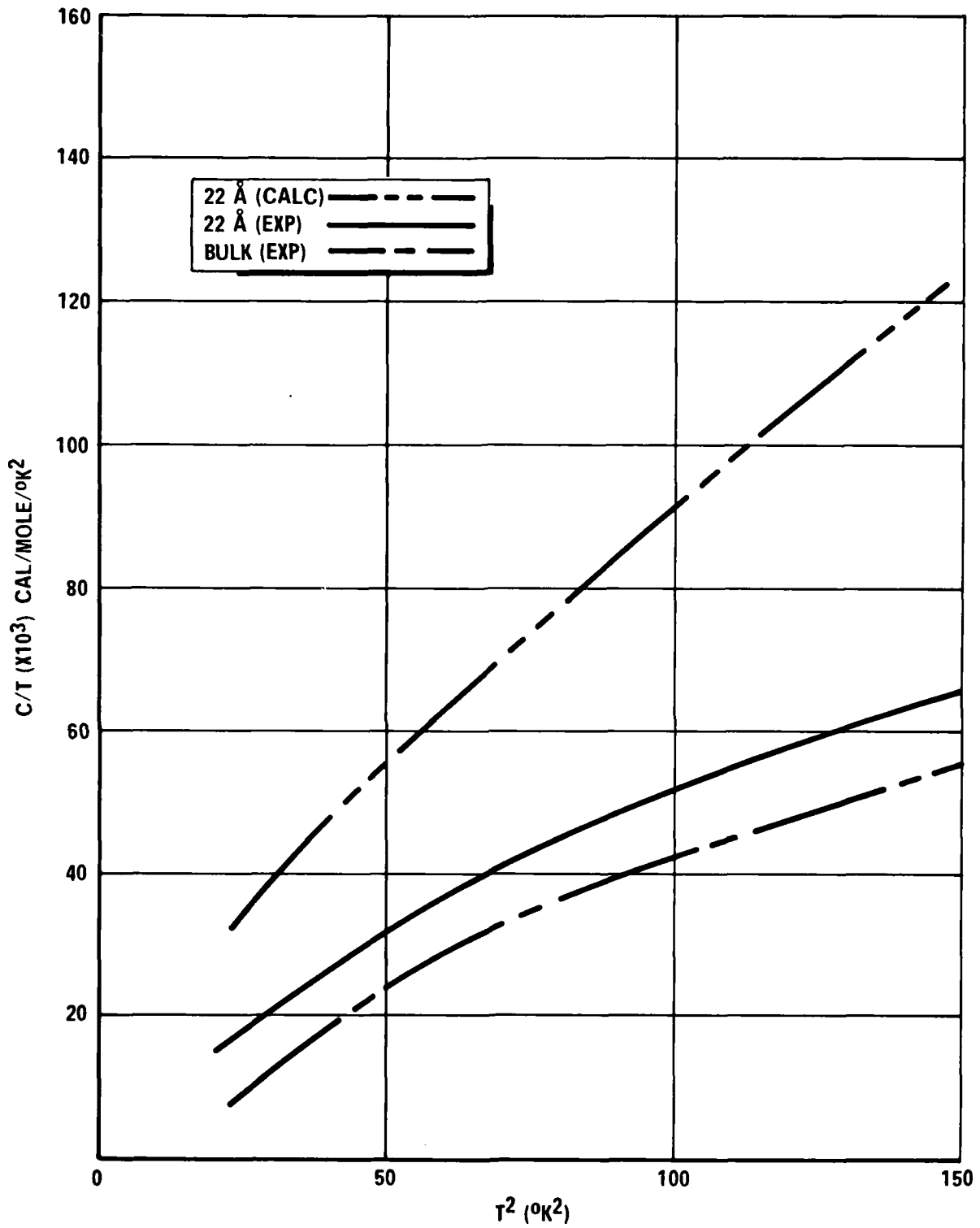


Figure 7. Specific Heat of Indium Ultrafines

of a specific heat enhancement than predicted, and take up a disproportionate share of the sample mass, causing the analysis to err both in the increment-per-particle to be expected as well as in the estimate of total number of particles which give this contribution.

The Comsa measurement program included electron micrograph studies of the palladium ultrafines which seems to confirm the narrow size distribution predicted by Granqvist. Based on this palladium data, we conclude that the LNDF distribution is acceptably narrow for purposes of achieving the full benefit predicted by the Montroll analysis.

In contrast to the Comsa program, Novotny prepared his samples by impregnating a porous glass with metal vapors. His program was carefully designed to determine the diameter of the capillary pores, but not their depth; his size distribution of the pore diameters appears to be relatively narrow.

The resulting metal particle shape, similar to the glass pore shape, apparently tends toward long cylinders instead of discrete separated spheres, and this could explain his conclusion, contradictory to Comsa, that the crystal habit is evident in the particles.

Novotny finds evidence of a significant surface enhancement effect, but the measured magnitude does not follow the prediction of Eq. 43 as applied to spherical particles of the pore diameter. The discrepancy is expected due to the fact that the long cylinders of metal in the glass capillary pores have a different specific surface than would spheres of the same diameter. Eq. 43 fits the data of Figure 6 reasonably well if we assume that the  $22\text{\AA}$  diameter metal cylinders approximate spheres of about  $130 - 150\text{\AA}$  diameter. For the  $22\text{\AA}$  indium particles, Novotny's results can be fit reasonably well under the assumption that the equivalent particle size is in the  $80 - 100\text{\AA}$  range, implying that the cylinders of indium in the pores are somewhat shorter than those of the lead.

If Novotny had measured the specific surface of his samples, thus taking into account their deviation from a simple spherical shape, then Eq. 24 could have been used directly without making an assumption of spherical structure. We can only speculate that the resulting correlation to his measurements might have been significantly better.

In summary then, the Novotny results do indeed detect a significant surface enhancement in both the indium and lead ultrafine cylinders produced by the porous glass test technique. Some combination of shape factor and/or non-homogeneity in the pore size distribution probably explains the fact that specific heat measurement of these cylinders deviates from the results predicted for simple spheres. In contrast to Novotny's work, the recently reported palladium data shows convincingly that spherical ultrafines can be produced (by the inert gas evaporation technique) and that the resulting size distribution is narrow enough that the Montroll approach reasonably accurately predicts the specific heat enhancement.

In order to verify that the "long cylinder" theory adequately explains the Novotny results, another set of measurements using spherical ultrafines of lead and indium will have to be performed.

## 2.8 Candidate Materials for Surface Specific Heat Enhancements

According to Eq. 25, the most important selection criterion for materials likely to show a large surface enhanced specific heat effect in the cryogenic region is the bulk Debye temperature. Of lesser importance are the bulk density and molecular weight of the candidate substances.

Since the Debye temperature actually varies slightly with temperature in the region where surface effects become important, the low temperature value,  $\Theta_0$ , has

been used in the following tabular summary, where available, instead of the conventional value of  $\Theta_D$ . The difference in the two is that  $\Theta_D$  is evaluated close to absolute zero while the latter is more an average value evaluated in the vicinity of  $\Theta_D/2$ .

To illustrate the differences which can be found, Table 1 lists some typical comparisons<sup>24</sup>.

Bulk Material	$\Theta_D$ (average)	$\Theta_D$ (low temperature)
Aluminium (Al)	385	426
Lead (Pb)	85	88
Indium (In)	140	109
Palladium (Pd)	275	262
Rubidium (Rb)	60	55
Mercury (Hg)	100	72

Table 1. Variation in  $\Theta_D$  and  $\Theta_D$  for Various Substances

Table 2 presents pertinent data for nineteen candidate materials which have been found to exhibit favorable values of Debye temperature.

Eight of these materials appear promising enough at first inspection that plots of molar specific heat for each are presented in Figures 8 through 15, and volumetric specific heat in Figures 16 through 23. These candidates include, in order, bismuth, mercury, indium, lanthanum, lead, selenium, thallium, and chromium chloride. Each figure illustrates calculated specific heat values in the 5 - 20°K range as determined from Eq. 43 for the bulk

TABLE 2  
EVALUATION OF CANDIDATE MATERIALS  
(listed alphabetically by symbol)

Substance	Symbol	Atomic number	Atomic weight M(g)	Debye temp. $\Theta$ (°K)	Bulk density $\rho$ (g/cm <sup>3</sup> )	$\frac{\text{cal}}{\text{mole}} \times 10^{-4}$	$\gamma$ (mole <sup>-1</sup> )	Plots of Specific Heat Included Herein	Rationale for Selecting/Rejecting Material for Further Study
Actinium	Ac	89	227	100	10.06	---	---	No	Radioactive material. <u>Hazardous</u> . Rejected.
Bismuth	Bi	83	209	120	9.8	0.05		Yes	Non toxic. Selected for Debye temperature characteristic despite its extremely low gamma contribution.
Cesium	Cs	55	133	39	1.9	7.64		No	Liquid at room temperature, density too low, explodes when in contact with cold water. <u>Hazardous</u> . Rejected.
Mercury	Hg	80	201	72	13.6	4.44		Yes	Selected due to low Debye temperature, even though liquid at room temperature and a cumulative respiratory poison.
Indium	In	49	115	109	7.73	4.40		Yes	Low toxicity. Selected due to low Debye temperature.
Gallium	Ga	31	70	125	5.9	1.43		No	Liquid near room temperature, low toxicity. Mercury chosen instead, as representative of this type of material, but with lower Debye temperature. Rejected.
Lanthanum	La	57	139	130	6.19	23.9		Yes	Highly reactive to oxygen, moderate toxicity. Selected in order to evaluate effect of high gamma contribution material.
Neodymium	Nd	60	144	150	7.0	---		No	Low toxicity, mildly reactive in air. Rejected. Lead, with a lower Debye temperature, chosen as a better candidate for exhibiting surface effects, even though it doesn't show the magnetic anomaly of Neodymium at low temperature.

TABLE 2 (Continued)

Substance	Symbol	Atomic number	Atomic weight M(g)	Atomic Debye temp. $T_D$ (°K)	Bulk density $\rho$ (g/cm <sup>3</sup> )	$\frac{\text{cal}}{\text{mole}} \times 10^{-4}$	$\frac{\text{gamma}}{\text{mole}} \times 10^{-4}$	Plots of Specific Heat included Herein	Rationale for Selecting/Rejecting Material for Further Study
Lead	Pb	82	207	108	11.36	8.3	Yes	Yes	Although a cumulative poison, experience in use of bulk lead in present refrigerator technology and low Debye Temperature make it a primary candidate for evaluation. Selected.
Praseodymium	Pr	59	141	120	6.77	---	No	No	Minor oxidation in air, non toxic, soft/malleable. Lead chosen instead of Pr due to its lower Debye temperature. (May be candidate for cluster structures). Rejected.
Rubidium	Rb	37	85	60	1.53	5.76	No	No	Liquid near room temperature, ignites spontaneously, burns in water, radioactive. Hazardous. Rejected.
Antimony	Sb	51	122	140	6.62	0.027	No	No	Relatively toxic. Debye temperature too high in comparison with lead. Rejected.
Selenium	Se	34	79	90	4.8	---	Yes	Yes	Practically non toxic, but several compounds extremely toxic. Selected for its favorable Debye temperature.
Tin	Sn	50	119	140	7.3	4.18	No	No	Low toxicity. Rejected. Indium chosen instead as a representative of this type of material due to its lower Debye temperature.
Tellurium	Te	52	128	130	6.24	---	No	No	Probably mildly toxic. Relatively high Debye temperature. Rejected in favor of lead.
Thorium	Th	90	232	140	11.7	11.2	No	No	Radioactive, requires AEC licensing, burns in air. Hazardous. Rejected.
Thallium	Tl	81	204	90	11.85	3.63	Yes	Yes	Although a suspected carcinogenic and highly toxic, it has a Debye temperature lower than lead, and similar properties. Selected.
Alums	--	--	--	80	---	---	No	No	Usually brittle crystals, due to water of hydration. Difficult to use as heat exchanger packing. Rejected.
Chromium Chloride	CrCl <sub>3</sub>	--	158	100	2.87	---	Yes	Yes	Chosen to exemplify material with low bulk density and favorable Debye temperature. Crystal soluble in acetone, suspected mildly toxic. Selected.

45

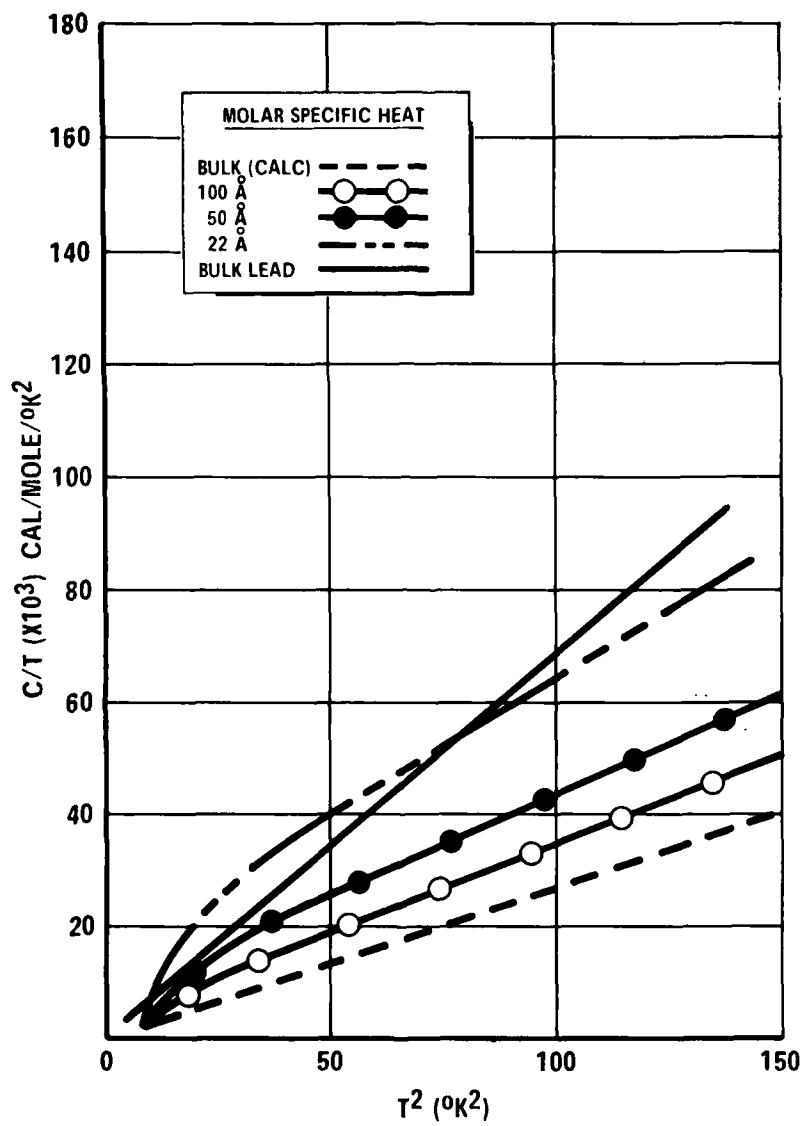


Figure 8. Molar Specific Heat of Bismuth Ultrafines

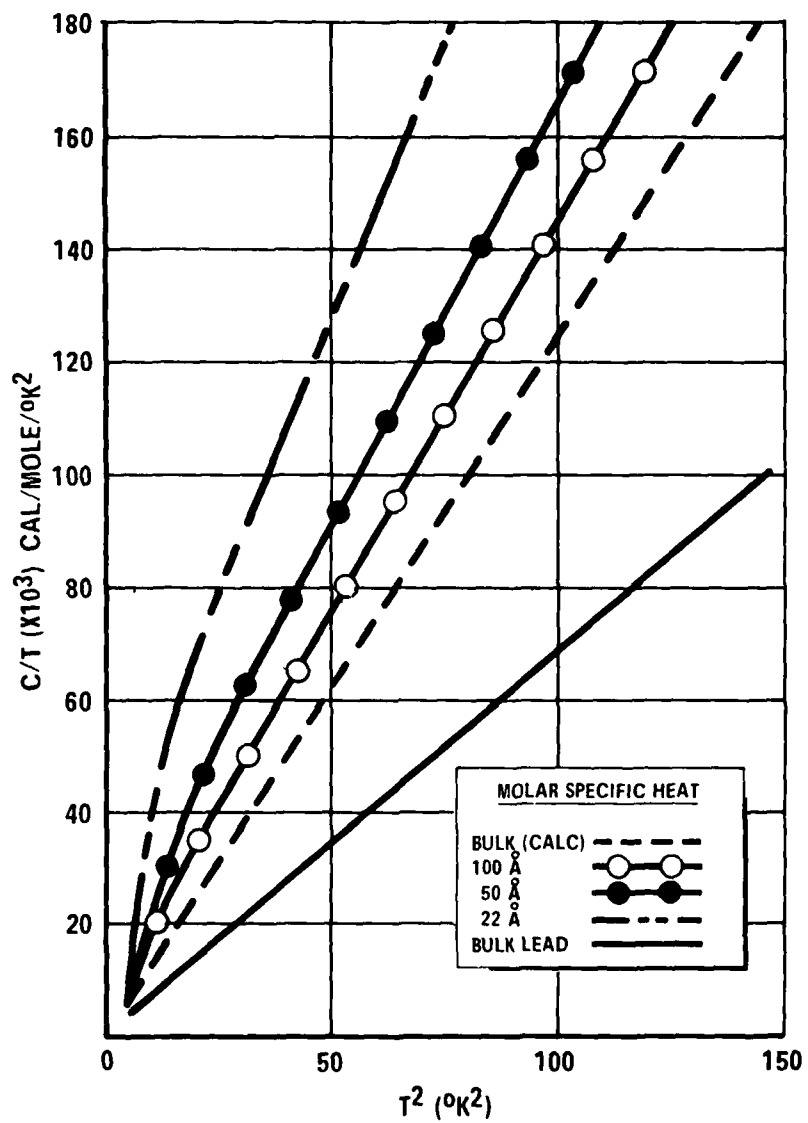


Figure 9. Molar Specific Heat of Mercury Ultrafines

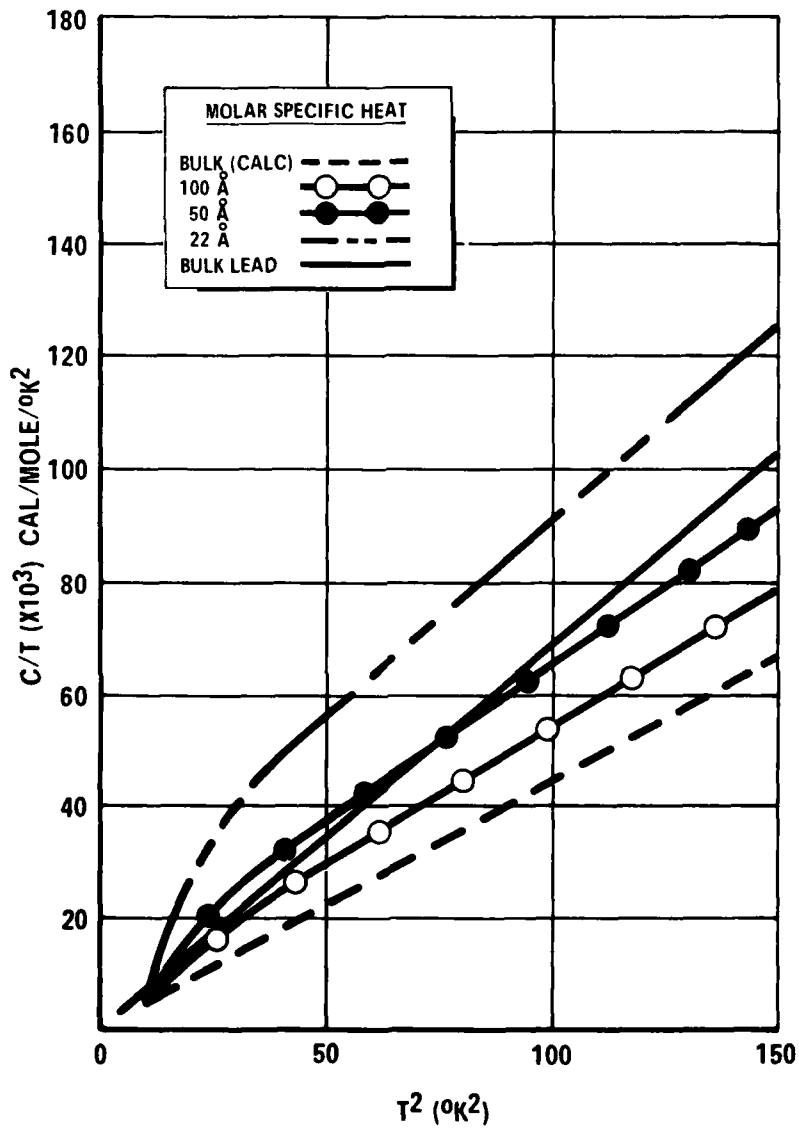


Figure 10. Molar Specific Heat of Indium Ultrafines

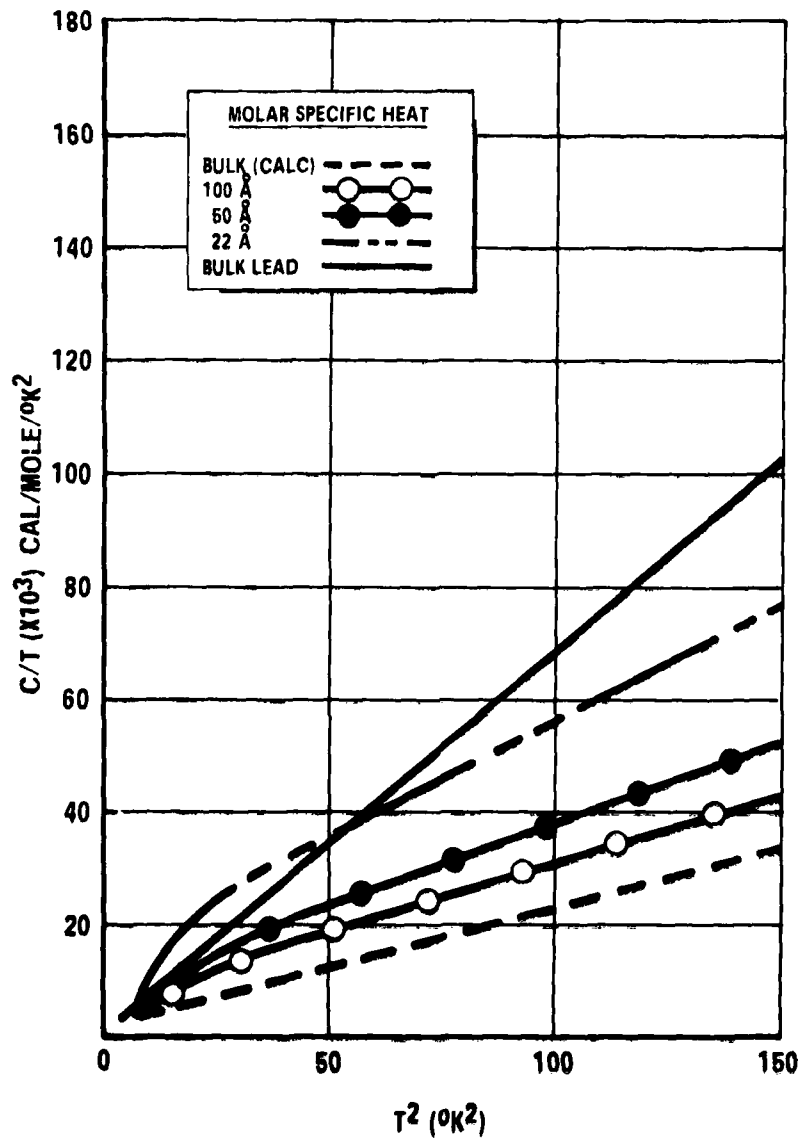


Figure 11. Molar Specific Heat of Lanthanum Ultrafines

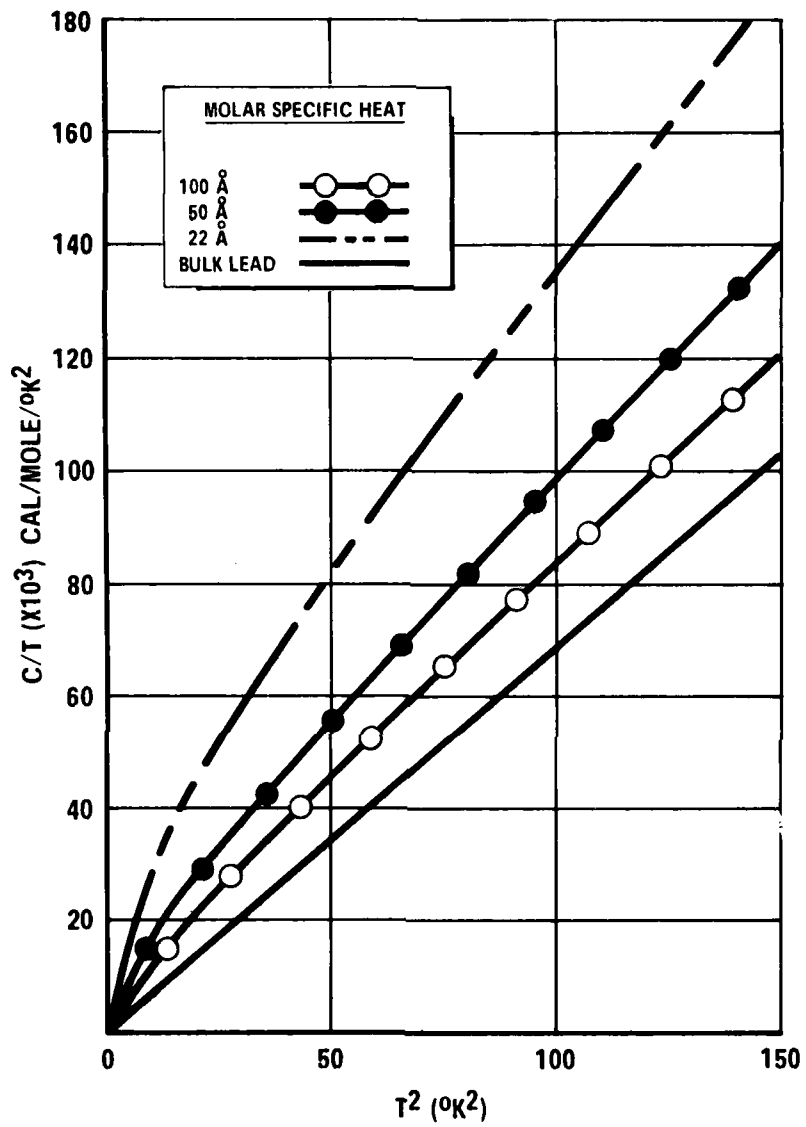


Figure 12. Molar Specific Heat of Lead Ultrafines

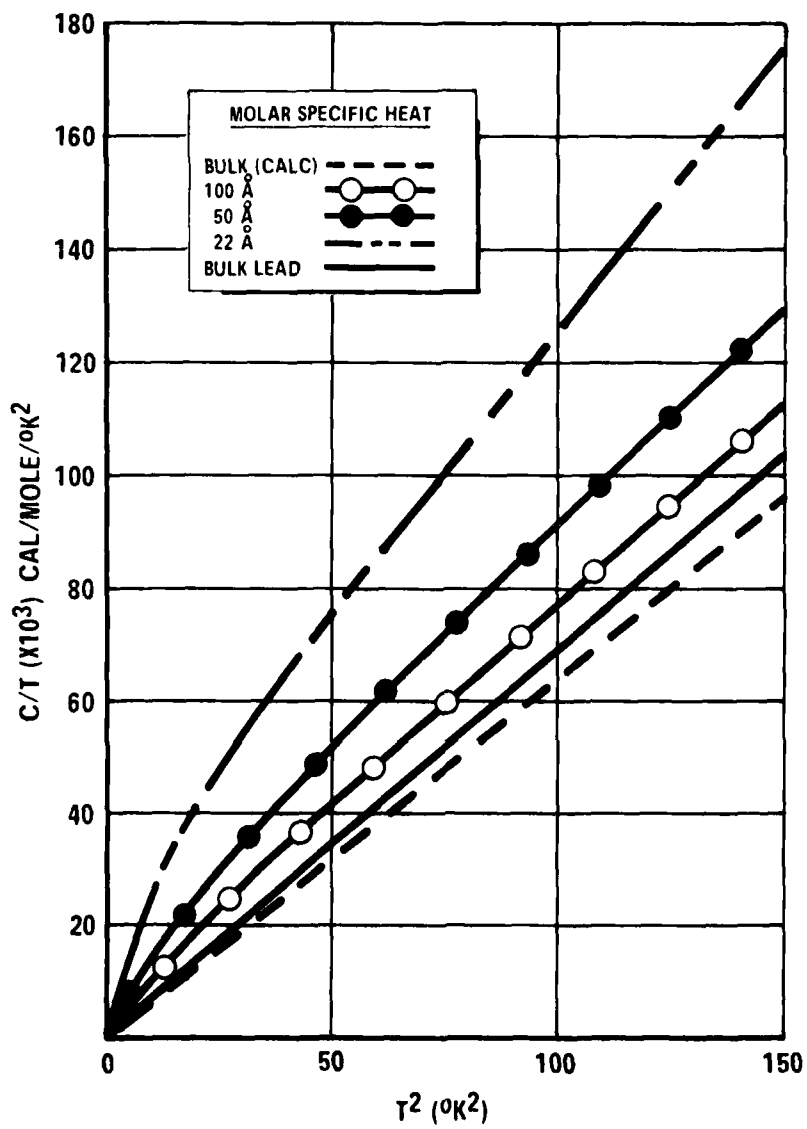


Figure 13. Molar Specific Heat of Selenium Ultrafines

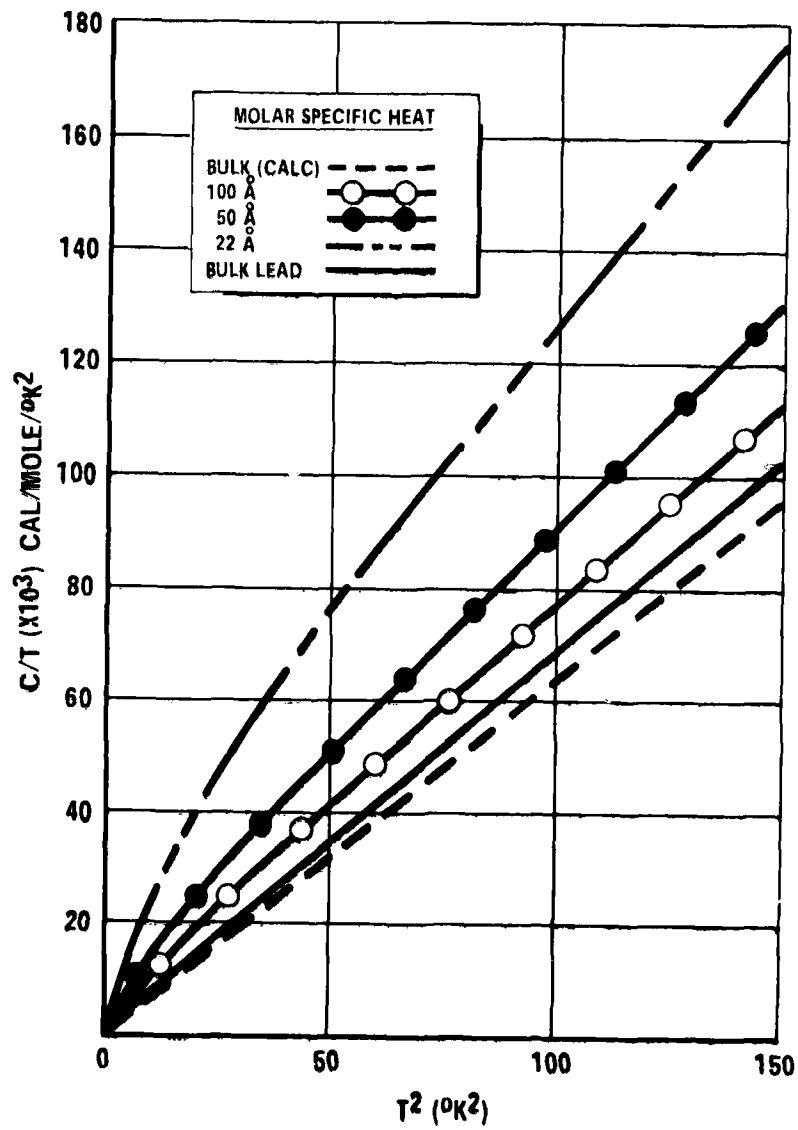


Figure 14. Molar Specific Heat of Thallium Ultrafines

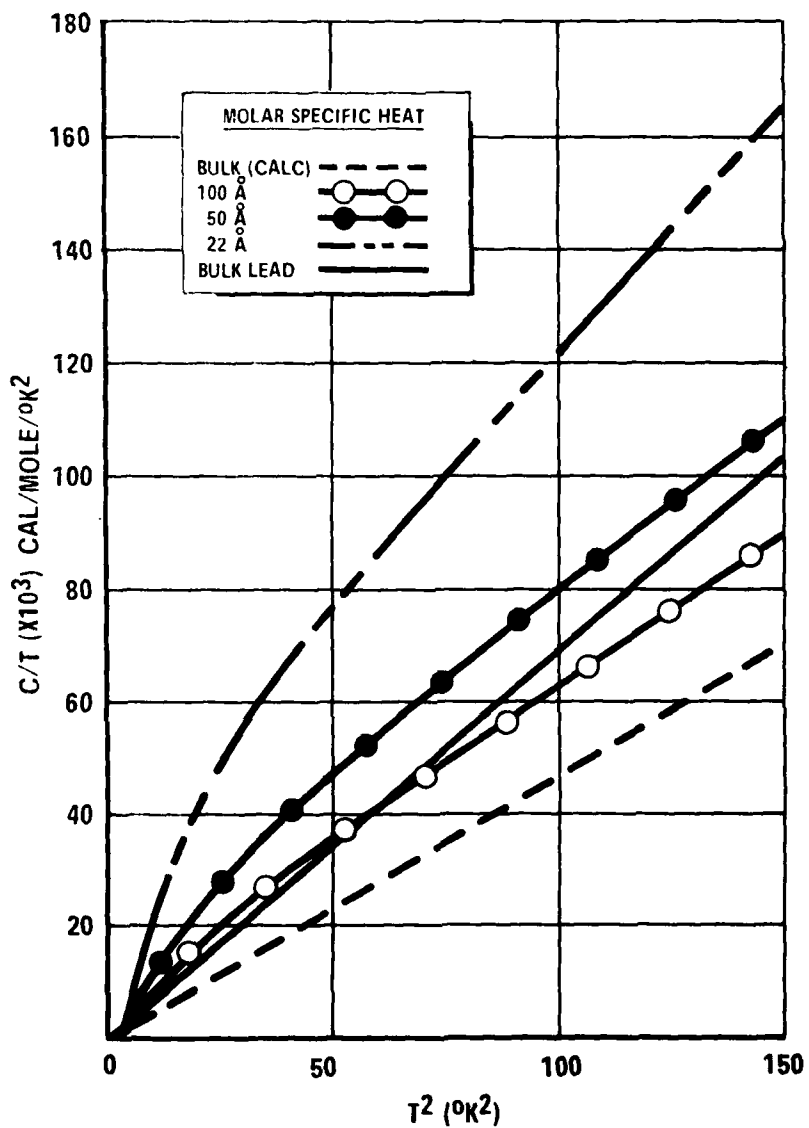


Figure 15. Molar Specific Heat of Chromium Chloride Ultrafines

material, 100 Å , 50 Å and 22 Å ultrafines, plotted against bulk lead as the baseline reference.

Upon inspection of these curves  $\text{CrCl}_3$  can be eliminated from further consideration because of its low density, and mercury, lead, and selenium remain as the primary candidates for the regenerator improvement experiment to be conducted in later phases of this program.

2.8.1 Interpretation of Specific Heat Enhancement Data. It was noted in Eq. 15 that the  $\beta T^3$  approximation for bulk material specific heat is strictly valid only at temperatures much lower than the characteristic Debye temperature of the solid. At temperatures greater than about  $\Theta_D/24$  the approximation shouldn't be used for high precision work, and at temperatures warmer than about  $\Theta_D/8$  the complete form of the Debye equation:

$$C_v = \frac{3}{x^3} \int_0^x \frac{x^4 e^x dx}{(e^x - 1)^2} \quad ; x = \frac{\Theta_D}{T} \quad (46)$$

yields lower specific heat values than does the approximation (Figure 24), becoming increasingly significant as T increases.

All measurements done on fine powders to date have been at temperatures where the simplified  $\beta T^3$  approximation for the bulk material applies. The data of Figures 3 and 4 on  $\text{MgO}$  and  $\text{NaCl}$  shows clearly that a significant surface enhancement in specific heat occurs at these fractional Debye temperature regions.

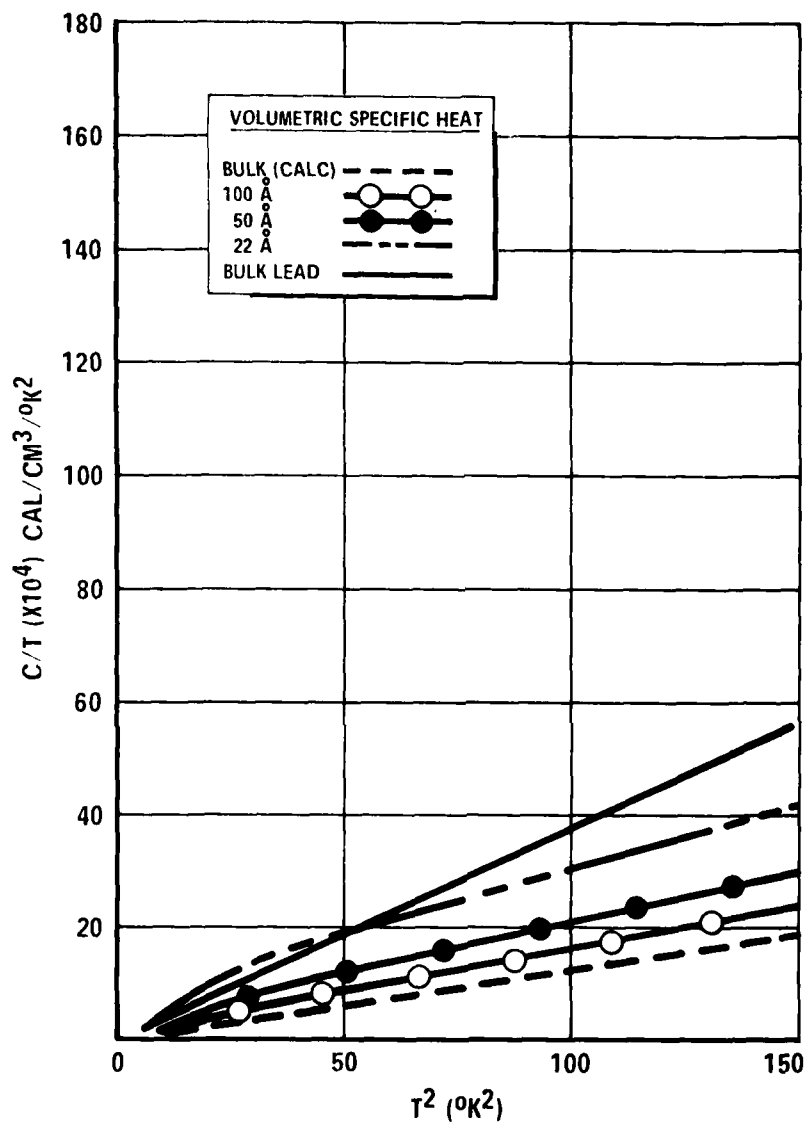


Figure 16. Volumetric Specific Heat of Bismuth Ultrafines

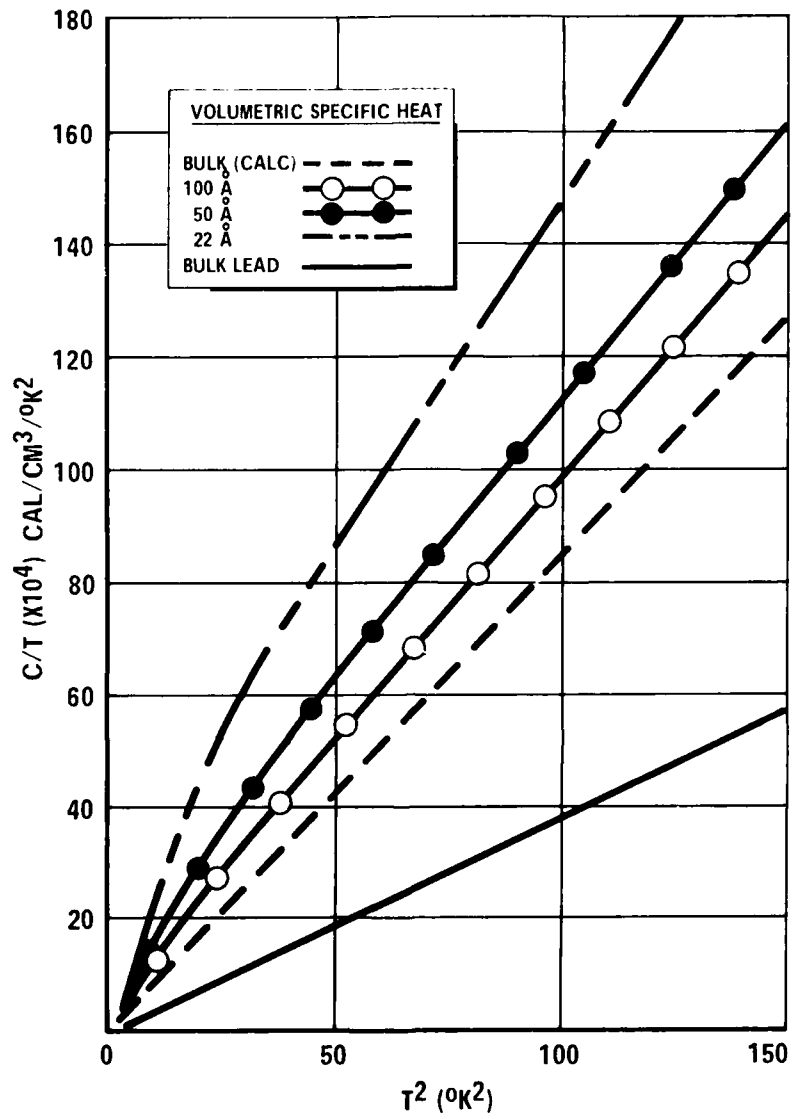


Figure 17. Volumetric Specific Heat of Mercury Ultrafines

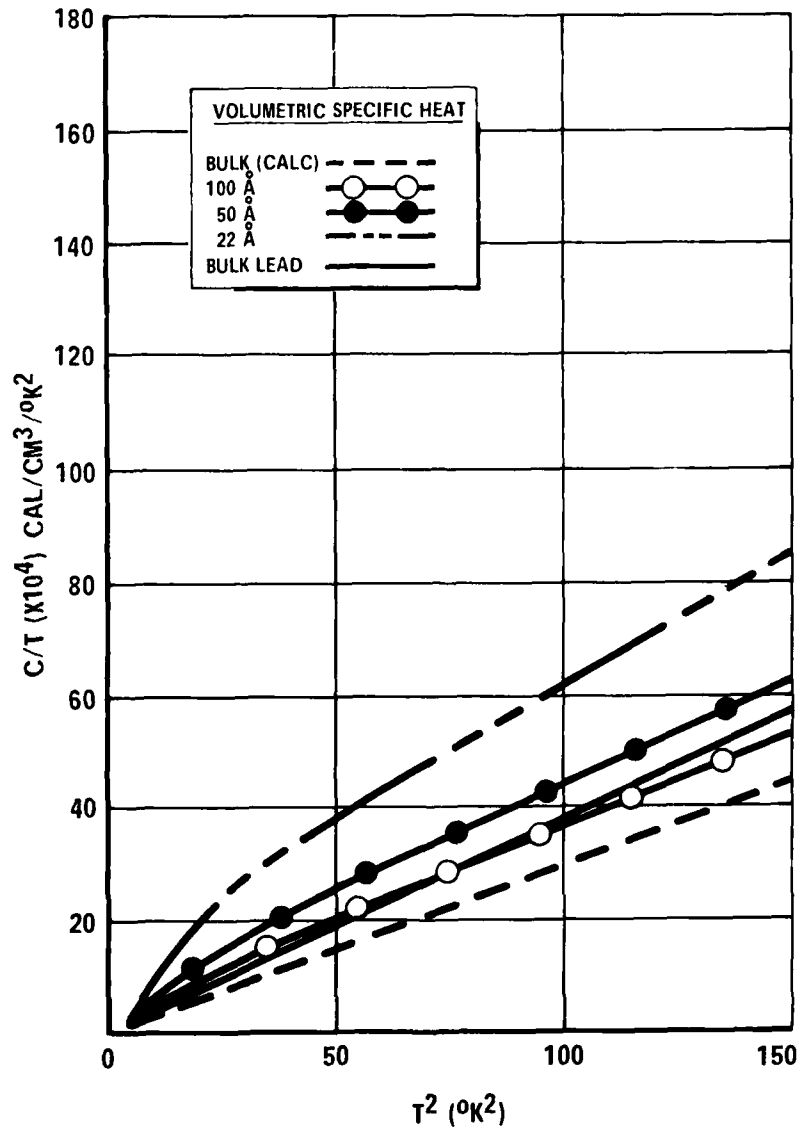


Figure 18. Volumetric Specific Heat of Indium Ultrafines

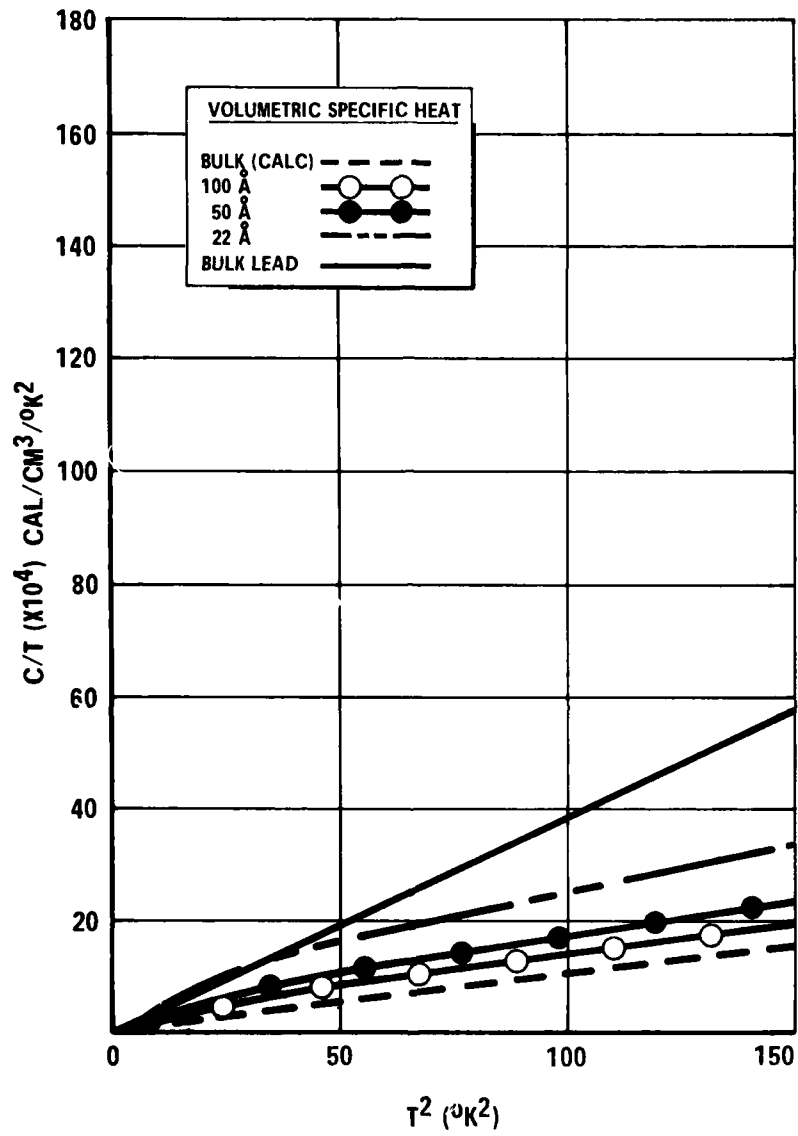


Figure 19. Volumetric Specific Heat of Lanthanum Ultrafines

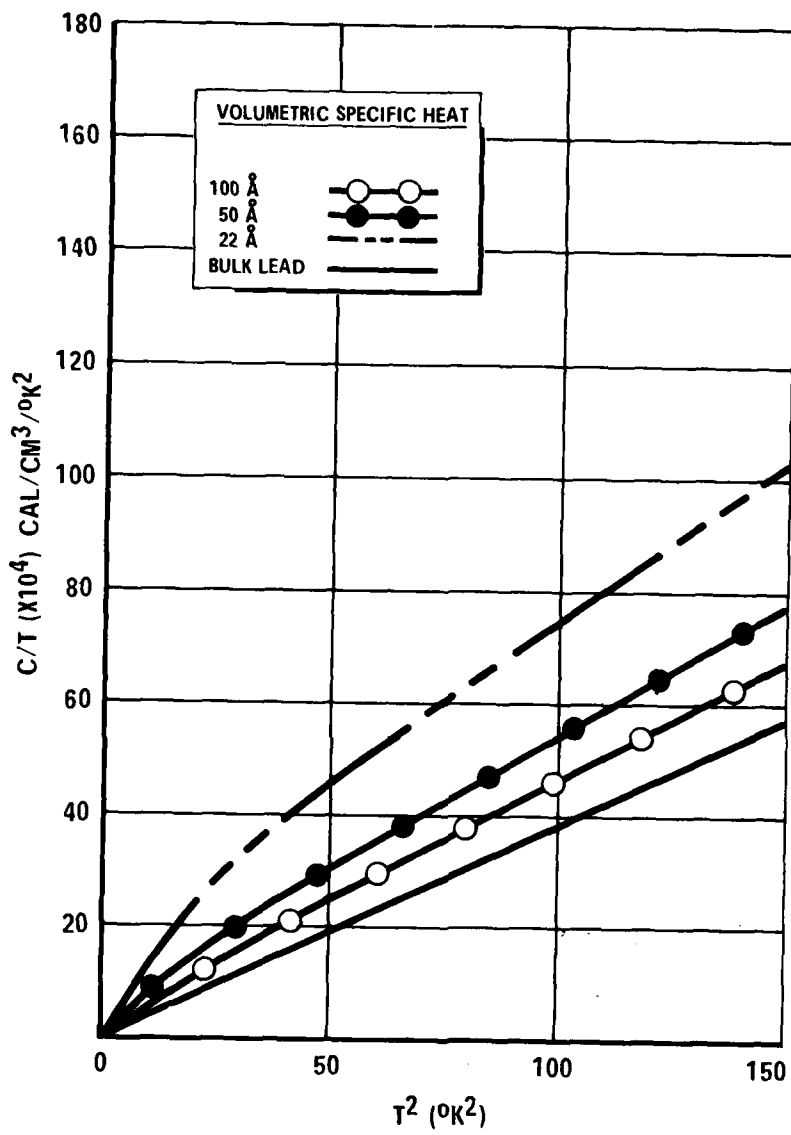


Figure 20. Volumetric Specific Heat of Lead Ultrafines

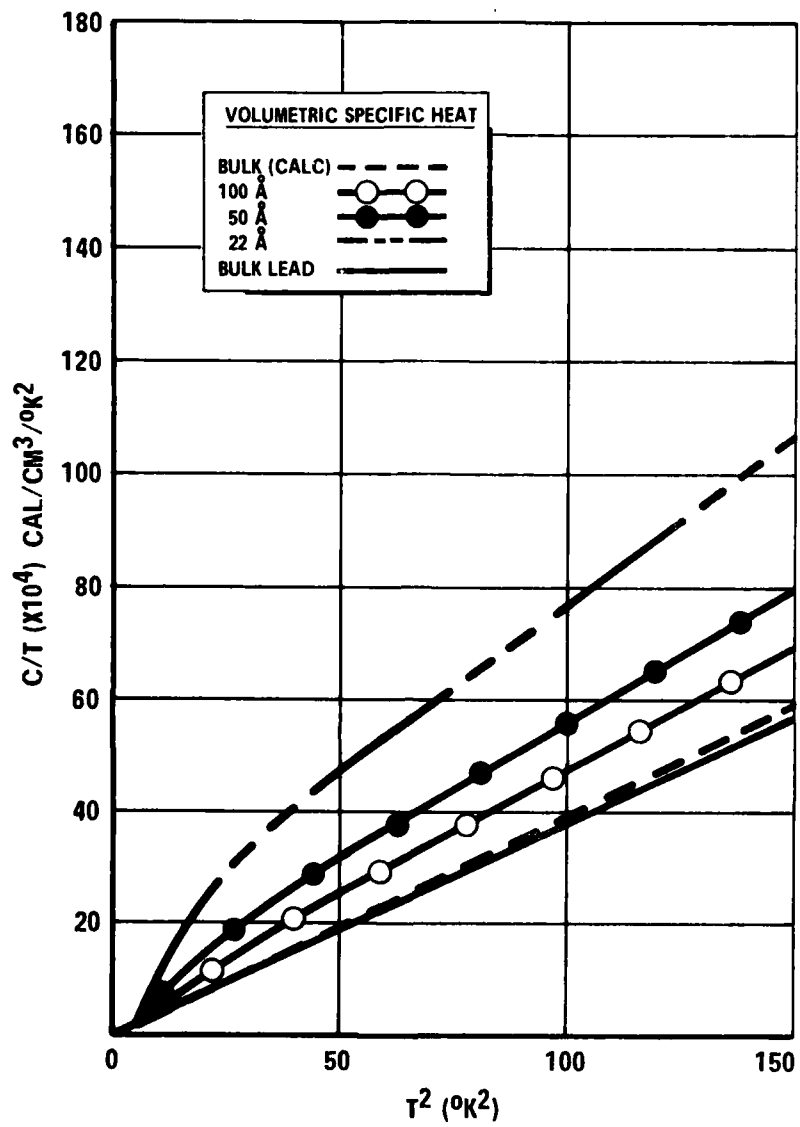


Figure 21. Volumetric Specific Heat of Selenium Ultrafines

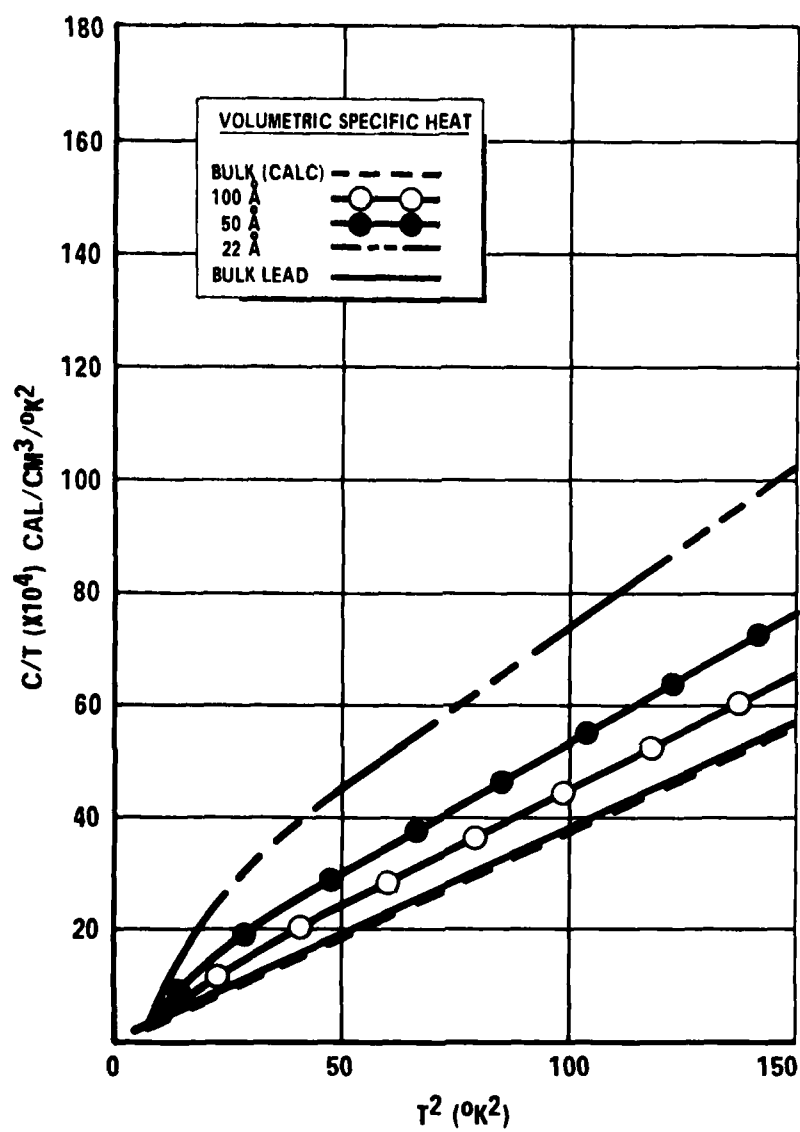


Figure 22. Volumetric Specific Heat of Thallium Ultrafines

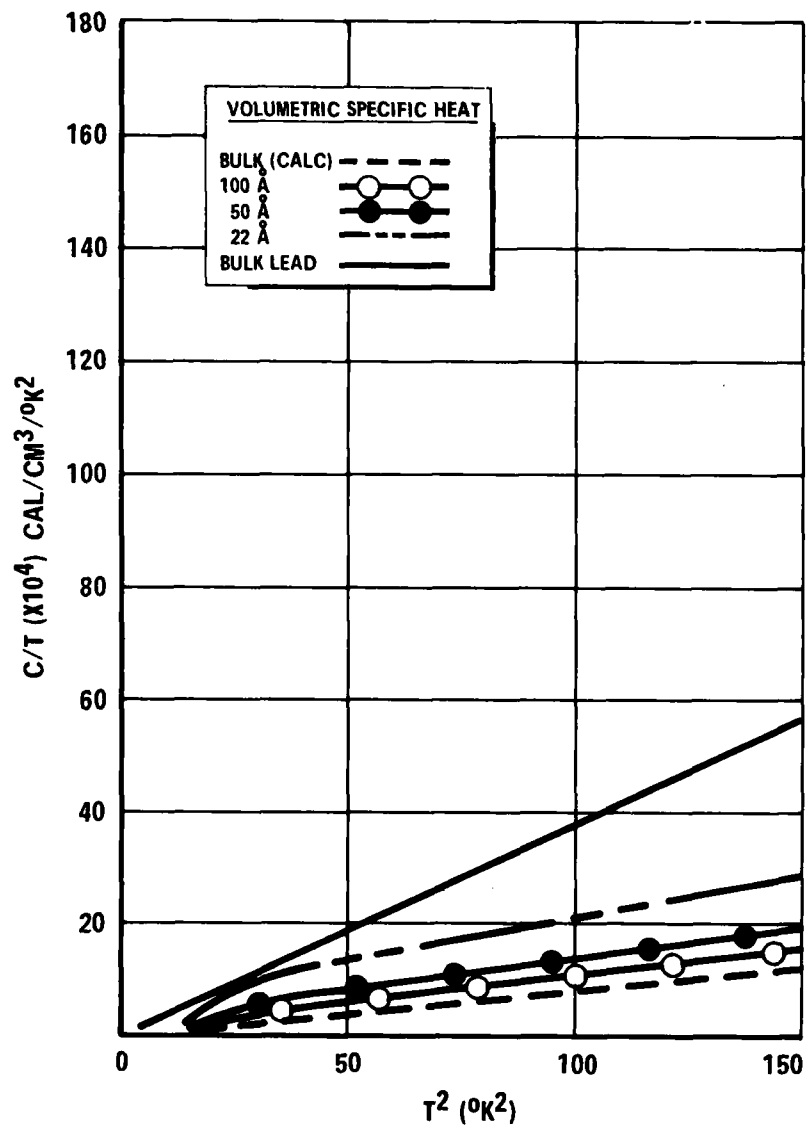


Figure 23. Volumetric Specific Heat of Chromium Chloride Ultrafines

The recent measurements on palladium ultrafines illustrate that the surface enhancement effect does occur similarly with metals, and further shows that the empirical form of the algorithm (Eq. 43) produces a conservative fit in this fractional  $\Theta_0$  region.

The warm end of these reported palladium measurements approached a temperature value of  $\Theta_0/8$ . There is no indication at that temperature that the enhanced specific heat is beginning to deviate from the value predicted by Eq. 43.

The Montroll-type theory isn't developed far enough to indicate the expected warm-end temperature limits on the enhancement, and no reported measurements have investigated this effect beyond the range of the palladium data.

In order to apply this surface specific heat theory to cryogenic refrigerator regenerator design it is necessary to predict the enhancement effect at temperatures as warm as about  $\Theta_0/3$ . Because Montroll's equation was derived under the limit  $T \rightarrow 0$ , we expect the  $\alpha T^2$  correction to be in error (similar to Debye's  $\beta T^3$  term) as the value of  $\Theta_0/T$  becomes smaller. Since no test data exists we must either assume that Eq. 43 is valid all the way out to the warm end of our interest, or else artificially assume some degradation in the computed value between  $\Theta_0/8$  (where palladium data is available) and  $\Theta_0/3$ . So as to attempt to keep performance projections conservative, we shall assume that the full calculated value of the enhancement increment is applicable as warm as  $\Theta_0/8$  -- as indicated by the palladium data -- and decreases percentagewise to zero (in a manner linear with temperature) at a value of  $\Theta_0/3$ . Figure 25 illustrates this hypothesized fall-off in the  $\alpha T^2$  term for our baseline material (lead). Specific heat values from this figure will be used in Section III when enhanced refrigerator performance predictions are compared with performance derived from conventional technology using lead spheres in the regenerator.

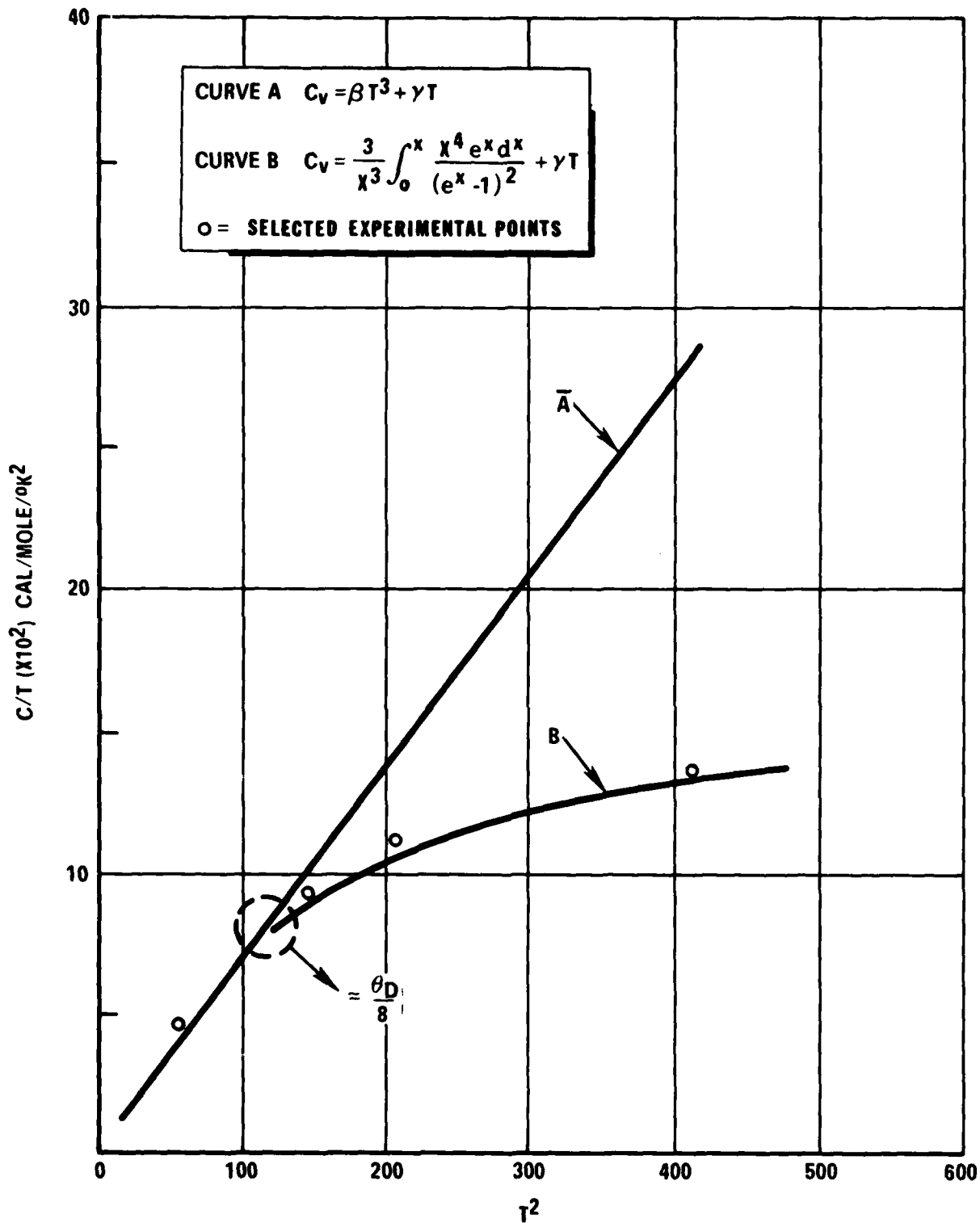


Figure 24. Comparison of Specific Heat Calculations for Lead

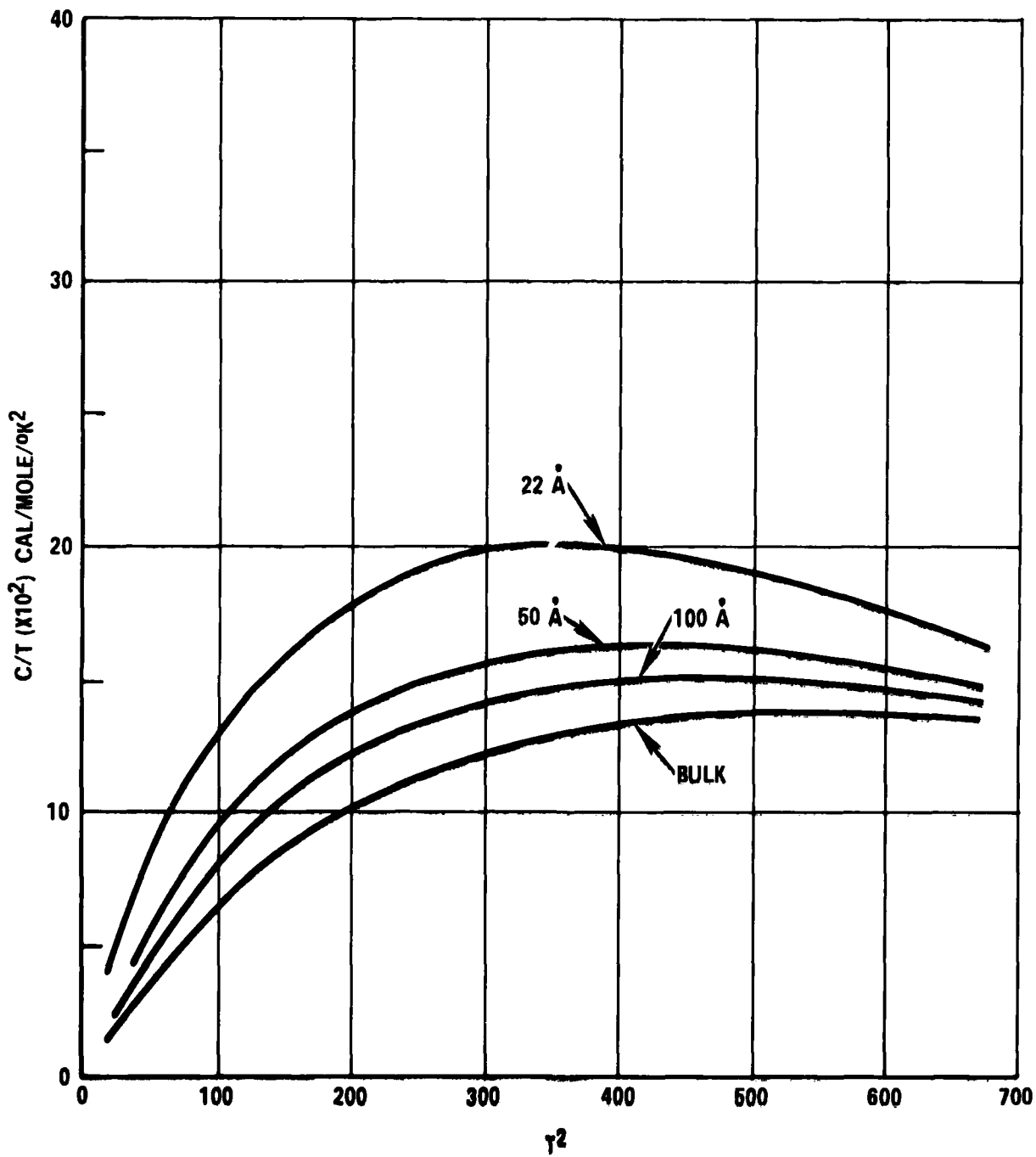


Figure 25. Weighted Curves for Lead Particle  $C_v$

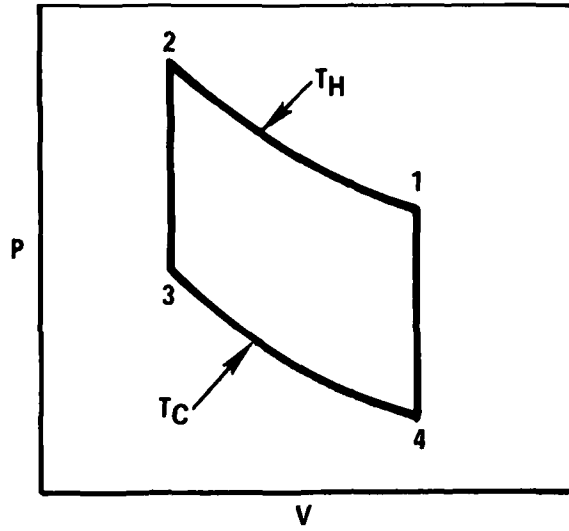
### III IDEALIZED REFRIGERATOR PERFORMANCE

#### 3.1 Introduction

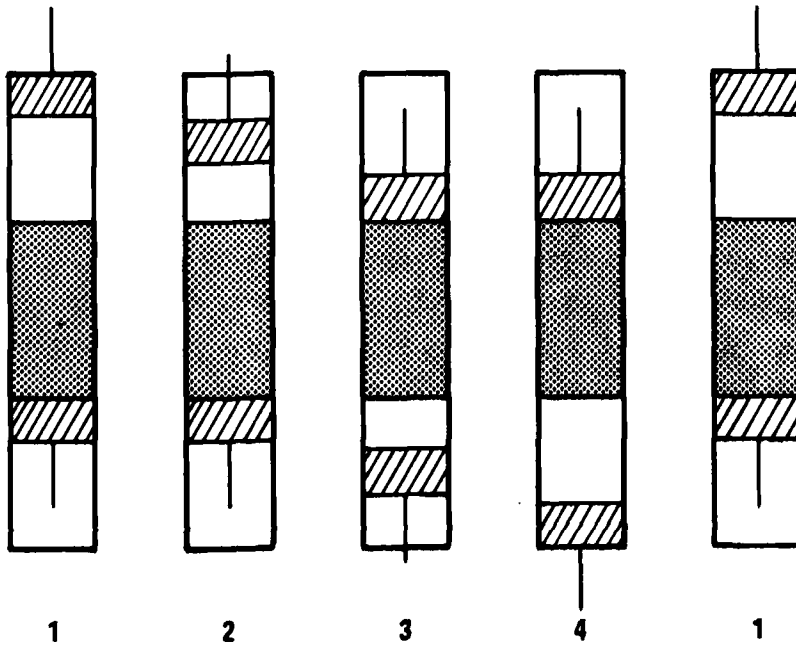
The mechanisms used to produce refrigeration at cryogenic temperatures have historically been inefficient devices, plagued with reliability problems and high input power requirements. In the early 1960s several research groups began showing promising results in applying the refrigeration version of the Stirling heat engine to the production of low temperatures. Used in this manner, the process is sometimes called the Kirk cycle, after an early researcher who reported its utilization to produce refrigeration. Following the more usual nomenclature, however, it will be referred to as the Stirling cycle in this report, and is shown graphically in Figure 26.

The second highly significant development came in that same time frame when Gifford and McMahon published a report describing a new thermodynamic cycle which now bears their names<sup>25</sup>. There has previously been a debate whether their disclosure actually represented a new thermodynamic concept or was merely a novel implementation of the Ericsson cycle shown in Figure 27. Regardless of how we argue the resolution of that question, the implementation of their concept resulted in high reliability and high performance machines when compared with prior technology.

The Stirling cycle and the Gifford-McMahon cycle refrigerators, as well as devices based on several other similar cycles not highlighted here, have in common the fact that they are designed around a periodic flow heat exchanger called a regenerator. The regenerator separates the hot working volume of these machines from the cold working volume, and is the keystone of machine performance.



a) IDEALIZED CYCLE



b) IDEALIZED IMPLEMENTATION

Figure 26 . Stirling Cycle Diagram

An ideal regenerator would have characteristics of zero pressure drop for gas flow between the hot and cold regions, infinite specific heat so as to cause a perfect temperature transition (between hot and cold) for the gas flowing through it, zero heat conductivity along the axis of the heat exchange matrix, and an infinitesimally small void volume in the gas flow paths. Obviously, these ideal requirements, even to the extent they are not mutually exclusive, cannot be satisfied. Consequently, the performance of the overall refrigerator is directly affected by the deviation of the regenerator from the ideal.

Because the Stirling cycle machine is subjected to relatively severe mechanical loading on dynamic components such as bearings and seals, a closely related thermodynamic process which minimizes these loads, known as the Vuilleumier (VM) cycle, was adopted for these refrigerators in the late 1960s. VM-based machines have incrementally improved the reliability of Stirling-type devices, and are leading candidates for long life space mission applications.

Some writers describe the VM cycle as merely a Stirling cycle modified so that the high pressure is produced by a thermal (rather than a mechanical) compressor. It is probably more accurate, however, to describe it as a variant of the Ericsson cycle, since mass flow out of the cold volume occurs during the expansion part of the cycle<sup>26</sup>. The thermodynamic process which is physically implemented in the VM refrigerators cannot conveniently be described on a temperature-entropy plot, because dynamic flow conditions are encountered throughout the cycle. Flow process thermodynamics are usually employed to analyze the performance of these machines.

The first law of thermodynamics, for steady flow processes through a control volume, is written as:

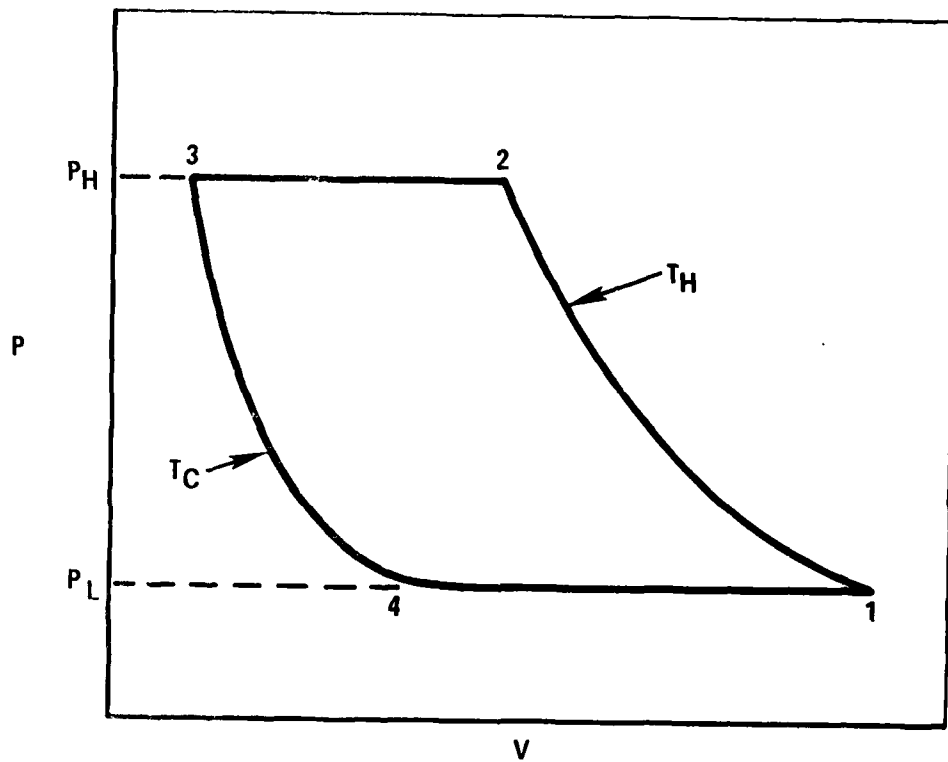


Figure 27. Ericsson Cycle Diagram

$$\dot{Q}_{Net} - \dot{W}_{Net} = \sum \dot{m} h_o - \sum \dot{m} h_i \quad (47)$$

when kinetic and potential energy terms are neglected.

$\dot{Q}_{Net}$  is net heat transfer rate to or from the system

$\dot{W}_{Net}$  is net work rate done by the system

$\sum \dot{m} h_o$  is the enthalpy sum for all flow outlets

$\sum \dot{m} h_i$  is the enthalpy sum for all flow inlets.

It is assumed that over the period of the process being analyzed there is no net storage of mass or energy in the control volume considered.

This approach is adapted to the analysis of the periodic flow associated with the expansion volumes of the regenerator-based refrigerators, and the equation for gross refrigeration capacity per cycle is usually expressed as:

$$Q_{exp} = W_{exp} - \Delta H_{exp} \quad (48)$$

where

$Q_{exp}$  indicates the heat absorbed in the actual expansion process (in contrast to the  $Q_{3-4}$  idealized quantity from Figure 26a)

$W_{exp}$  is the work done by the expanding gas, and

$\Delta H_{exp}$  is the enthalpy change of the gas during the expansion process.

Helium is almost always employed as the working gas in refrigerators of this type, since it liquefies only at pressures and temperatures lower than those normally achieved in the cycle. For purposes of computing gross refrigeration, the assumption is often made that helium behaves as an ideal gas, following the relationship:

$$PV = mRT \quad (49)$$

where  $m$  is the mass of gas involved in the process, and  $R$  is the gas constant.

For a closed system, the first law of thermodynamics is, in analogy to Eq. 2 :

$$dU = \delta Q - \delta W \quad (50)$$

where the symbols indicate that  $dU$  is an exact differential whose value depends only on the state of the thermodynamic system, while  $\delta Q$  and  $\delta W$  are inexact differentials and represent infinitesimal quantities whose values depend on the particular process followed in taking the working substance from state to state.

Since

$$\delta W = PdV \quad (51)$$

we can write

$$dU = \delta Q - PdV \quad (52)$$

and for a constant volume process, we showed in Eq. 5 that

$$\left(\frac{\partial U}{\partial T}\right)_V = \frac{dU}{dT} = \left(\frac{\delta Q}{dT}\right)_V = C_V, \quad (53)$$

since the internal energy of an ideal gas is a function of temperature only, i.e.:

$$U = U(T). \quad (54)$$

Since we define enthalpy as

$$H = U + PV, \quad (55)$$

we can write for an ideal gas

$$H = U + mRT; \quad (56)$$

and since all terms on the right side of the equation are solely functions of temperature, it follows that  $H$ , likewise, is only a function of temperature.

Consequently, if the control volume selected for the regenerator flow analysis includes both the regenerator and the expansion volume, and it is postulated that inlet and exit gas are at the same temperature (i.e., a 100% efficient regenerator), then the equation for gross refrigeration can be rewritten as:

$$Q'_{exp} = \int_{exp} P dV \quad (57)$$

where the prime ( $i$ ) emphasizes that the ideal gas assumption was employed to achieve this simplification, and the symbol  $\int_{exp}$  indicates that the work term is integrated over the expansion cycle.

In summary then, for VM cycle refrigerators the estimate for gross refrigeration production uses either Eq. 48 or the ideal-gas simplification, Eq. 57. As a matter of fact, since all the cycles of interest as-implemented deviate from the ideal  $P$ - $V$  diagrams, these two equations can be applied to any of these machines to estimate the actual output.

The first successful attempt to analyze the performance of non-idealized, as-implemented Stirling machines was reported by Schmidt in the 1860s<sup>27</sup>. His analysis recognized that realizable machines would employ sinusoidal drives for the reciprocating elements rather than the "square wave" drives implied in the piston movements of Figure 26.

His theory requires, among other simplifications, the assumptions of isothermal compression and expansion, and further assumes the regenerator operates with 100% efficiency. In spite of the fact that his model is still highly idealized, it represented a striking improvement over the cycle analysis equations based on the pure **P-V** diagram for the refrigerator.

This theory has been further refined in recent years. The Philips Laboratories, Eindhoven, Netherlands have been heavily engaged in research and development of Stirling devices for several decades. Early emphasis was on the Stirling engine as a prime mover; however, as early as 1945 Rinia and duPré of that organization were involved in preliminary work on refrigerators. More recently, computer assisted design analyses of VM refrigerators have been published. Correlation between as-built performance and the computer-predicted capability is reportedly good in at least one case of a high capacity VM machine developed for the Air Force<sup>28</sup>.

### 3.2 Stirling Cycle Analysis

For ease in understanding the concepts to be presented in this report -- specifically, the concept of improving overall refrigerator performance by a technique to increase the specific heat of regenerator matrix materials -- it is particularly convenient to avoid both the Schmidt analysis and the flow process analysis and to work with a true cycle which can be described on a **P-V** state diagram. Consequently, the Stirling cycle of Figure 26a will be used hereafter as our model for discussing this effect.

The idealized cycle achieves the same theoretical coefficient of performance (COP) as the theoretical Carnot cycle, whose limiting performance forms an alternate definition of the second law of thermodynamics. COP is defined as:

$$(COP)_{ad} = \frac{Q_{3-4}}{W_{net}} \quad (58)$$

Where the subscript  $id$  means idealized (or Carnot) COP,

$Q_{3-4}$  means the gross heat absorbed in going from State 3 to 4 of Figure 26, and  $W_{net}$  is the difference between the theoretical work of compression at the higher temperature and the expansion work available. For the idealized cycle:

$$(COP)_{id} = \frac{T_c}{T_H - T_c} \quad (59)$$

Before proceeding to consider the effect of regenerator efficiency on machine performance as well as the effect of adding multiple stages, it is useful to list the heat and work balance equations for the cycle. For the isothermal compression 1-2 we can apply the first law from Eq. 2 as:

$$Q_{1-2} = W_{1-2} \quad (60)$$

and our sign convention requires that  $Q$  be numerically positive for heat absorbed by the system, and  $W$  be numerically positive for work done by the system.

Treating the helium as an ideal gas,

$$W_{1-2} = -mRT_H \ln P_2/P_1 \quad (60a)$$

thus

$$Q_{1-2} = -mRT_H \ln P_2/P_1 \quad (60b)$$

For the isochoric process 2-3, the first law becomes,

$$Q_{2-3} = U_{2-3} \quad (60c)$$

and consequently

$$Q_{2-3} = mc_v (T_c - T_H) \quad (60d)$$

and, of course

$$W_{2-3} = 0. \quad (60e)$$

With similar arguments,

$$W_{3-4} = Q_{3-4} = m R T_c \ln \frac{V_4}{V_3} \quad (60f)$$

and

$$Q_{4-1} = m c_v (T_H - T_c) \quad (60g)$$

while

$$W_{4-1} = 0. \quad (60h)$$

We thus find that,

$$W_{\text{Net}} = W_{1-2} + W_{3-4} \quad (61)$$

or

$$W_{\text{Net}} = -m R \ln \frac{V_1}{V_2} (T_H - T_c). \quad (61a)$$

3.2.1 Simple Regenerator Model. In the ideal cycle of Figure 26, the heat transfer in both Steps 2-3 and 4-1 is accomplished in the high efficiency periodic flow heat exchanger referred to earlier as a regenerator. In the figure the entire mass of helium contained in the cycle is required to be transformed exactly between the two temperature levels as it passes through the regenerator. In real machines it is not possible to achieve such perfect heat transfer, and consequently the gas exiting from the cold end of the regenerator will be warmer than  $T_c$  by some  $\Delta T$ .

We can define regenerator efficiency ( $\epsilon$ ) in terms of the heat actually transferred during the flow process:

$$\epsilon = \frac{Q_{2-3}^{\text{act}}}{Q_{2-3}^{\text{id}}} \quad (62)$$

where the superscript act refers to the heat actually transferred during the process and id refers to the idealized amount of heat which should have been transferred to properly "fit" the cycle diagram. We know from the earlier derivation that:

$$Q_{2-3}^{\text{id}} = mc_v (T_c - T_H). \quad (63)$$

if we define the regenerator heat loss as

$$Q_R = Q_{2-3}^{\text{id}} - Q_{2-3}^{\text{act}} \quad (64)$$

we can show

$$Q_R = (1 - \epsilon) mc_v (T_H - T_c). \quad (65)$$

It is also necessary to recognize that in a real machine the gross refrigeration produced in the process 3-4 is "used up" by the sum of (A) the external load being cooled ( $Q_{\text{ext}}$ ), (B) the regenerator heat loss ( $Q_R$ ), and (C) various other stage losses associated with the design of the particular machine of interest ( $Q_{\text{s.l.}}$ ). This can be expressed as:

$$Q_{3-4} = Q_{\text{ext}} + Q_R + Q_{\text{s.l.}} \quad (66)$$

We saw earlier that,

$$Q_{3-4} = mRT_c \ln P_2/P_1 \quad (67)$$

This can be rearranged as

$$Q_{3-4} = (\gamma - 1) mc_v T_c \ln P_2/P_1 \quad (68)$$

where

$$\gamma = c_p/c_v \quad (69)$$

Then

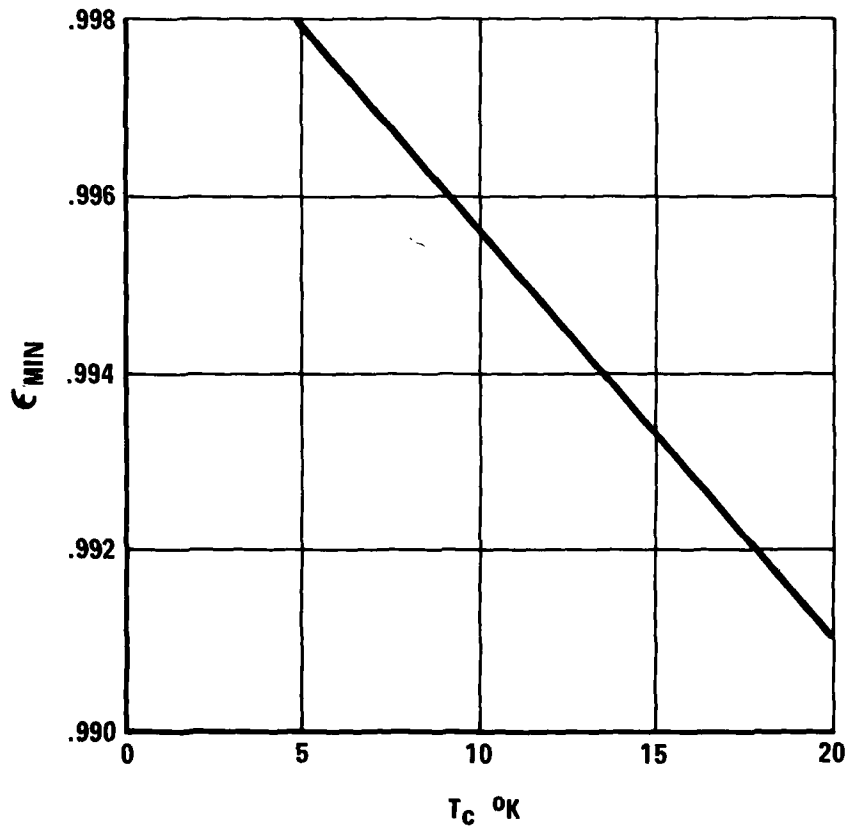
$$\frac{Q_R}{Q_{3-4}} = \frac{(1 - \epsilon) (T_H/T_c - 1)}{(\gamma - 1) \ln(P_2/P_1)} \quad (70)$$

Equation 70 can be solved to determine that minimum efficiency which allows all the gross refrigeration to be consumed by the regenerator heat loss (this approach can be modified to include  $Q_{2L}$ ).

Thus:

$$\epsilon_{\min} = 1 - \frac{(\gamma - 1) \ln(P_2/P_1)}{(T_H/T_c - 1)} \quad (71)$$

A graph of Eq. 71 is included as Figure 28. In this limiting case there is no net refrigeration left to cool an external heat load.



FOR HELIUM,  $\frac{P_2}{P_1} = 1.4$ ,  $T_H = 324^\circ\text{K}$ ,  $\gamma = 1.4$

**Figure 28. Minimum Required Regenerator Efficiency vs. T<sub>c</sub> (Cold Stage)**

Now, the theoretical, or design, efficiency  $\epsilon_0$  of a periodic flow regenerator can be expressed as:

$$\epsilon_0 = \frac{\lambda_0}{\lambda_0 + 1} \quad (72)$$

where  $\lambda_0$  is the theoretical number of heat transfer units associated with the regenerator design.

The value for the number of design heat transfer units is computed as:

$$\lambda_0 = \frac{A_T U_{AV}}{C_g} \quad (73)$$

where  $A_T$  is the heat transfer surface area

$U_{AV}$  is the overall coefficient of heat transfer, approximated for our purposes by the convection heat transfer coefficient,  $h$ ,

and  $C_g$  is the gas flow stream capacity rate  
 $= \dot{m} c_p$ .

We can thus write the approximation,

$$\lambda_0 \approx \frac{A_T h}{\dot{m} c_p} \quad (74)$$

Since the convection coefficient,  $h$ , is not always accurately computed from basic heat transfer principles, it is useful to determine it indirectly for a particular heat exchanger configuration from experimental evaluation of the Stanton number,  $N_{ST}$ , a dimensionless heat transfer modulus defined as:

$$N_{ST} = \frac{h}{G C_p} \quad (75)$$

where  $G$  is the regenerator flow-stream mass velocity,

$$G = \dot{m} / A_c \quad (76)$$

with  $A_c$  being the minimum free-flow area of the heat exchanger.

If we neglect entrance, exit, and flow acceleration effects in the regenerator, Fanning's equation which describes the flow pressure drop due to core friction can be written as:

$$\frac{\Delta P}{L} = \frac{f}{2} \frac{G^2}{\rho} \frac{1}{r_h} \quad (77)$$

where  $\Delta P$  is core pressure drop  
 $L$  is length of the flow path  
 $f$  is the Fanning friction factor  
 $\rho$  is average gas density  
 and  $r_h$  is the hydraulic radius of the flow path

defined as

$$r_h = \frac{L A_c}{A_T} \quad (78)$$

If we define the heat transfer "J" factor as,

$$J = N_{ST} N_{PR}^{2/3} \quad (79)$$

where  $N_{PR}$  is the Prandtl number:

$$N_{PR} = \frac{\mu C_p}{k} \quad (80)$$

then Fanning's equation can be rewritten to relate the pressure drop and heat transfer characteristics of the regenerator in the form:

$$\frac{\Delta P}{\lambda_0} = \frac{G^2 f}{2 J} \frac{N_{PR}^{3/2}}{\rho} \quad (81)$$

Consequently, the required length of the regenerator heat transfer matrix can be determined by combining the two forms of Fanning's equation.

$$L = \frac{\rho_h \lambda_0 N_{PR}^{3/2}}{J} \quad (82)$$

3.2.2 Multiple Stage Refrigeration. Up to this point we have been considering a simple "single stage" refrigerator wherein a single regenerator was used to span the temperature range between  $T_H$  and  $T_C$ .

It has been found experimentally, however, that machines capable of achieving temperatures lower than 50 - 70°K achieved their maximum efficiencies if several stages of cooling were employed. This staged cooling allows heat leaks to be intercepted at temperatures warmer than the desired design temperature. In addition, the stage concept allows extra refrigeration to be made available (for example, to cool radiation shields at these intermediate stage temperatures) with a relatively modest penalty in work-input, compared with providing that same quantity of refrigeration at the lowest design temperature.

In order to understand the performance of a typical three-stage refrigerator a model can be developed wherein the gas expanded at each stage undergoes a series of processes which each can be described on a P-V diagram as illustrated in Figure 29. Each volume of gas works

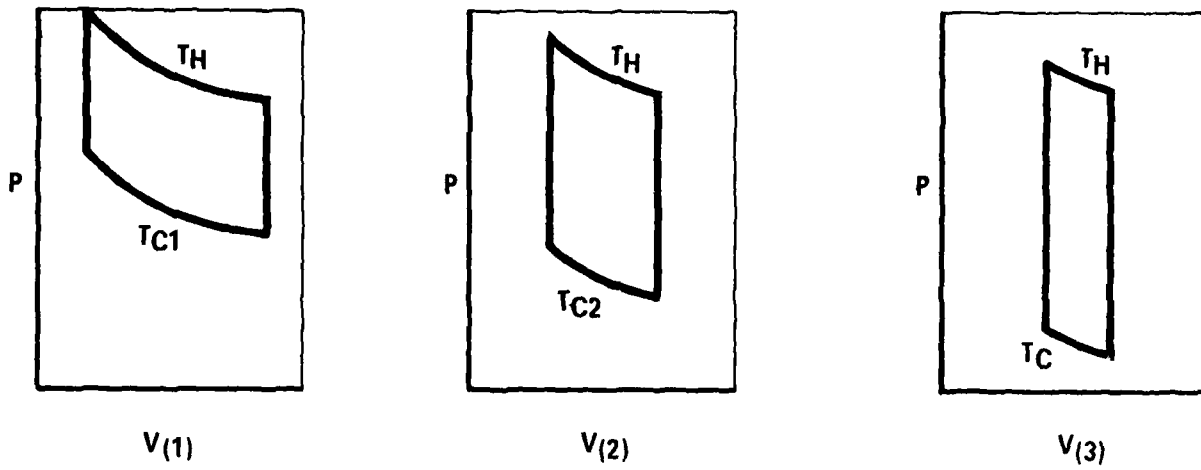
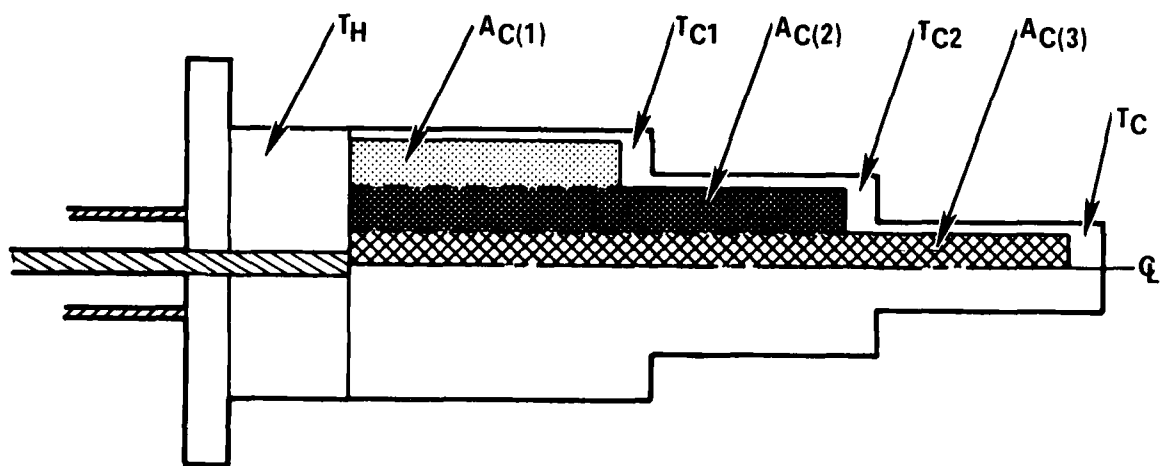


**Figure 29. P-V Diagram Representation for Multiple Stage Refrigerator**



$A_C(1)$  : FLOW CROSS SECTION FOR STAGE 1  
 $A_C(2)$  : FLOW CROSS SECTION FOR STAGE 2  
 $A_C(3)$  : FLOW CROSS SECTION FOR STAGE 3

Figure 30. Idealized Gas Flow Paths for Multiple Stage Refrigerator

between temperature limits established by the cold working temperature of that stage and some  $T_H$  established typically by the crankcase ambient temperature of the machine.

The flow path for each stage is conveniently conceptualized as shown in Figure 30. Neglecting mixing (which is immaterial as long as we have "perfect" regenerators), the gas to be expanded at the first (warmest) refrigeration stage can be considered to flow through the length of the first stage regenerator, requiring some free-flow area  $A_{c(1)}$  of the overall regenerator frontal area. Likewise the gas to be expanded in Stages 2 (intermediate stage) and 3 (coldest stage) will require the amount of flow area designed as  $A_{c(2)}$  and  $A_{c(3)}$ , respectively. We can express the total required free flow area of this first stage regenerator as:

$$A_c^{(1)} = A_{c(1)} + A_{c(2)} + A_{c(3)} \quad (83)$$

Similarly, the total free flow area of the second stage is,

$$A_c^{(2)} = A_{c(2)} + A_{c(3)} \quad (84)$$

and for the third stage,

$$A_c^{(3)} \equiv A_{c(3)} \quad (85)$$

since flows earmarked for the warmer stages undergo their expansion at that earlier stage and then flow back to the ambient temperature crankcase.

It may be useful to think of this multi-stage process as three devices operating in parallel (not in series), each one independently undergoing the processes shown in Figure 29, only coincidentally thermodynamically coupled

AD-A686 098

SCITECH CORP SANTA ANA CA  
LOW TEMPERATURE REGENERATOR STUDY.(U)  
AUG 79 P J WALSH

F/O 13/1

UNCLASSIFIED

APPDL-TR-79-0009

F33618-78-C-3025  
NL

2 of 2

2025-08-08



END

DATE

FILED  
3 - 80

DDC

via the common mechanisms of the refrigerator. To further belabor this point, the overall regenerator temperature gradient required for proper heat transfer between  $T_H$  and  $T_C$  during the two isochoric processes of the cycle is provided in part by the first stage regenerator (from  $T_H$  to  $T_{C1}$ ), in part by the second stage regenerator (from  $T_{C1}$  to  $T_{C2}$ ), and finally by the third stage regenerator (from  $T_{C2}$  to  $T_C$ ). It is only in this sense that we can talk about the stages being arranged in "series" in this particular model.

Equations 60 through 85 must be evaluated for each refrigeration stage during the process of designing a multi-stage machine. For purposes of this study program, however, our chief interest focuses only on the variation in performance of the coldest stage of such a device caused by variations in the specific heat of the material used as the heat storage matrix in the regenerator.

Recognizing that no stage of a multi-stage refrigerator operates as an ideal heat pump, still we lose very little in generality by assuming that whatever the regenerator efficiency and stage losses associated with the first and second stages of a particular device happen to be, they do not change with a variation in third stage matrix specific heat, and therefore treating the two warmer stages as having perfect regenerators.

Having made this assumption, the work input necessary to absorb the heat loads of these warmer stages can be computed based on Carnot performance then merely scaled up in accordance with the relationship a manufacturer's typical machine has to the theoretical minimum power requirements.

3.2.3 Cold Stage Analysis. When we focus on the performance of the third stage regenerator, we find that its actual

efficiency ( $\epsilon$ ) differs from the theoretical design efficiency ( $\epsilon_0$ ), being a strong function of the ratio of total matrix (thermal) stream capacity ( $C_R$ ) to the gas (thermal) stream capacity ( $C_g$ ). The matrix stream capacity is defined as follows:

$$C_R = \int_0^L \frac{M_R}{\tau_c} c_m(L) dL \quad (86)$$

where

$M_R$  is the total mass of heat transfer packing traversed by the gas stream during the cycle, and is equal to twice the regenerator mass ( $m_R$ )

$\tau_c$  is the cycle time required for the system to pass through all the states of the P-V diagram, and the functional notation  $c_m(L)$  emphasizes the fact that the cold stage matrix specific heat can vary with axial location.

We can also define blow time ( $\tau_B$ ) as the time required for the helium gas to pass through the regenerator in either direction, and approximate this time by the relationship

$$\tau_B \cong \frac{1}{2} \tau_c \quad (87)$$

Thus

$$C_R \cong \int_0^L \frac{m_R}{\tau_B} c_m(L) dL \quad (88)$$

If we make the further approximation that the specific heat of helium gas is constant in this temperature region, then the gas stream capacity relationship is

$$C_g \cong \dot{m} c_p \quad (89)$$

and consequently,

$$C_R / C_g \cong \frac{\int_0^L m_R c_m(L) dL}{\dot{m} c_p \tau_B} \quad (90)$$

Current design technology takes this variation in the ( $C_R / C_g$ ) ratio into account by "derating" the theoretical design value for the number of transfer units ( $\lambda_0$ ) depending on the average value of this ratio for the matrix. The relationship is<sup>29</sup>:

$$\lambda = \lambda_0 \left[ 1 - (C_R/C_q)^{\lambda_0} \right] \quad (91)$$

where  $\lambda$  is the number of transfer units actually achieved in the regenerator initially designed to provide a value of  $\lambda_0$ .

This equation is not physically realistic\*, since it equals zero at a point where  $C_R = C_q$ , and it predicts negative values of  $\lambda$  if the matrix stream capacity is less than the gas stream capacity. We expect regenerator performance to suffer seriously, of course, when this ratio becomes small, but there is no a priori reason that heat exchanger performance should dramatically cease when the ratio is unity.

Lambertson<sup>30</sup> analyzed this variation of regenerator efficiency as a function of stream capacity ratio, assuming a constant specific heat for the matrix lengths, by employing a finite difference heat balance network and iterating it using a digital computer. His results show conclusively that the number of transfer units -- and hence the actually achieved efficiency ( $\epsilon$ ) -- are finite even when the ratio is unity along the entire matrix length. Note that the actually achieved efficiency and the actually achieved value for transfer units are related by an equation similar to the defining equation for theoretical efficiency:

$$\epsilon = \frac{\lambda}{\lambda + 1} \quad (92)$$

-----  
\* Depending, of course, on how the designer determines the "average" values to be assigned to  $C_R$  and  $C_q$ .

In actuality, since the stream capacity parameter of the matrix varies along the length of the regenerator due to the matrix specific heat fall-off with temperature, we will find that the ratio will (typically) approach a value of unity only towards the cold end of the regenerator.

If we consider the first increment of gas flowing through the regenerator during the "hot blow" half cycle (i.e., gas flow from  $T_h$  toward  $T_c$ ), the gas will be cooled so as to approximate the roughly linear temperature gradient of the matrix until this stream capacity ratio attains some low value approaching unity. At these low values of the ratio the gas will continue to be cooled, but will itself tend to more rapidly warm up the lowest temperature segment of the matrix since the specific heat fall-off of the solid now results in the gas stream capacity being comparable to -- or even greater than -- that of the matrix. When the second and later increments of gas reach this same point along the regenerator length, the warmer matrix temperature now obtaining means that poorer heat transfer will take place. Consequently, the overall effect results in a regenerator which "looks" to be shorter than the design length (since the expected linear temperature gradient at the cold end is distorted), so the effective number of transfer units,  $\lambda$ , is less than the theoretical design value,  $\lambda_0$ , as can be seen from Eq. 82 .

Results stemming from Lambertson's finite difference network analysis can be fit empirically (for a limited range of  $\lambda_0$  values and  $(C_r/C_g)$  ratios) with an equation of the form:

$$E = E_0 \left[ 1 - I (C_r/C_g)^k \right] \quad (93)$$

Lambertson's analysis was limited to conditions where the  $(C_r/C_g)$  ratio ranged from 1 - 5 and where values

of  $\lambda_0$  varied from 1 - 10. Howard and Bahnke<sup>31</sup> subsequently used similar finite difference iteration techniques to extend these results to values of  $\lambda_0$  in excess of 200. The range of the Howard calculations encompasses values of the variables ( $C_R/K_g$ ) and  $\lambda_0$  usually encountered in cryogenic refrigerator design.

The form of Eq. 93 was fit to the Howard data set using a multi-linear regression technique, with the resulting value for the coefficients:

$$\epsilon = \epsilon_0 \left[ 1 - .0587 (C_R/K_g)^{-1.93} \right] \quad (94)$$

The published data set includes too few points to allow a comprehensive assessment of the fit achieved, but based on the data available a correlation coefficient of about 95% was obtained. The empirical equation predicts efficiency values which differ by a maximum of about  $\pm .5\%$  from the Howard results. Even this small variance is undesirable, but since experimental verification of the published data has apparently not been undertaken - at least not to this third decimal point accuracy - further work to improve the statistical fit is not warranted.

Since the value of  $C_R$  varies along the length of the regenerator it is apparent that the actually achieved efficiency also varies.

We can express this effect best with the concept of actually achieved efficiency per segment:

$$\epsilon_L^{(i)} = \epsilon_0 \left[ 1 - .0587 \left( \frac{C_R^{(i)}(L)}{C_g^{(i)}(L)} \right)^{-1.93} \right] \quad (95)$$

where  $\epsilon_L^{(i)}$ ,  $C_R^{(i)}(L)$  and  $C_g^{(i)}(L)$  are average values of the efficiency, matrix capacity and gas capacity, respectively, for the  $i^{th}$  segment of the regenerator.

The smaller these (hypothetical) regenerator segments, the more accurate should be the efficiency prediction derived from this equation.

For purposes of this study program, we shall assume that the portions of the heat transfer supplied by the first stage regenerator and the second stage regenerator are idealized, and these two regenerators operate with 100% efficiency. Consequently, gas exiting the second stage regenerator during the "hot blow" will be assumed to be at exactly  $T_{c2}$ , the second stage operating temperature, as indicated in Figure 30.

We shall arbitrarily subdivide the final length of this heat transfer gradient, the so-called third stage regenerator, into three segments, shown in Figure 31, each of which has an efficiency ( $\epsilon_L^{(i)}$ ) associated with it; each  $\epsilon_L^{(i)}$  shall be considered a function of the capacity ratio only.

Since the mass flow through the regenerator is the same in both the cold blow and the hot blow period, it can be shown that for steady state operation the regenerator efficiency can be alternatively expressed in terms of average exit temperatures instead of the heat quantities of Eq. 62. Thus, in general,

$$\epsilon = \frac{\Delta T_{\text{actual}}}{\Delta T_{\text{theoretical}}} \quad (96)$$

or for the total cold gradient of our model:

$$\begin{aligned} \epsilon_{cc} &= \frac{\Delta T_{\text{actual}}}{T_H - T_C} \\ &= \frac{(\Delta T)_{1st\ STG} + (\Delta T)_{2nd\ STG} + (\Delta T_{\text{actual}})_{3rd\ STG}}{T_H - T_C} \end{aligned} \quad (97)$$

Based on this analytical approach, the efficiency equations for the three cold-end segments of Figure 31 can be approximated as:

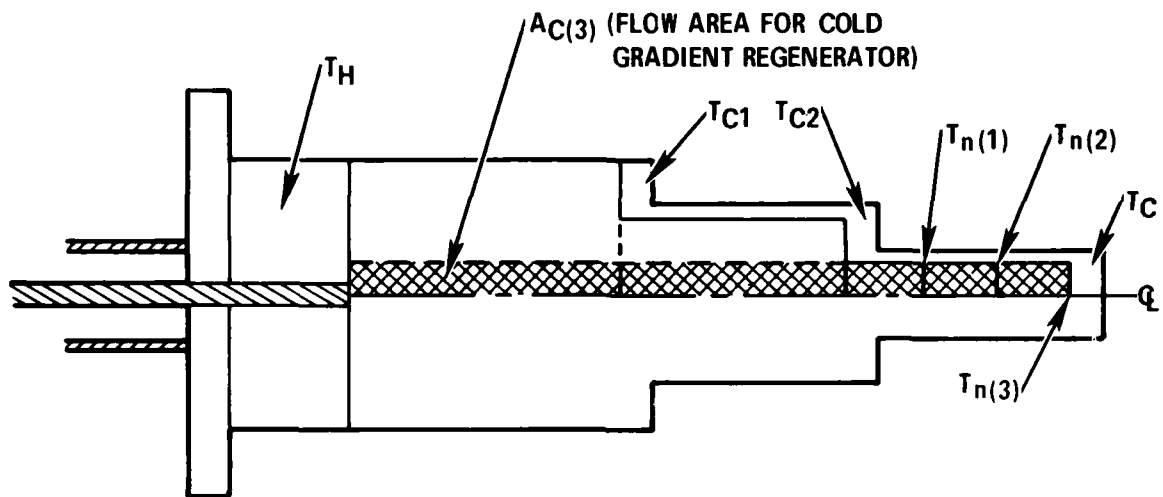


Figure 31. Idealized Refrigerator Model With Segmented Cold Gradient Regenerator

$$\epsilon_3^{(1)} = \frac{T_{c2} - T_{m1}}{\frac{1}{3}(T_{c2} - T_c)} \quad (98)$$

$$\epsilon_3^{(2)} = \frac{T_{m1} - T_{m2}}{\frac{1}{3}(T_{c2} - T_c)} \quad (99)$$

$$\epsilon_3^{(3)} = \frac{T_{m2} - T_{m3}}{\frac{1}{3}(T_{c2} - T_c)} \quad (100)$$

where  $T_{m3}$  is the actual exiting gas average temperature.

The  $\epsilon_3^{(i)}$  can be computed from Eq. 95 sequentially for each of the three segments (using the segment-average for the capacity ratio) and the resulting value used to solve for the actual temperature difference produced in each segment. This done, the effective efficiency for the overall cold gradient regenerator can be computed using the formula of Eq. 97

$$\text{where } \Delta T_{\text{actual}} = T_{c2} - T_{m3} \quad (101)$$

Although this approach is not rigorously accurate (because in actuality each of the segment temperatures is time-varying during a "blow") it should provide a better prediction of regenerator performance than the conventional approaches of assigning a single "lumped" average value to the capacity ratio based on the expected temperature distribution of the matrix.

### 3.3 Refrigerator Performance Calculation

So long as we keep clearly in mind the physical model just developed of three refrigerator stages operating in parallel, it is convenient to treat the third-stage regenerator as if it were a serial heat exchanger, operating between the limits  $T_{c2}$  and  $T_c$ . Conventional design techniques involve the determination of machine size parameters based on the efficiency of this third-stage regenerator computed as:

$$\epsilon_3 = \frac{T_{c2} - T_{m3}}{T_{c2} - T_c} \quad (102)$$

which is a logical extension of Eqs. 98, 99 and 100 .

Heretofore in this report, all design equations have been derived based on the refrigeration produced as the working fluid is taken through one complete cycle of the PV diagram of Figure 26. In order to apply these equations to compute flow and power requirements under dynamic operating conditions, several further approximations will be required. We earlier defined the cycle time,  $\tau_c$ , as the time required for the system to achieve all the states of the P-V diagram; consequently, it is evident that

$$\tau_c \cdot \frac{N}{60} = \tau_c \cdot m = 1 \quad (103)$$

where  $m$  is the number of cycles per second and  $N$  is the RPM of the mechanism.

It was also noted that

$$\tau_B \cong \tau_c / 2 \quad (104)$$

where  $\tau_B$  is the "blow time" when gas flows through the regenerator.

The total mass of gas available for expansion during each cycle is then approximately the average regenerator flow rate multiplied by the flow time or:

$$m = \dot{m} \tau_B \cong \dot{m} \tau_c / 2 \quad (105)$$

The total refrigeration produced per second, is then evidently,

$$\dot{Q} = Q m \quad (106)$$

Thus, from Eq. 60 ,

$$\dot{Q}_{1-2} = -\frac{1}{2} \dot{m} R T_H \ln \frac{v_1}{v_2} \quad , \quad (107)$$

$$\dot{Q}_{2-3} = -\frac{1}{2} \dot{m} c_v (T_c - T_H) \quad (108)$$

$$\dot{Q}_{3-4} = \frac{1}{2} \dot{m} R T_c \ln \frac{v_1}{v_2} \quad (109)$$

$$\dot{Q}_{4-1} = \frac{1}{2} \dot{m} c_v (T_H - T_c) \quad . \quad (110)$$

Regenerator efficiency from Eq. 62 can likewise be defined in terms of refrigeration rate,

$$\epsilon = \left( \dot{Q}_{2-3}^{act} \right) / \dot{Q}_{2-3}^{id} \quad , \quad (111)$$

so that the number of transfer units required in order for a regenerator to operate between the limits  $T_H$  and  $T_c$  is found in the following manner:

Since

$$\lambda_{\text{ROD}} = \frac{\epsilon \dot{Q}_{2-3}}{\dot{Q}_R} = \frac{\epsilon \dot{m} c_p \Delta T}{2 \gamma \dot{Q}_R} \quad (112)$$

We rearrange and find,

$$\lambda_{\text{ROD}} \approx \frac{1}{\ln(P_3/P_4)} \frac{\dot{Q}_{3-4}}{\dot{Q}_R} \frac{c_p}{R \gamma} \left( \frac{T_H - T_C}{T_C} \right) \quad (113)$$

so long as we recognize from Figure 28 that regenerator efficiency must exceed 0.99 for practical refrigerators. The mass flow rate required to provide the desired refrigeration is approximately

$$\dot{m}_{\text{ROD}} \approx \frac{2 \dot{Q}_{3-4}}{R T_C \ln(P_3/P_4)} \quad (114)$$

In order to assess whether or not small particle technology can provide a worthwhile benefit to refrigerator efficiency, a set of calculations has been performed comparing the performance of a conventional lead ball regenerator with a regenerator employing various sizes of ultrafines. The ultrafines as pointed out in the preceding section, achieve an improved heat capacity at low temperature due to the large surface to volume ratio of the material.

If the ultrafines were merely packed into the regenerator shell as a powder bed, the pressure drop for required values of  $\lambda_0$  would be so high that no refrigeration could be produced. The equation to describe pressure drop through a powder bed is the Kozeny-Carmen equation<sup>31</sup>:

$$\Delta P = \frac{S_v^2 \cdot K \cdot (1-\phi) \cdot L \cdot \dot{m}_c \mu}{A \phi^2} \quad (115)$$

where  $S_v$  is the volume specific surface

$A$  is the cross sectional area of the bed

$\phi$  is the porosity of the pack

$L$  is the length of flow path

$\mu$  is the gas viscosity

$\dot{m}_c$  is the rate of flow corrected for compressibility  
 and  $K$ , the Kozeny constant, equals 5 for spherical particles.

It can easily be verified that for even small flow values the pressure drop is prohibitive. It is evident, then, that the ultrafines must be processed into bulk shapes to be useful as regenerator elements. The feasibility of achieving this compacting and shaping, as well as the effect this would have on the surface to volume enhanced specific heat contribution are discussed in Section IV.

For purposes of the refrigeration comparison calculations, it will be assumed that the ultrafines are processed into a shape with a hydraulic radius comparable to the conventional lead ball regenerator. For 0.005 in. balls which will be considered the baseline packing for the regenerator matrix we find

$$r_h (.005 \text{ balls}) = .00136 \text{ cm.} \quad (116)$$

For comparison, if a fine mesh screen were used,

$$r_h (400 \text{ mesh}) = .00139 \text{ cm.} \quad (116a)$$

For convenience, we will assume the ultrafines are compacted into spherical shapes of the baseline packing size so the enhanced performance can be directly compared to a bulk lead regenerator of similar configuration.

Although several materials were identified in Section II which evidence a greater surface specific heat enhancement, it is likely that initial testing of this effect will employ ultrafines of lead since its toxicity characteristics are well known and there is

some experience to be drawn upon in both handling the material and producing powders of the required size. Thus, the curve of Figure 25 can be used to determine the specific heat characteristics of the heat exchanger. These values are tabulated in Table 3 for the four test cases for which refrigerator performance calculations have been performed:

- Case I -  $T_H = 35^\circ\text{K}$ ,  $T_C = 15^\circ\text{K}$
- Case II -  $T_H = 35^\circ\text{K}$ ,  $T_C = 10^\circ\text{K}$
- Case III -  $T_H = 35^\circ\text{K}$ ,  $T_C = 5^\circ\text{K}$
- Case IV -  $T_H = 15^\circ\text{K}$ ,  $T_C = 5^\circ\text{K}$ .

In order to obtain numerical results for refrigerator performance, the baseline model of Table 4 was assumed.

The values in the table are intended to be compatible with calculations for the High Capacity Vuilleumier Refrigerator performance, as determined by the Vuilleumier Cycle Cryogenic Refrigerator Optimization Computer Program<sup>32,33</sup>. That program is tailored to the Hi-Cap VM machine whereas the calculations reported here are based on the idealized Stirling cycle of Figure 26, so power estimates and sizing can't be directly compared between the two. However, the Hi Cap results allow us to assign physically realistic values to our model for gross heat loads and operating temperatures for the three stages,

In particular, it should be noted that the ratio of regenerator heat loss to gross third stage refrigeration,  $(\dot{Q}_2/\dot{Q}_{3-4})$  as determined by that program and as used in Table 4 is typical of well designed Stirling cycle or VM cycle machines, and the gross third-stage refrigeration of 2.785w is a typical value needed to produce a net of about 0.3w available for the external load at about  $10^\circ\text{K}$ . The difference between the gross output and net output is the sum of the regenerator loss, which we primarily focus on in this report, and the other stage losses treated in detail elsewhere<sup>34</sup>.

	TEST CASE 1 $T_H = 35^\circ\text{K}$ $T_C = 15^\circ\text{K}$				TEST CASE 2 $T_H = 35^\circ\text{K}$ $T_C = 10^\circ\text{K}$				TEST CASE 3 $T_H = 35^\circ\text{K}$ $T_C = 5^\circ\text{K}$				TEST CASE 4 $T_H = 15^\circ\text{K}$ $T_C = 5^\circ\text{K}$			
	BULK	100Å	50Å	22Å	BULK	100Å	50Å	22Å	BULK	100Å	50Å	22Å	BULK	100Å	50Å	22Å
$C_{pm}(T_H)$	.0696	.0696	.0696	.0696	.0696	.0696	.0696	.0696	.0696	.0696	.0696	.0696	.0334	.0386	.0439	.0573
$C_{pm}(m)$	.0792	.0792	.0792	.0792	.0721	.0755	.0789	.0677	.0695	.0737	.0778	.0882	.0206	.0246	.0287	.0390
$C_{pm}(m^2)$	.0606	.0662	.0719	.0862	.0460	.0519	.0578	.0728	.0334	.0386	.0439	.0573	.0070	.0090	.0108	.0156
$C_{pm}(T_C)$	.0334	.0386	.0489	.0573	.0130	.0160	.0190	.0265	.0017	.0025	.0032	.0057	.0017	.0025	.0032	.0051

Table 3. Specific Heat Values for Third Stage Regenerator  
(Tabulated Values, in Joules/cm<sup>3</sup>/K, Correspond to  
Endpoints of Segmented Model -- Fig. 23)

TABLE 4  
 BASELINE REFRIGERATOR MODEL

1) Crankcase temperature	324°K
2) First-stage temperature	67°K
3) First-stage gross output	57 w
4) Second-stage temperature	35°K, Case 1, 2, 3 15°K Case 4
5) Second-stage gross output	22 w
6) Regenerator efficiency for first stage and second stage	100%
7) Mechanism operating speed	600 RPM
8) Base cycle pressure	40 atm
9) Expansion pressure ratio	1.4
10) Third-stage parameters.	
a) Regenerator hydraulic radius (.005 lead spheres)	0.0013 cm
b) Regenerator Reynolds Number (optimized so f/j is at 16.6)	500
c) $\dot{Q}_{3-4}$ (gross output)	2.785 w
d) $\dot{Q}_R/\dot{Q}_{3-4}$	0.395
e) Net refrigerator output	0.3 w
f) Maximum regenerator pressure drop	0.5 atm

### 3.3.1 Interpretation of Calculated Results

The results of refrigerator performance analysis are presented in Table 5. For each test case, the required third-stage values of  $\dot{m}_{R0D}$  and  $\lambda_{R0D}$  to satisfy the baseline model conditions of Table 4 were computed from Eqs. 113 and 114 .

Using an iterative approach a design value for heat transfer units ( $\lambda_0$ ) for the (bulk material) lead sphere matrix was assumed, then sizing calculations were performed and the appropriate derating factors (to account for low temperature specific heat fall-off) were applied. The resulting value of "effective" number of transfer units was compared with the  $\lambda_{R0D}$  value (from Eq. 114 , and the iteration was continued until a reasonable agreement was achieved. This iterative technique determined the "design" value,  $\lambda_0$  , to be employed for sizing the physical parameters of the mechanism.

For each test case three additional iterative computations were performed; one each for the spheres made of 100A<sup>o</sup>, 50A<sup>o</sup> and 22A<sup>o</sup> lead ultrafines. The iterative technique again showed an optimum design value associated with that size of ultrafines, to be employed for sizing the mechanism. The optimized values of  $\lambda_0$  give rise to values for effective efficiency which differ between the bulk material spheres and the compacted spheres of ultrafines. This incremental change in efficiency is the basis for a potential savings in input power, for a reduction in physical size, or for an increase in the refrigeration available to the external heat load -- thus providing a kind of safety factor to allow for better temperature control of the load.

It is important to understand the implications of the increased efficiency and the options for improvement which are presented.

Option 1. Reduction in the Design Value of Transfer Units

In general, an enhanced specific heat obtained through the use of ultrafines in the regenerator matrix allows the refrigerator designer to select a lower design value for  $\lambda_0$  than if he were working with conventional matrix materials. Several parameters can be traded off to optimize the method of lowering the design value but Eq. 117 gives some insight as to the benefit which will accrue.

$$L = \frac{\eta_r \lambda_0 N_{FR}^{2/3}}{J} \quad (117)$$

The variables are to some extent functionally inter-related, but it can be seen that a lower value of  $\lambda_0$  allows the designer to either proportionally reduce the regenerator length or to increase the hydraulic radius. In the one case he is opting to reduce the size of his machine and in the other to reduce the flow friction losses in the regenerator. In addition to reducing the thermodynamic flow friction losses this latter approach will contribute to improved reliability by lowering the loads on bearings and seals. This first option is not considered to be the most advantageous way of capitalizing on the specific heat enhancement.

Option 2. More Capacity at  $T_c$  for the External Load

For a given design value for  $\lambda_0$ , an improved matrix specific heat results in a greater value for regenerator efficiency, since the effective value for  $\lambda$  increases. If the regenerator efficiency is improved, then the regenerator losses are reduced,

$$\dot{Q}_R = (1 - \epsilon) \dot{Q}_{2-3} \quad (118)$$

This reduction in regenerator heat loss is directly available as added capacity for the external load since from Eq. 66 :

$$\dot{Q}_{3-4} = \dot{Q}_{ext} + \dot{Q}_R + \dot{Q}_{s.L.} \quad (119)$$

For the same gross refrigeration, and no change in stage losses, a reduction in  $\dot{Q}_R$  directly increases the available  $\dot{Q}_{ext}$ . If the designer elects this option, he will still design to the same  $\lambda_0$  value, but will achieve a safety factor over the designed net capacity as indicated in the table.

Option 3. Reduction of Input Power for the Same Safety Factor in Net Refrigeration

If the designer of current technology refrigerators must provide the same safety factor which could be achieved automatically through the use of ultrafine particles in the regenerator matrix, he must increase the gross refrigeration to overcome the poorer efficiency of conventional materials. The increase in gross output must be achieved through increased mass flow rate, which in turn produces a larger absolute value of regenerator loss for the same effective efficiency value. Eq. 70 can be rearranged as,

$$\dot{W}_R = \frac{\dot{Q}_R}{(\text{COP})_{id} \left\{ \frac{(T_H/T_C - 1)}{(\delta - 1)(\lambda + 1) \ln(P_2/P_1)} \right\}} \quad (120)$$

so that the power requirement can be computed from the regenerator loss value and the effective number of transfer units. Values of input power are compared in the table versus a percentage safety factor provided, a) automatically through the use of ultrafines, and b) by way of increased mass flow when conventional technology is employed.

MATRIX PACKING OF .005 DIAMETER SPHERES MANUFACTURED FROM LEAD	TEST CASE I $T_H = 35^\circ K$ $T_C = 15^\circ K$ $\dot{Q}_R \text{ ROD} = 0.5394 \text{ gM/SEC}$ $\lambda_{\text{ROD}} = 20.3$										TEST CASE II $T_H = 35^\circ K$ $T_C = 10^\circ K$ $\dot{Q}_R \text{ ROD} = 0.8077 \text{ gM/SEC}$ $\lambda_{\text{ROD}} = 38$						
	BULK	PARTICLES				BULK	PARTICLES				BULK	PARTICLES					
		100Å	50Å	22Å	22Å		100Å	50Å	22Å	22Å		100Å	50Å	22Å	22Å		
DESIGN VALUE $\lambda_0$	107	102	99	91	107	107	107	107	107	107	107	107	107	167	167	167	167
THIRD STAGE REGENERATOR SIZE PARAMETERS $L(C_M^1)$	2.78	2.65	2.56	2.37	/	/	/	/	/	/	/	/	/	4.34	4.06	3.82	3.40
$A_C(C_M^2)$	.062	.061	.060	.058	/	/	/	/	/	/	/	/	/	.117	.113	.109	.103
$V_M(C_M^3)$	.28	.26	.25	.22	/	/	/	/	/	/	/	/	/	.83	.75	.69	.57
EFFECTIVE VALUE $\lambda$	20.6	20.3	20.5	20.4	20.6	23.0	25.3	30.2	38.0	38.0	38.2	38.0	38.0	38.0	45.1	51.2	66.7
REGENERATOR LOSS $\dot{Q}_R$ (WATTS)	/	/	/	/	1.0308	.9279	.8482	.7141	/	/	/	/	/	1.0713	.9081	.7937	.6180
% NET REFRIGERATION REQUIREMENT ACHIEVED	/	/	/	/	100	134	161	206	/	/	/	/	/	100	154	193	251
USABLE REFRIGERATION SAFETY FACTOR	/	/	/	/	0	34	61	106	/	/	/	/	/	0	54	93	151
INPUT POWER FOR A REGENERATOR OF BULK MATERIAL TO PROVIDE EQUIVALENT SAFETY FACTOR. $\dot{W}$ (WATTS)	/	/	/	/	447	455	457	461	/	/	/	/	/	471	481	486	494

Table 5. Predicted Regenerator Improvements Obtainable From Small Particle Technology. (sheet 1 of 2)

MATRIX PACKING OF .005 DIAMETER SPHERES MANUFACTURED FROM LEAD	TEST CASE III: $T_H = 35^\circ K$ $T_C = 5^\circ K$ $\dot{m} \lambda_{ROD} = 1.615 \mu M/SEC$ $\lambda_{ROD} = 91.3$										TEST CASE IV: $T_H = 15^\circ K$ $T_C = 5^\circ K$ $\dot{m} \lambda_{ROD} = 1.615 \mu M/SEC$ $\lambda_{ROD} = 30.4$					
	DESIGN VALUE	PARTICLES			BULK	PARTICLES			BULK	PARTICLES						
		100Å	50Å	22Å		100Å	50Å	22Å		100Å	50Å	22Å				
$\lambda_0$	309	285	266	231	309	309	309	309	309	309	309	483	483	483		
$L(C_{M1})$	8.03	7.40	6.90	5.99												
$A_C(C_{M2})$	.318	.305	.295	.275												
$V_M(C_{M3})$	4.17	3.68	3.32	2.69												
EFFECTIVE VALUE	91.3	91.2	91.3	91.3	91.3	110.1	127.4	165.2	30.4	30.4	30.4	30.4	49.4	68.6		
REGENERATOR LOSS					1.0880	.9035	.7876	.6038				1.0645	.6635	.4803		
% NET REFRIGERATION REQUIREMENT ACHIEVED					100	162	202	261				100	234	295		
USABLE REFRIGERATION SAFETY FACTOR					0	62	102	161				0	134	195		
INPUT POWER FOR A REGENERATOR OF BULK MATERIAL TO PROVIDE EQUIVALENT SAFETY FACTOR.					543	562	73	588				815	859	875		

Table 5. Predicted Regenerator Improvements Obtainable From Small Particle Technology. (sheet 2 of 2)

\* Apparent discrepancy in regenerator sizes between test case III and test case IV is due to the fact that only three segments are used in the segmented model and case III requires five segments for accurate calculations.

Using Test Case II of Table 5 to illustrate these options, the following conclusions can be drawn from values tabulated.

1. If  $22 \text{ \AA}$  particles are used to form the .005 in diameter lead spheres in the regenerator matrix, the design value of  $\lambda_0$  for this  $35^\circ\text{K}$  to  $10^\circ$  stage can be reduced from 167 (required for solid lead spheres) down to 131. This reduction shortens the regenerator from 4.34 cm down to 3.40 cm, decreases the critical flow area from  $.117 \text{ cm}^2$  to  $.103 \text{ cm}^2$ , and reduces the lead volume requirements in the matrix from  $.83 \text{ cm}^3$  to  $.57 \text{ cm}^3$ .
2. Alternatively, if the original sizing calculations are used and the refrigerator uses a design value for  $\lambda_0$  of 167, the spheres made of  $22 \text{ \AA}$  particles will provide an effective value for transfer units of 66.7, as compared with the bulk material value of 38. Additionally, the regenerator loss will decrease to  $.6180w.$ , as opposed to  $1.0713w.$  for the bulk material, providing a 151% safety factor for the  $0.3w.$  net refrigeration requirement.
3. Using this same design value of 167 for  $\lambda_0$ , the 151% safety factor will be achieved with a refrigerator power input of  $471w.$ . If the bulk material were used, and a comparable safety factor were desired, mass flow rate would have to be increased and the minimum input power necessary to achieve the needed gross refrigeration increase would be  $494w.$

## IV ULTRAFINE PARTICLE TECHNOLOGY

### 4.1 Introduction

In an earlier section of this report it was determined that finely divided powders show an increase in the low temperature specific heat value when compared with the bulk material. This effect is at least approximately proportional to specific surface of the sample. This proportionality probably holds at least down to particle diameters of 20 - 30 Å.

For maximum improvement in the performance of cryogenic refrigerators it is obviously desirable to maximize the specific heat of the material used to store energy in the regenerator matrix. Thus it is of interest to determine whether this desired improvement can be effected by utilizing small particle technology to take advantage of this specific heat enhancement.

Calculations presented earlier indicate that a worthwhile improvement in regenerator performance due to this effect would require that particles 100 Å in diameter or smaller be used to make up the heat exchanger matrix. Particles of this size category are usually referred to as ultrafines, and are comparable in size, at least in the low end of the range, to some of the larger single molecules. Consequently, we are approaching a physical limit of what can be still called a particle when we consider substances much below 100 Å.

In the past decade numerous technical reports have been published regarding the production, measurement, and handling of small particles of both dielectric and metal substances. Because metal powders have potentially a larger specific heat for a given Debye temperature value, generally higher bulk densities, and generally more favorable mechanical properties, they are more attractive than dielectrics for use in low temperature regenerator experiments.

Much of the early work in production and handling

techniques for ultrafine powder, however, involved dielectric materials instead of metals. These materials are not generally as hazardous to work with as the pure metals, which tend to be highly reactive as well as being, in many cases, highly toxic.

#### 4.2 Production of Particles

There are a surprisingly large number of ways that ultrafine particles can be produced. Rather than survey all of the possible methods in this report, the reader is cited to several excellent review articles which themselves provide numerous references<sup>35</sup>.

Several of the methods, including the electrostatic precipitation and inert gas evaporation methods, seem to show up repeatedly in the literature. We can thus conclude that the resulting particle production, especially from the inert gas technique is more or less reliable and that the size distribution is narrow enough to satisfy scientific measurement requirements.

Most of the ultrafine powder samples first used for specific heat measurements of dielectric materials in the 1950s were produced by an electrostatic precipitation process, wherein the crystal was heated in a dry atmosphere until it vaporized. The smoke particles thus produced were collected in a high voltage alternating current electrostatic precipitator. They were subsequently handled under scrupulously anhydrous conditions since exposure to moisture caused an increase in particle size. Specific surfaces of sodium chloride as large as  $96 \text{ m}^2/\text{gm}$  (corresponding to about  $1000 \text{ \AA}$  cube edge) have been prepared by this method. Smaller particles of  $\text{MgO}$ , having a specific surface of  $166 \text{ m}^2/\text{gm}$  (corresponding to about  $100 \text{ \AA}$  cube edge), were produced by Lien and Phillips<sup>36</sup> using a dehydration technique, the details of which were not reported by them.

Other methods which reportedly yield predictable and reproducible results include the decomposition of

specially prepared metal-organic compounds<sup>37</sup> -- apparently used primarily for the preparation of refractory oxides -- and the high temperature decomposition of carbonyl vapor<sup>38</sup>, which was an early method used to produce particulates of high purity metal.

Much of the recent work with metals involves one variation or another of the inert gas evaporation method. In this technique a pure metal sample is homogeneously and rapidly heated, often either by induction heating or temperature-stabilized oven techniques, to produce a super-saturated vapor within an inert gas atmosphere of the evaporation apparatus.

Nucleation and growth of the metal particles begins in the gas atmosphere. During this process traces of impurities are highly undesirable since they will cause oxides, nitrides, or other contaminated forms of the particles to grow. Success of this method in producing narrow size distributions of ultrafine high purity particles seems to be related to the size of the inert gas molecule, as well as to the ability to rapidly achieve a highly super-saturated condition of the vapor. This high degree of supersaturation is conducive to the formation of a large number of condensation nuclei and to subsequent slow growth, which allows a reasonable (but short) time to collect the ultrafines -- often on a water-cooled surface which inhibits further nuclei development. The particles so collected must be stored in vacuum or in an inert gas atmosphere since the high surface to volume ratio results in a large excess surface energy which not only tends to form agglomerations of particles but also results generally in strong pyrophoric tendencies.

An interesting variation on this inert gas evaporation technique will be discussed in a later section as the best candidate system for providing a production scale-up of the technology, should the later test phases of this program confirm the current analytical predictions of refrigerator efficiency improvement.

4.2.1 Measurement and Grading of Ultrafine Powders. The BET adsorption isotherm technique, introduced earlier, has been the accepted standard method of determining the area of finely divided powders since its inception. In this method the amount of gas (typically nitrogen maintained near its condensation point) which adsorbs on the active surface of the powder is determined by measuring a change in pressure of the test chamber before and after the adsorption process takes place. This method is time consuming and requires precise process controls, but provides a highly accurate result.

There have been recent attempts to develop less time consuming dynamic gas flow techniques utilizing air permeability measurements to determine powder surface areas, but in general the accuracy is questionable and the range of measurement capability doesn't extend to the ultrafines which are of interest for this program.

An important disadvantage of the BET method is that it measures only total surface area, and doesn't allow a determination of the distribution of particle sizes within a sample. Size distribution is critically important for the regenerator specific heat enhancement application because only those particles below about  $100 \text{ \AA}$  in size will evidence a large enough enhancement effect so as to improve regenerator efficiency. Consequently, if a given test sample of suitable "average" particle size were made up of an extreme bi-modal distribution, e.g. one group of  $300 \text{ \AA}$  and one of  $10 \text{ \AA}$  particles, the resulting measurable enhancement in specific heat could conceivably be almost nil, depending on the numbers of members of each distribution which combined to produce the average surface area of the sample.

Because of the growing industrial interest in ultrafine powders for high performance magnets, self-lubricated bearings, and dispersion strengthened alloys, considerable experimental and theoretical work in the past decade has

addressed the question of size distribution.

Since the BET method cannot investigate the size distribution function, electron microscope techniques are commonly employed for this purpose. Although many researchers also employ this instrument to estimate the actual specific surface area of a powder sample, there is apparently no consensus that it can replace the BET method for area determination.

Granqvist and Buhrman<sup>39</sup> have reported that ultrafine powders tend to take a spherical shape, rather than follow the appropriate crystal habit, if the particle diameter is below about 200 Å. They further determined that, provided the inert gas evaporation technique is used, the size distribution follows a log normal distribution function with standard deviation in the range  $1.36 \leq \sigma \leq 1.60$ .

They corroborated this theory with extensive electron microscope studies of ultrafines produced from aluminium oxides, chromium, iron, cobalt, nickel, copper, gallium, magnesium, zinc, and tin.

Consequently, if the inert gas evaporation method of producing ultrafines is employed, the question of how to grade and separate the particles to be used in later test phases of the current program disappears.

4.2.2 Predicted Availability of Test Materials. There is no longer any question that gram-size samples of spherical ultrafine metal particles, with nominal diameters of about 50 Å, and acceptably narrow size distributions, can be produced. In order to advance into the next phase of this program, however, it is necessary to determine how to acquire such powders made from the materials identified earlier as the best candidates for the refrigerator efficiency improvement application.

The powder metal industry does not currently work with powders much smaller than 400 mesh. A 400 mesh screen has openings of about 45 μm on a side. Particles which

pass through such a screen are obviously smaller than the opening, but still two-to-three orders of magnitude larger on average than the ultrafines which will exhibit a sufficiently enhanced specific heat effect for purposes of the regenerator application.

An extensive survey of the leaders in this powder metal industry has demonstrated convincingly that 50 - 100 Å powders are not currently available off the shelf.

A survey of industrial research laboratories which specialize in materials development also turned up negative results. This survey included companies like Union Carbide, Celanese, Dupont, Bethlehem Steel, Hercules Inc., GCA Corp., and Ethyl Corp., among others. Of this group only Ethyl Corp. reported prior experience in ultrafine particle production (of aluminum). Their activity was discontinued some time back for economic reasons.

Finally, a survey of academic institutions was conducted, using author names and institutions obtained from recently published papers on small particles. Based on this effort it was determined that Cornell University, Ithaca, N.Y., has the capability currently to produce particles of the size and distribution characteristics necessary for further experimental work on this program. Based on discussions with personnel from that organization, indium must be eliminated from the list of candidate materials presented earlier since its ultrafines are apparently exceedingly soft and tend to form films instead of collectible particles. Lead and selenium, our other two primary candidates, are considered by them to be viable materials for particle production, with the toxicity characteristics of the latter needing more investigation.

As noted earlier, the preferred method of particle preparation is the inert gas evaporation technique which was analyzed in detail by the researchers at Cornell. For production scale-up of the particle production,

providing that test results in later program phases remain encouraging, a variation of the inert gas technique has already been pioneered by a Japanese laboratory. Yatsuya, Mihama, and Uyeda<sup>40</sup> recently reported on a vacuum evaporation technique which captures the newly formed ultrafines in the oil film flowing outboard under the influence of centrifugal force on a rotating disc inside the bell jar. This is essentially a continuous production operation, and the particles are subsequently separated from the oil by distillation techniques. The researchers have projected that the technique is suitable for reasonably large scale production.

#### 4.3 Methods of Regenerator Production

Very little work has been done to date to develop techniques for handling ultrafine powders and forming or shaping materials made from them. Since, as noted, the particles can't be employed in a refrigerator merely as a packed power bed due to pressure drop considerations, it is necessary to fabricate special regenerator elements from them.

In the process of forming the particles into usable shapes, care must be taken not to destroy the high surface to volume ratio which gives rise to the enhanced specific heat effect.

Several classes of methods suggest themselves for forming the ultrafines into usable configurations. First, techniques from the powder metallurgy industry can be applied. In forming powdered metal components, a two-stage approach is commonly followed. The raw powders are initially pressed into a "green compact" stage, where the amount of surface welding or alloying is minimal and is related to the pressure of compacting. This green compact has generally poor mechanical properties until it is heated to just under the melting temperature and "sintered", wherein heavier surface welding takes place.

Heavy surface welding is obviously undesirable for our application, since discrete particle characteristics must be preserved. Thus, an optimum green compacting pressure must be determined to provide maximum strength of the element with an acceptable level of alloying or welding as determined from specific heat measurements.

There is a precedent for this approach. The experiment of Comsa, et al, on palladium ultrafines, noted earlier, was designed so that the powders were compacted into a small pellet before the specific heat was measured. This processing yielded a Montroll effect which fit the analytical predictions exceedingly well. However, they did not make any determinations of the mechanical strength of the compact.

An advantage in this approach is that the metal compact will act as a helium sponge in the regenerator, since the large surface to volume ratio will encourage an adsorbent-adsorbate relationship. A disadvantage in the approach is that there will be a tendency, the seriousness presently unknown, for the lightly welded ultrafines to break off from the compact and move with the gas flow through the regenerator as a smoke. In addition to causing an undesirable virtual heat leak through this "pumping" action, the ultrafines conceivably could cause bearing and seal deterioration if they are not contained inside the regenerator.

With present technology, it is impossible to positively contain free particles smaller than about 200 Å. Consequently if the individual particles break away from the compact some migration will take place.

One interesting approach to this problem comes from the field of powder metallurgy itself. Studies into the porosity of metal compacts employ a process called mercury porosimetry. In this technique, liquid mercury under high pressure is forced into the pore structure of the formed element. The pore volume is determined

by the amount of mercury which flows during the pressure cycle. Since the pore structure is the mirror image of the compact, we can expect that the mercury will flow into a three dimensional shape which itself is characterized by a high surface to volume ratio. Current technology allows mercury to penetrate pore sizes as small as  $18 \text{ \AA}$  with pressures achievable with commercial equipment<sup>41</sup>.

From Figure 17 it is known that mercury has a better low temperature specific heat than lead, and also that the surface enhancement for large surface to volume ratios is the highest of any material surveyed to date. Consequently, if the porosimetry approach does indeed yield the mirror image structure, the potential for a complementary effect to the lead enhancement is available.

Since mercury easily alloys with many metals, including lead, it can be expected that surface alloying will take place when the two metals are in contact. This will increase the strength of the green compact, and probably eliminate any objections to using mercury in the regenerator applications founded on its vapor pressure characteristics.

What is currently an unknown, however, is the effect this surface alloying will have on the specific heat enhancement effect. It is believed that the alloy interface will form a wave reflection or scrambling boundary for the low frequency acoustic vibrations, and that this will allow the full Montroll effect to be observed. Until the tests are conducted, however, this is speculation. If the theory developed in Section II for the cluster structure materials proves accurate, however, those materials provide some evidence that the surface enhancement effect survives when ultrafine particles are embedded, and even alloyed, into a metal matrix binder.

The next most feasible approach to containing the particles inside a regenerator draws on the current state of thin film membrane technology. A survey of several organizations involved in both cellulose acetate

and teflon membrane research has provided encouragement that a quantity of ultrafines can be mixed into a batch of the membrane substance and rolled into thin sheets. Estimates of achievable particle-to-membrance density in the 50 - 80% range (by volume) have been obtained.

There are several possible ways of utilizing the sheet material. Membranes of this type are commonly used as filters or separators. They can perform this function because a network of precisely sized pores forms when the substance cures initially. The pore size can be controlled over wide limits, with the smallest diameter being about 0.2  $\mu\text{m}$  for the cellulose acetate and .035  $\mu\text{m}$  for the teflon. Since 400 mesh screen has a pore size in the tens of microns and a hydraulic radius comparable to the lead spheres currently used in regenerators, a membrane formed to approximate a screen of this size could potentially serve as a regenerator element "wafer".

Advantages to this permeable membrane approach include ease of forming the regenerator elements and positive containment of the particles. Disadvantages include the fact that mechanical strength of a membrane is low, and pressure cycling of the helium gas in a regenerator could pose a problem over time.

Lastly, it is attractive to consider merely "gluing" the ultrafines together and avoiding the problems and unknowns inherent in the powder metallurgy and thin membrane technology approaches just discussed.

It has been suggested that an organic binder like GE7031 varnish, which has a good thermal conductivity at low temperature, could be treated chemically so that it would form into a hard compact upon curing. Using centrifuge techniques, the density of ultrafines could be raised to a sufficiently high level in the liquid varnish, and then droplets of approximately the desired size for regenerator elements could be formed and cured.

In addition to the GE varnish approach, a low melting point ceramic which itself has favorable low temperature specific heat characteristics has been suggested as such a binder<sup>42</sup>.

Of the various methods discussed, only the green compact approach has any experimental evidence to directly support its viability. Consequently, based on work by Comsa, et al noted earlier, the best candidate for forming the ultrafines into suitable regenerator elements is this one.

It is unavoidable that a significant amount of developmental work must be invested in this aspect of the application for the program to progress beyond this first phase.

#### 4.4 Safety Considerations

The pyrophoric tendencies of ultrafine metal powders have been noted earlier. In addition to this potential fire and explosion danger, however, the inhalation of these powders can produce a significant health hazard.

For obvious reasons, most inhalation studies have focussed on particles larger than the ultrafines of interest for regenerator applications. Although monodisperse particles in the 20 - 100 Å size can now be reliably produced, fractional micron particles are more commonly available and have been used extensively for clinical experiments.

Based on the work done to date, the number of inhaled particles deposited in the respiratory tract reaches a minimum value at equivalent sphere diameters of 0.3  $\mu\text{m}$ <sup>43</sup>. The deposition fraction increases on both sides of this value, implying that in the ultrafine size region the inhalation problem must be regarded as a danger.

Since lead is likely to be the initial material tested in later phases of this program some discussion

of its hazards is warranted. Lead can enter the body via the skin, by ingestion, or by inhalation. Since inhalation is the most common cause of lead poisoning, and lead vapors are probably comparable in particle size to the ultrafines to be employed on this program, the Occupational Safety and Health Administration guidelines for atmospheric content of lead can serve as a starting point for program safety considerations. Any exposure of humans to concentrations of lead exceeding 0.6 milligrams per cubic meter of air is considered a serious health hazard, and the highest permissible average concentration over an eight hour day is 0.2 milligram per cubic meter.

Safety procedures must also be implemented to periodically monitor the lead content of blood and urine samples from all personnel working in the vicinity.

Lead is not on the State of California, Division of Industrial Safety, list of carcinogenic substances, so no special licensing requirements must be met to work with the substance. Prudent experiment design, however, will employ vented glove boxes and approved personal respirators for personnel in direct contact with the experiment itself.

## CONCLUSIONS

### 5.1 Small Particle Specific Heat

Although early measurement programs on the low temperature specific heat of finely divided materials provided inconsistent results and were plagued with experimental difficulties, recent work in the United States and abroad confirms that a significant specific heat enhancement is available for ultrafines with an equivalent diameter below 100 Å.

Theoretical work to predict this enhancement has been under development for nearly three decades. Rigorous models from lattice dynamics technology are complex to use and currently do no better at predicting the magnitude of the specific heat effect than simple models patterned after conventional Debye analysis.

Based on its excellent correlation to experimental specific heat values for palladium ultrafines, the modified Montroll equation presented in Section II is an accurate enough predictor of enhanced specific heat values for purposes of this intended application.

Applying that equation to the group of low Debye temperature substances which are candidates for use in later experimental phases of this program, we conclude that lead is the best choice for initial experimental work.

### 5.2 Small Particle Availability

There is no doubt that ultrafine particles of nominally 50 Å diameter, with an acceptably narrow size distribution, can be produced using the inert gas evaporation technique. Since the powdered metal industry is not yet working with sub-micron particles -- although there is a recent major thrust in this direction -- a source of lead ultrafines for use on this program has been difficult to locate.

Discussion with research leaders in this field has established that Cornell University has the capability of producing the materials. Cornell may be the only organization in the United States capable of doing this work, although similar capability probably can be located in several foreign research centers. No negotiations have been undertaken to buy the particles from Cornell, but preliminary contacts have been made.

#### 5.3 Cryogenic Refrigerator Performance

As part of this program it was necessary to develop a new regenerator performance model based on the prior work of several researchers to predict efficiency vs. specific heat effects at low temperature. This new model, when applied to four test cases typical of cryogenic refrigerator performance requirements, predicts significant improvements in operating characteristics when selected ultrafine materials are used to form the heat transfer elements in the regenerator matrix.

In particular, the model indicates that the size of the cold stage mechanism can be reduced, a significant safety factor (by way of excess refrigeration capacity) can be provided, a significant power savings can be achieved, or an optimum combination of these three new degrees of freedom can be selected. These savings are judged to be a significant benefit to existing refrigerator technology.

#### 5.4 Regenerator Element Producibility

Of the questions addressed during this research study, the one which is least confidently answered involves the producibility of regenerator elements. Based on recently reported measurement results, a green compact of the powdered material can be formed without destroying the surface enhanced specific heat which is characteristic of the ultrafines. The suitability of

such a compact for use in a periodic flow regenerator, due to mechanical strength considerations, can only be determined by experimental simulations and evaluation.

Several other fabrication techniques have been identified and determined to be candidates for forming regenerator elements. Each of them, however, must be further evaluated experimentally because very little work on the forming and shaping of sub-micron powders has been reported in the literature. This is a new technological area.

The fabrication techniques selected for initial use during the later phases of this program will be the green compact method, and the green compact method combined with the mercury porosimetry technique described in the text.

#### 5.5 Safety

Experimental work with ultrafines of lead introduces additional hazards beyond the toxicity problem normally encountered. The large surface to volume ratio of the powder results in a high energy, exposed surface area. This large surface area will react readily with oxygen (or similar substances) and tends to spontaneously burn or explode. This problem is minimized by storing and handling the materials only in an inert gas environment.

The ultrafines pose an inhalation danger, very similar to lead vapor, thus escalating the health considerations, and normal safety precautions require the use of a vented laboratory hood or glove box, as well as the use of personal respirators for workers who directly contact the material. With these precautions, the hazards can be reduced to an acceptably low level.

#### 5.6 Summary

In summary, the expected small particle specific heat enhancement at low temperature has been verified

to exist. New regenerator analysis models have been developed as part of this program to predict the magnitude of technology improvement to be achieved through use of these materials in cryogenic regenerators.

It has been determined that laboratory techniques for forming the particles have been developed to an advanced state by several research groups. No proven technology currently exists for forming and shaping the particles to a configuration suitable for the cryogenic regenerator application, but no insurmountable problems in this development area have been identified.

Safety considerations will require that special precautions be observed in working with the materials, but again no insurmountable problems are anticipated.

Based on the results of this current program phase, the achievable improvement in refrigerator performance which should be realized through use of small particle technology warrants a continuation of this research activity. The experiment plan for later program phases is included as an appendix.

## REFERENCES

1. A. J. Dekker, Solid State Physics, Prentice Hall, Inc., Englewood Cliffs, 1961, pp. 51-53.
2. K. S. R. Gopal, Specific Heats At Low Temperatures, Plenum Press, New York, 1966, pp. 40-47.
3. E. W. Montroll, "Size Effect In Low Temperature Heat Capacities", J. Chem. Phys. 18, 183 (1950).
4. D. Y. Maa, "Distribution of Eigentones In A Rectangular Chamber At Low Frequency Range", J. Acous. Soc. Am. 10, 235 (1939). Also see, R. H. Bolt, J. Acous. Soc. Am. 10, 228 (1939).
5. J. H. Barkman, R. L. Anderson, and T. E. Brackett, "Low Temperature Specific Heat of Finely Divided Sodium Chloride", J. Chem. Phys. 42, 1112 (1965).
6. D. G. Naugle and R. E. Allen, "Simple Model For Surface Specific Heats", J. Chem. Phys. 63, 991 (1975).
7. M. Du Puis, R. Mazo, and L. Onsager, "Surface Specific Heat Of An Isotropic Solid At Low Temperatures", J. Chem. Phys. 33, 1452 (1960). Also see, R. Stratton, J. Chem. Phys. 37, 2972 (1962).
8. H. P. Baltes and E. R. Hilf, Solid State Commun. 12, 369 (1973).
9. T. S. Chen, G. P. Alldredge, and F. M. de Wette, "Studies Of Vibrational Surface Modes In Ionic Crystals", Surf. Sci., 62, 675 (1977).
10. A. J. Dekker, op. cit., p. 213
11. W. F. Giauque and R. C. Archibald, J. Am. Chem. Soc. 59, 561 (1937).
12. J. A. Morrison and D. Patterson, "The Heat Capacity Of Small Particles Of Sodium Chloride", Trans. Far. Soc. 52, 764 (1956).
13. S. Brunauer, P. H. Emmett, and E. Teller, "Adsorption Of Gases In Multimolecular Layers", J. Am. Chem. Soc. 60, 309 (1938).
14. D. S. MacIver and P. H. Emmett, "Adsorption of Nitrogen On Pure Sodium Chloride", J. Phys. Chem. 60, 824 (1956).
15. W. H. Lien and N. E. Phillips, "Heat Capacity Of Small Particles of  $M_2O$  Between  $1.5^{\circ}$  and  $4^{\circ}K$ ", J. Chem. Phys. 29, 1415 (1958).<sup>g</sup>

16. J. H. Barkman, R. L. Anderson, and T. E. Brackett, op. cit..
17. G. H. Comsa, D. Heitkamp, and H. S. Rade, "Effect Of Size On The Vibrational Specific Heat Of Ultrafine Palladium Particles", Solid State Comm. 24, 547 (1977).
18. V. Novotny and P. P. M. Meincke, "Thermodynamic Lattice And Electronic Properties of Small Particles", Phys. Rev. B, 8, 4186 (1973).
19. E. S. R. Gopal, op. cit., Chapt. 4.
20. K. Schroder, "Effect Of Magnetic Clusters On The Specific Heat Of Ni-Cu And Fe-V Alloys", J. Appl. Phys. 32, 880 (1961).
21. G. Jura and K. S. Pitzer, "The Specific Heat Of Small Particles At Low Temperatures", J. Am. Chem. Soc. 74, 6030 (1952).
22. E. W. Collings, F. J. Jelinek, J. C. Ho, and M. T. Mathur, "Magnetic And Thermal Properties Of Stainless Steel And Inconel At Cryogenic Temperatures", Adv. in Cryo. Engr. 22, 159 (1976).
23. C. G. Granqvist and R. A. Buhrman, "Ultrafine Metal Particles", J. Appl. Phys. 47, 2200 (1976).
24. E. S. R. Gopal, op. cit., Chapt. 2-3.
25. W. E. Gifford and H. O. McMahon, "A New Refrigeration Process", Proc. 10th Int. Cong. of Refrig. (1959).
26. G. Walker, Stirling-Cycle Machines, Clarendon Press, Oxford, 1973, p. 134.
27. See G. Walker, op. cit., Chapt. 4.
28. R. White, Computer Program For Optimizing Three-Stage Vuilleumier Cycle Cryogenic Refrigerators, Air Force Flight Dynamics Laboratory, Wright Patterson Air Force Base, Ohio, 45433, AFFDL-TR-76-27, Feb. 1976.
29. K. W. Cowans, 5<sup>0</sup>K Vuilleumier Cryogenic Refrigerator, Air Force Flight Dynamics Laboratory, Wright Patterson Air Force Base, Ohio, 45433, AFFDL-TR-72-10, Feb. 1972, p. 43.
30. T. J. Lambertson, "Performance Factors Of A Periodic-Flow Heat Exchanger", Trans. ASME 80, 586 (1958).
31. G. D. Bahnke and C. P. Howard, "The Effect Of Longitudinal Heat Conduction On Periodic-Flow Heat Exchanger Performance", Trans. ASME 86, 105 (1964).

32. R. L. Grob, M. A. Kaiser, and M. J. O'Brien, "Specific Surface Area Analyses: Applications And Limitations", Am. Lab. 7, 13 (1975).
33. J. Denney, Principal Investigator, Vuilleumier Cycle Cryogenic Refrigerator Optimization Computer Program, Report P78-193, Hughes Aircraft Co., Culver City, California, April 1978. Also see, Closed Cycle Cryogenic Cooler Technology And Applications, Air Force Flight Dynamics Laboratory, Wright Patterson Air Force Base, Ohio, 45433, AFFDL-TR-73-149 Vol. 1, Dec. 1973 p. 163 (R. White, "Program For Predicting V-M Cooler Off Design Performance").
34. B. Leo, Designers Handbook For Spaceborne Two-Stage Vuilleumier Cryogenic Refrigerators, Air Force Flight Dynamics Laboratory, Wright Patterson Air Force Base, Ohio, 45433, AFFDL-TR-70-54, June 1970.
35. N. A. Fuchs and A. G. Sutugin, Highly Dispersed Aerosols, Ann Arbor Science Publishers, Ann Arbor, 1970 (Chapt. 1).
36. W. H. Lien and N. E. Phillips, op. cit.
37. C. T. Lynch, K. S. Mazdeyasni, and J. S. Smith II, "Preparation and Properties of Refractory Oxides From Metal-Organic Compounds", Proc. Third Intl. Sym., High Temperature Technology, Asilomar, California, 1967.
38. N. A. Fuchs and A. G. Sutugin, op. cit., p. 22.
39. C. G. Granqvist and R. A. Buhrman, op. cit.
40. S. Yatsuya, K. Mihama, and R. Uyeda, "A New Technique For The Preparation of Extremely Fine Metal Particles", Japan J. Appl. Phys. 13, 749 (1974).
41. J. S. Hirschhorn and K. H. Roll, Editors, Perspectives In Powder Metallurgy, Vol. 5 Advanced Experimental Techniques In Powder Metallurgy, Plenum Press, New York, 1970 p. 225.
42. Personal communication, Dr. W. N. Lawless, April 17, 1979.
43. Job Health Hazards Series Pamphlet, "Lead", OSHA 2230, U.S. Dept. of Labor, June 1975

## APPENDIX

### TEST PLAN

#### 1.0 Introduction

The Low Temperature Regenerator study program is divided into several phases. The first phase, now completed, encompassed both a literature survey and the development of analytical models for small particle specific heat, regenerator efficiency, and overall refrigerator performance.

The second phase is designed to include the production, as well as mechanical and thermal testing, of small particles and small particle composites. In addition, the regenerator performance efficiency models developed in Phase 1 will be evaluated and optimized.

The third phase will compare computed values of improved regenerator performance with measured results derived from a refrigerator test bed as well as from simulated dynamic testing in a regenerator test fixture upgraded from the efficiency model test cryostat which will be used in Phase 2.

This test plan details the test logic and requirements for the Phase 2 work. Successful completion of the tasks outlined herein will provide the management and technical information necessary to move into Phase 3 and conduct simulated dynamic testing and actual refrigerator testing of the proposed regenerator design. The Phase 3 program will evaluate the predictions of input power savings and refrigeration capacity improvements derived from the Phase 1 and Phase 2 work.

#### 2.0 Scope of Test Plan

This test plan addresses verification and test activities in two distinct Phase 2 areas; evaluation of small particle (and small particle composite) specific heat enhancement, and evaluation of the segmented regenerator performance model discussed earlier in this report.

### 3.0 Technical Requirements

#### 3.1 Small Particle Specific Heat

Because of the lack of reported measurement results for materials which are candidates for regenerator matrix packings, the specific heat of selected materials produced in several batches will be evaluated. The sampling strategy will be designed to preclude a situation where suspected anomalies due to production peculiarities adversely affect conclusions. Unless toxicity, safety, or producibility problems force a reconsideration, the two test materials will be lead and selenium.

#### 3.2 Small Particle Composites

Small particle composites formed from two different materials and several different production techniques will be evaluated for mechanical and thermal characteristics at room temperature and (selectively) at low temperatures. The redundancy in this approach will again allow evaluation of any anomalies which could cloud results of the measurements. The composites will be formed as, a) pressed green compacts, b) mercury impregnated pressed green compacts, c) permeable membranes loaded with the ultrafines, and d) ultrafines dispersed in a binder and processed to wafer, spherical or cylindrical shapes.

##### 3.2.1 Physical Characteristics

A wafer configuration of the four forms of composites will be used for a preliminary evaluation of physical characteristics of ultrafines. This evaluation will be conducted in two parts. First, to determine binding integrity, a strip of ordinary bond paper sandwiched between the weighed wafer and a 100 gm weight will be pulled for two inches; then the wafer shall be inspected and re-weighed to determine loss of ultrafines due to abrasion. Second, a fracture test will be conducted both at room temperature and at 77°K. This test will consist of applying an axial force (via a 1/16" diameter

ball-end rod) to the wafer, and incrementally increasing the load until significant deformation or fracturing of the composite is observed.

### 3.2.2 Thermal Characteristics

The composites will be evaluated as to heat capacity characteristics in the range from 5 to 100<sup>o</sup>K. In addition to the four types of composites defined in Paragraph 3.2, heat capacity measurements will also be performed for up to two cluster structure materials (as defined in Section II) and/or selected "anomaly" materials which evidence large entropy effects in the low end of the temperature range.

### 3.3 Regenerator Efficiency Equation

In order to test and verify the accuracy of the segmented regenerator efficiency equation developed in Section III, a progressive evaluation program is required. This program encompasses the following four test sequences:

- Test Sequence I - Constant Regenerator Matrix Stream Capacity and constant gas stream capacity.
- Test Sequence II - Multi-segmented Matrix Stream Capacity and constant gas stream capacity.
- Test Sequence III - "Continuously" Variable Matrix Stream Capacity and constant gas stream capacity.
- Test Sequence IV - "Continuously" Variable Matrix Stream Capacity and variable gas stream capacity.

Sequences I, II, and the initial testing of Sequence III will be conducted with the regenerator operating between room temperature and 77<sup>o</sup>K. The remainder of Sequence III as well as Sequence IV will be conducted with the regenerator operating as low as the liquid helium temperature range.

### 3.3.1 Sequence I Evaluation

With an experimental regenerator (R1) built up of material of known specific heat, the Lambertson-London finite difference method of calculating efficiency, as well as the empirical equation from Section III of this report will be evaluated. The reciprocity effects of  $C_r$  and  $C_g$  on regenerator efficiency (i.e. the effect on efficiency of increases of  $C_r$  versus decreases of  $C_g$ ) will be explored. A determination will be made whether or not axial heat conduction must be accounted for in order to correlate measured efficiency with calculated values. Test conditions will encompass NTU values up to about 200 and  $C_r/C_g$  values ranging from 3 or 4 down to below unity.

### 3.3.2 Sequence II Evaluation

With an experimental segmented regenerator (R2) built up of two or three segments of known specific heat, the segmented regenerator model derived in Section III will be evaluated. As in Sequence I, reciprocity effects for high NTU values and low  $C_r/C_g$  ratios will be investigated, and a determination of the importance of axial heat conduction will be accomplished.

### 3.3.3 Sequence III Evaluation

With an experimental regenerator (R3) built up of a larger number of divided segments, the segmented regenerator model of Section III will be applied to approximate the continuously variable matrix.  $C_r$  and  $C_g$  reciprocity characteristics will be investigated again for high NTU value and low  $C_r/C_g$  ratios. Results will be compared with calculated values from the segmented regenerator model, and the importance of axial heat conduction on performance predictions will be assessed.

### 3.3.4 Sequence IV Evaluation

The regenerators used in the Sequence III program will be re-evaluated in the 77 - 5°K range where the specific heat and thus the stream capacity of helium

gas is a function of temperature at the pressure of interest. As before, test results will be compared with calculated predictions, and the importance of axial heat conduction will be evaluated. During a sub-part of this sequence the helium gas flow rate will be varied in a linear manner so that a preliminary model for predicting time varying flow and phase angle effects can be empirically compiled.

#### 4.0 Test Sequence Requirements

#### 4.1 Specific Heat Measurements

The planning network for specific heat measurements is shown in Figure 32. The schedule of tests depicted therein is designed to provide the information base necessary to, a) verify the magnitude of surface enhanced specific heat for powders and powder composites, and b) perform a preliminary evaluation of the mechanical characteristics of powder composites for use in regenerator fabrication. This information will be used to define the scope of follow-on Phase 3 work and to evaluate whether to design and build a prototype regenerator using these effects.

#### 4.1.1 Description of Test Activity Blocks (per Figure 32)

<u>Block No.</u>	<u>Title</u>	<u>Discussion</u>
1	Procure Powders	Ultrafine powders meeting the size distribution requirements of Section II of this report will be procured.
2	Procure Basic Membranes	Cellulose acetate-based and teflon-based membrane materials with defined pore sizes will be procured.

<u>Block No.</u>	<u>Title</u>	<u>Discussion</u>
3	Build Specific Heat Cryostat	A specific heat cryostat will be fabricated from the design package developed as part of the Phase I program.
4	Calibrate Cryostat	Using a specimen of known specific heat, the cryostat will be calibrated in the 5 - 100°K range.
5	Preliminary Membrane Evaluation	The pressure drop of gaseous He <sup>4</sup> a) through a 10 cm cylindrical stack of membrane wafers and b) through a wound spiral cylinder 10 cm in length will be determined. Coarse determination of brittleness/durability at 78°K will be performed.
6	Decision Block	Based on pressure drop and durability tests a go-no go decision will be made with regard to further fabrication and testing of membrane composites.
7	Size Distribution Assessment	After receipt of ultrafines from the vendor and just prior to further processing or use, a size distribution measurement shall be performed. Results will be compared with vendor data to assess long term agglomeration characteristics.

<u>Block No.</u>	<u>Title</u>	<u>Discussion</u>
8	Specific Heat Measurement (Powder)	Using the calibrated cryostat the specific heat of several batches of the various ultra-fine materials shall be determined. Statistical design shall be employed to determine the number of sets of measurements required.
9	Press Compacts	Several compacts, the actual quantities determined by statistical analysis, shall be pressed from batches of each material being evaluated.
10	Mechanical Characteristics	The binding integrity and fracture tests of Para. 3.2.1 will be conducted both before and after cold cycling the composites to liquid helium temperature.
11	Decision Block	Based on an assessment of the composite's mechanical characteristics, a decision will be made whether or not to continue to evaluate the material for use in regenerator matrix fabrication.
12	Form "Binder" Composites	Several composites, the actual quantity determined by statistical analysis, shall be formed in wafer or cylindrical shapes by dispersing ultrafine powders in a binder solution.

<u>Block No.</u>	<u>Title</u>	<u>Discussion</u>
13	Mechanical Characteristics	The binding integrity, particle adhesion characteristics, and formability will be evaluated both before and after cold-cycling the composite.
14	Decision Block	Based on an assessment of the composite's mechanical characteristics, a decision will be made whether or not to continue to evaluate the material for use in regenerator matrix fabrication.
15	Mercury Impregnation	Using mercury porosimetry techniques, a selected number of pressed compacts will be impregnated with mercury so as to completely fill the void volume.
16	Mechanical Characteristics	The binding integrity and fracture tests of Para. 3.2.1 will be conducted both before and after cold cycling the composites to liquid helium temperature.
17	Decision Block	Based on an assessment of the composite's mechanical characteristics, a decision will be made whether or not to continue to evaluate the material for use in regenerator matrix fabrication.
18	Produce Loaded Membranes	Membrane materials will be loaded with ultrafine powders. For cellulose-based membranes, the

<u>Block No.</u>	<u>Title</u>	<u>Discussion</u>
18 continued	Produce Loaded Membranes	forming solution will be loaded to a high density prior to curing as a membrane. The teflon-based membrane material will be loaded by fusing techniques after formation, unless a more efficient process can be developed by the supplier.
19	Mechanical	The binding integrity, particle adhesion characteristics, and formability will be evaluated both before and after cold-cycling the composite.
20	Decision Block	Based on an assessment of the composite's mechanical characteristics, a decision will be made whether or not to continue to evaluate the material for use in regenerator matrix fabrication.
21	Specific Heat Measurement (Cluster Materials)	Using the calibrated cryostat, the specific heat of selected cluster materials (see Section II) in both bulk and wire screen form, if available, will be measured.
22	Specific Heat Measurement ("Anomaly" Material)	Using the calibrated cryostat, the specific heat of selected materials showing an entropy anomaly in the temperature range of interest will be determined.

<u>Block No.</u>	<u>Title</u>	<u>Discussion</u>
23	Size Distribution Assessment	A size distribution determination of samples of ultrafines from several batches of each material shall be performed. Results shall be compared with the earlier measurements (Block 7) to further assess agglomeration characteristics.
24	Analysis of Powder Specific Heat	An analysis shall be performed to determine if the achieved surface enhanced specific heat correlates with predicted values as determined from the Section II equation.
25	Specific Heat Measurement (Composite Materials)	Using the calibrated cryostat, the specific heat of samples of each composite material shall be determined. Statistical design shall be employed to determine the number of sets of measurements required.
26	Selection of Regenerator Materials	Based on the measurements and observations collected, the best candidate materials for use in regenerator fabrication will be selected.

#### 4.2 Regenerator Efficiency Measurements

The planning network for regenerator efficiency model evaluation is shown as Figure 33. The schedule of tests depicted therein is designed to provide the information base necessary to, a) verify the validity of the segmented regenerator model (see Section III), b) evaluate the

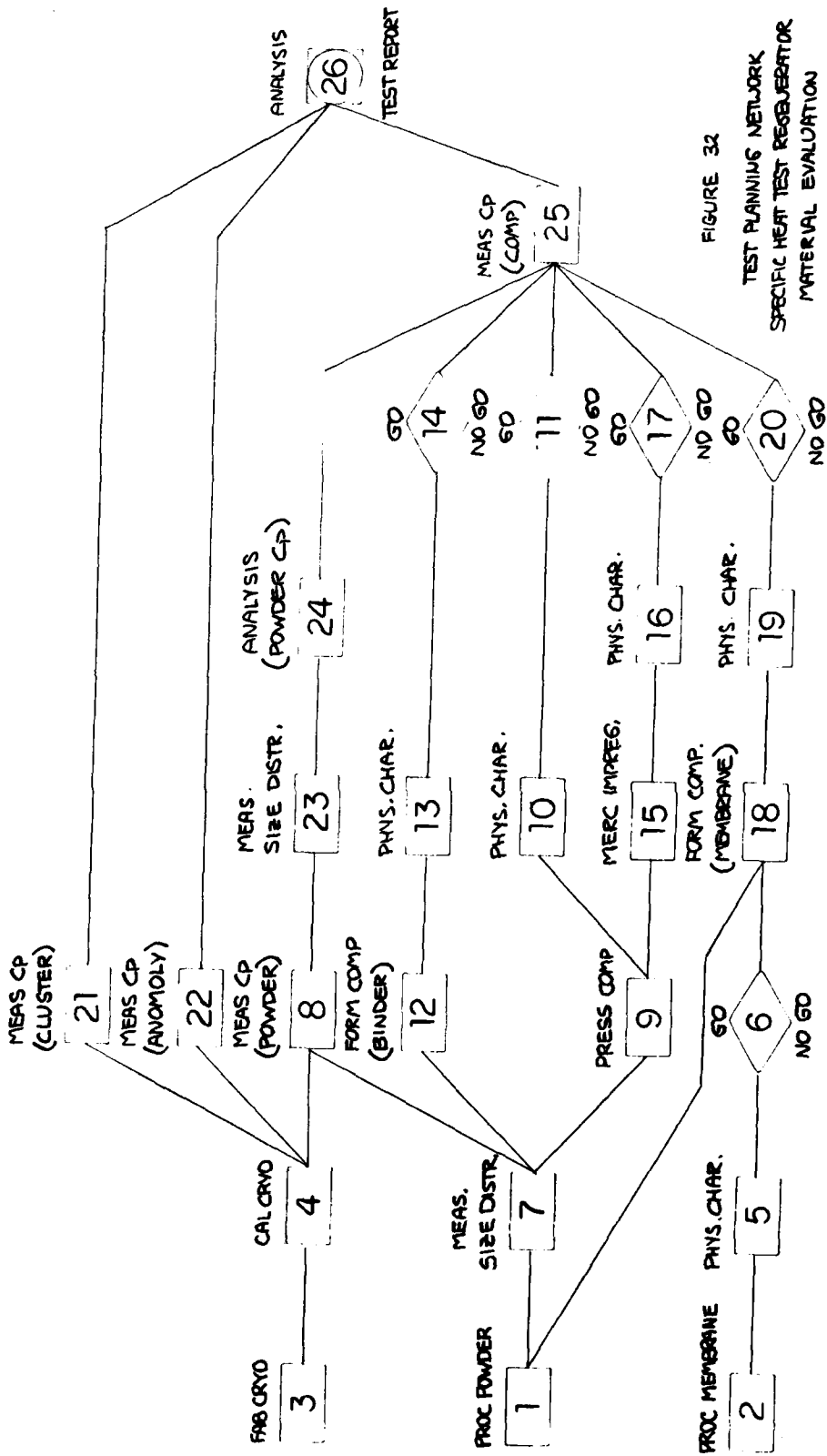


FIGURE 32

TEST PLANNING NETWORK  
 SPECIFIC HEAT TEST REEQUIPATOR  
 MATERIAL EVALUATION

importance of axial heat conduction and, c) investigate the reciprocity characteristics of  $C_r$  and  $C_g$  variations. This information will be used to verify the predictions of improved refrigerator performance derived from the small particle enhanced specific heat.

4.2.1 Description of Test Activity Blocks (per Figure 33)

<u>Block No.</u>	<u>Title</u>	<u>Discussion</u>
1	Measure Test Material Specific Heat	Using the calibrated specific heat cryostat, the heat capacity of screen and/or sphere materials to be used in this test program will be evaluated in the 5°K to 77°K range.
2	Build Regenerator Test Cryostat	Based on the design package developed during Phase 1, the regenerator test fixture will be constructed.
3	Fabricate Regenerator (R1)	A regenerator body will be fabricated and 150, 200 and 325 mesh screens of two different test materials (stainless steel and phosphor bronze) will be punched to size, so that the matrix packings can be conveniently interchanged.
4	High Temperature Baseline Test	The regenerator test cryostat will be baselined in the 300 - 77°K range using the R1 regenerator housing with .005 - .009" dia. lead spheres, as well as 150 mesh screen packing. Test results will be compared where possible with similar measurements by Gifford <sup>(1)</sup> and Lechner <sup>(2)</sup> in order to assess the fixture performance.

<u>Block No.</u>	<u>Title</u>	<u>Discussion</u>
5	Measure Regenerator R1 Efficiency (Test Sequence I)	The R1 regenerator using all combinations of screen mesh materials and sizes will be evaluated in the 300 - 77°K range. Square wave flow patterns will be utilized and peak helium flow rates will be varied in the 2.5 - 25 SCFM range. Blow times will be varied from 50 - 500 ms. Efficiency must be determined to three significant figures.
6	Low Temperature Baseline Test	The regenerator test cryostat will be baselined in the 77 - 5°K range using the R1 regenerator housing with .005 - .009" dia. lead sphere packing. Test results will be evaluated against the calculated values extrapolated from Block 4 results.
7	Fabricate Regenerator R2	A regenerator will be fabricated in such a manner that it can be partitioned into two (as well as three) segments of matrix material. Each segment will be packed with a matrix of pre-selected heat capacity.
8	Fabricate Regenerator R3	A regenerator will be fabricated in such a manner that it can be partitioned into more than three segments of matrix material. Each segment, not necessarily of equal lengths, will be packed with a matrix of pre-selected total heat capacity.

<u>Block No.</u>	<u>Title</u>	<u>Discussion</u>
9	Verify Lambertson-London Model	Using the data obtained from Block 5, the $C_r/C_g$ capacity ratio effect on efficiency will be investigated. Effects of axial heat conduction and wall effects will be considered.
10	Measure Regenerator R2 Efficiency (Test Sequence II)	The R2 regenerator using appropriate combinations of screen mesh materials and sizes will be evaluated in the 300 - 77°K range. Square wave flow patterns will be varied in the 2.5 - 25 SCFM range. Blow times will be varied from 50 - 500 ms. Efficiency must be determined to three significant figures.
11	Measure Regenerator R3 Efficiency (Test Sequence III)	The R3 regenerator using appropriate combinations of screen mesh materials will be evaluated in the 300 - 77°K range. Square wave flow patterns will be utilized and peak helium flow rate will be varied in the 2.5 - 25 SCFM range. Blow times will be varied from 50 - 500 ms. Efficiency must be determined to three significant figures.
12	Verify Segmented Regenerator Model	Using the data obtained from Blocks 10 and 11, the $C_r/C_g$ capacity ratio effect on segment efficiency and overall regenerator performance will be investigated. Effects of axial heat conduction will be considered.

<u>Block No.</u>	<u>Title</u>	<u>Discussion</u>
13	Measure Low Temperature Regenerator Efficiency (Test Sequence IV)	Using preselected combinations of matrix packings in the R2 and R3 regenerators, performance will be evaluated in the 77 - 5°K range. Square wave flow patterns will be utilized and peak helium flow rates will be varied in the 2.5 - 25 SCFM range. Blow times will be varied from 50 - 500 ms. Efficiency must be determined to three significant figures.
14	Final Model Assessment	Using the data obtained from Block 13, the $C_r/C_g$ capacity ratio effect on low temperature regenerator efficiency and overall performance will be investigated. Effects of axial heat conduction will be considered.

-----  
 (1) W. E. Gifford, Basic Investigation of Cryogenic Refrigeration Methods, Air Force Flight Dynamics Laboratory, Wright Patterson Air Force Base, Ohio, 45433, AFFDL-TR-68-61 (June 1968).

(2) R. A. Lechner, Investigation of Regenerators and Pulse Tube Cryogenic Coolers, United States Army Electronics Command, Fort Monmouth, N.J., ECOM-3409 (May 1971).

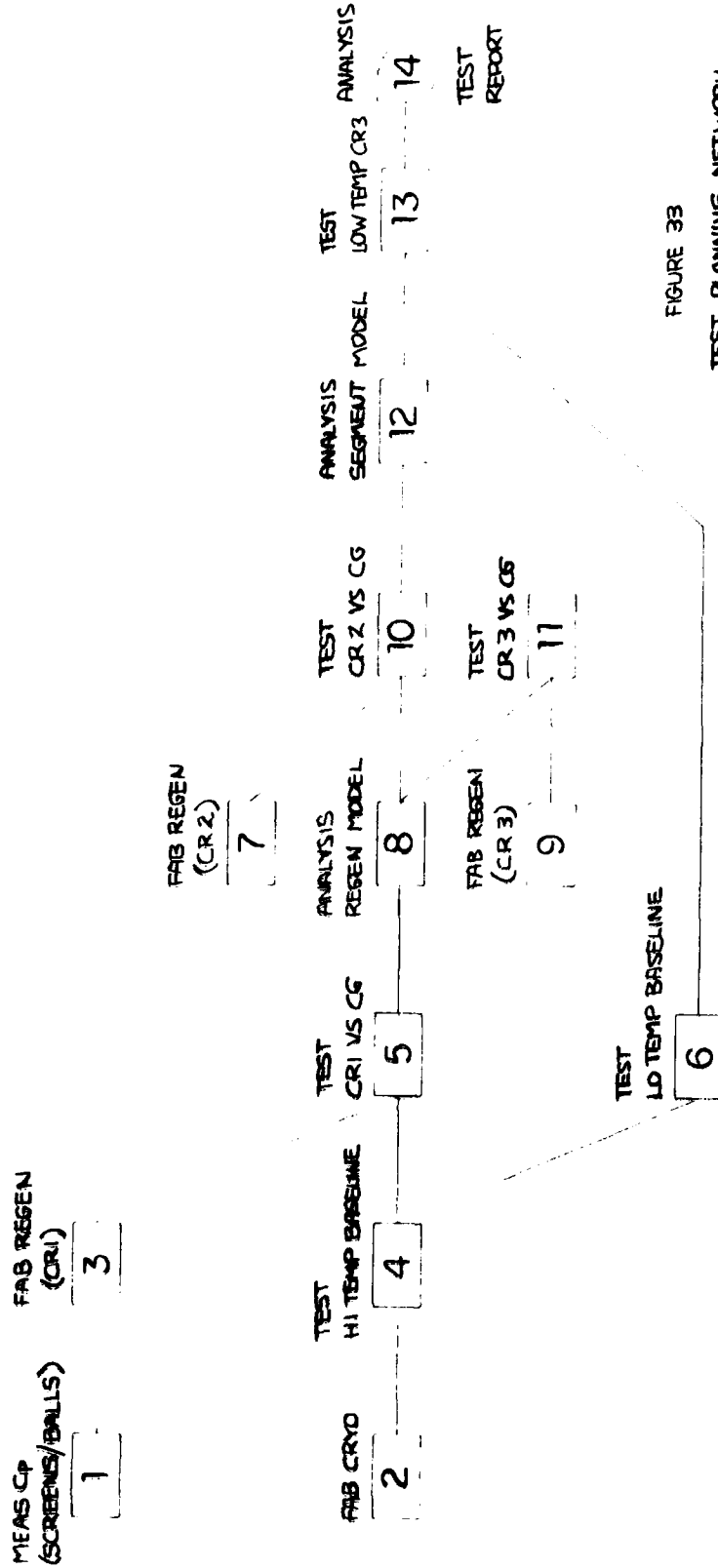


FIGURE 33  
TEST PLANNING NETWORK  
REGENERATOR PERFORMANCE  
MODEL EVALUATION